Norwegian University
of Life Sciences

Master's Thesis 2021 60 ECTS
Faculty of Chemistry, Biotechnology and Food Science
Morten Kjos

Uncovering a functional link between CozE proteins and lipoteichoic acid biosynthesis in *Staphylococcus aureus*

Maria Disen Barbuti
Biotechnology

Acknowledgements

This master thesis was completed as part of the Master programme in Biotechnology at the Norwegian University of Life Sciences (NMBU). The work was conducted in the Molecular Microbiology research group at the Faculty of Chemistry, Biotechnology and Food Science (KBM) between August 2020 and June 2021.

I particularly want to express gratitude to my main supervisor, Dr. Morten Kjos, for his continuous guidance throughout this entire process, both during the laboratory work and the writing process. Thank you for all your great ideas and comments regarding my thesis, and for always taking time out of your day to answer my questions. I also want to thank my co-supervisor, Dr. Daniel Straume, for his practical advice in the laboratory and for giving me, together with Dr. Morten Kjos, the opportunity to work on such an interesting topic. The knowledge I have gained during this process is invaluable.

In fact, everyone at the Molecular Microbiology research group deserves a huge thanks for providing a great work environment, with professional inputs as well as funny stories. I have really enjoyed my time in the laboratory, working with all of you. I want to give a special thanks to Maria Victoria Heggenhougen, for helping me get started with laboratory work, Ine Myrbråten, for assisting me with immunoblotting and for proofreading my thesis, and lastly Zhian Salehian, for assisting me with difficult overlap extension PCRs and for helping me finish all my experiments when NMBU closed due to SARS-CoV-2. I also want to thank my fellow master students, Henriette Sætre Olsen, Marie Leangen Herigstad, and Anna Teigen Schultheiss, for their support and entertainment in the laboratory during this year.

Lastly, I would like to thank my family and friends for all the love and support they have given me throughout my five years at NMBU.

Maria Disen Barbuti

Ås, June 2021

Abstract

Staphylococcus aureus is a common and successful human pathogen. Infections caused by *S. aureus* have become an urgent challenge in nosocomial and community settings, due to their multiple virulence mechanisms and ability to rapidly evolve resistance to novel antibiotics. Development of new therapeutic approaches to counteract the emergence of (multi) antibiotic resistant *S. aureus* strains is critical. Antibiotics that target bacterial cell division and teichoic acid biosynthesis has garnered interest in recent years. However, staphylococcal cell division is still not fully understood. In a previous study, the so-called CozE proteins found in *S. aureus*, CozEa and CozEb, have been demonstrated to play an important role in proper cell division, but the molecular mode of action by which the CozE proteins work are unknown.

In this work, the cellular functions of the CozE proteins were investigated further. Construction and characterisation of single and double *cozE* mutants confirmed that *cozEa* and *cozEb* constitute a synthetic lethal gene pair in *S. aureus*. Based on these results, we hypothesised that CozEa and CozEb possibly had a link to biosynthesis of lipoteichoic acids (LTAs) in *S. aureus*. By constructing a panel of mutant strains with knockdown of the *cozE* genes and LTA synthesis/modification genes, followed by growth assays, phase contrast- and transmission electron microscopy, we uncovered that two LTA biosynthesis genes (*ugtP* and *ltaA*) have pairwise synthetic genetic interactions with the *cozE* genes. Knockdown of *cozEa* and *cozEb* together is detrimental to wild-type *S. aureus* cells, and knockdown of these genes in a Δ*ugtP* background perpetuated the cell lysis phenotype observed in wild-type background. On the other hand, knockdown of both *cozE* genes in Δ*ltaA* background did remarkably not result in any apparent alterations to their growth rate or morphology. Normal cell growth and cell division were re-established in these Δ*ltaA* mutant strains. Anti-LTA immunoblot assays with cell lysates from the different mutants revealed that CozEb play a unique role in controlling LTA polymer length. *S. aureus* Δ*cozEb* mutants displayed abnormally long LTA polymers, reminiscent of LTA found in mutants affecting LTA glycolipid anchor synthesis (Δ*ugtP* and Δ*ltaA*). Subcellular localisation analysis by fluorescence microscopy of these proteins were also performed. Together, the results obtained in this work clearly demonstrates a functional link between CozE proteins and LTA biosynthesis in *S. aureus*, and the CozE proteins are predicted to perform this function upstream of either UgtP or LtaA.

Sammendrag

Staphylococcus aureus er en vanlig og vellykket human patogen. Infeksjoner forårsaket av *S. aureus* er en økende utfordring, både i helseinstitusjoner og utenfor, på grunn av deres mangfoldige virulensmekanismer og evne til å utvikle motstandsdyktighet mot nye antibiotika. Utvikling av nye behandlingsmetoder for å motvirke fremveksten av (multi)resistente *S. aureus*-stammer er svært viktig. Forskere har vist økt interesse for antibiotika som angriper bakteriell celledeling og biosyntese av teikoinsyre de siste årene. Celledelingen hos stafylokokker er imidlertid ikke fullstendig forstått enda. I en tidligere studie har de såkalte CozE-proteinene i *S. aureus*, CozEa og CozEb, vist seg å spille en viktig rolle i celledeling, men den molekylære virkningsmåten til disse proteinene er ukjent.

I dette arbeidet ble funksjonene til CozE-proteinene undersøkt nærmere. Konstruksjon og karakterisering av enkle og doble *cozE*-mutanter, bekreftet at *cozEa* og *cozEb* utgjør et syntetisk letalt genpar i *S. aureus*. Basert på disse resultatene, formulerte vi en hypotese om at CozEa og CozEb muligens hadde en kobling til biosyntese av lipoteikoinsyrer (LTAer) i *S. aureus*. Ved å konstruere et panel av mutanter med «knock-down» av *cozE*-genene og LTA-syntese/modifikasjonsgener, etterfulgt av vekstanalyser, fasekontrast- og transmisjonselektronmikroskopi, avdekket vi at to LTA-syntesegener (*ugtP* og *ltaA*) har syntetiske genetiske interaksjoner med *cozE*-genene. «Knock-down» av *cozEa* og *cozEb* sammen er svært skadelig for *S. aureus* celler, og «knock-down» av disse genene i en Δ*ugtP* bakgrunn forsterket cellelysis-fenotypen observert i villtype bakgrunnen. Derimot «knock-down» av begge *cozE*-genene i Δ*ltaA* bakgrunn resulterte tilsynelatende ikke i endringer i vekst eller morfologi. Normal cellevekst og -deling ble gjenopprettet i disse Δ*ltaA* mutantene. Anti-LTA immunoblot-analyser med cellelysat fra de forskjellige mutantene avslørte i tillegg at CozEb spiller en unik rolle når det kommer til å kontrollere lengden på LTA-polymerer. *S. aureus* Δ*cozEb*-mutanter produserte unormalt lange LTA-polymerer, som minner om LTAene man finner i mutanter med forstyrret LTA glykolipidanker-syntese (Δ*ugtP* og Δ*ltaA*). Subcellulære lokaliseringsanalyser, ved bruk av fluorescensmikroskopi, ble også foretatt med disse proteinene. I sum viser resultatene i dette arbeidet tydelig tilstedeværelsen av en funksjonell kobling mellom CozE-proteiner og LTA-biosyntese i *S. aureus*, og CozE-proteinene ser ut til å utføre denne funksjonen oppstrøms for enten UgtP eller LtaA.

Index

1 Introduction

1.1 *Staphylococcus aureus*

Staphylococcus aureus is a Gram-positive, spherical bacterium that can cause a wide range of infectious diseases (Lowy, 1998). It was first described in 1880 by Sir Alexander Ogston who was studying puss from abscess. Microscopic observations of Gram stained "Micrococci" from the pus, revealed that some of the "micrococci" were clustered together like grapes, hence the name *Staphylococcus*, meaning bunch of grapes (*staphyle*) and berry/grain (*kokkos*) in Greek (Bhunia, 2018; Ogston, 1882, 1984). *Staphylococcus* was further differentiated in 1884 by Friedrich Julius Rosenbach based on colony colour. Rosenbach proposed the name *S. aureus*, derived from the Latin word *aurum* meaning gold, because of its characteristic golden pigmentation (Liu et al., 2005; Rosenbach, 1884; Stryjewski & Corey, 2014). *S. aureus* has remained an important human pathogen since its discovery by Ogston, infecting millions of patients worldwide (Stryjewski & Corey, 2014). *S. aureus* is currently one of 55 recognised species belonging to the *Staphylococcus* genus (**Figure 1.1**), nevertheless, it is still considered the most pathogenic (Euzéby, 2021; van Belkum et al., 2009). The staphylococcal species are all non-spore forming, non-motile facultative anaerobes performing either aerobic respiration or fermentation (Harris, Foster, & Richards, 2002).

1.1.1 Epidemiology and pathogenesis

S. aureus is a common commensal of human and animal skin, nares, and gastrointestinal tracts (Bhunia, 2018). Approximately 20% of the human population is permanently carriers of *S. aureus* in their nose (persistent carriers), while approximately 60% are intermittent carriers with varying frequencies. Meaning that the majority of the population will carry *S. aureus* in their lifetime (Jenkins et al., 2015; Williams, 1963). It is not necessarily harmful to be a nasal carrier of *S. aureus*, the bacterium is actually a part of the normal microbiota of of asymptomatic carriers. However, carriers are at higher risk of infections and they presumably play an important role in the spread of *S. aureus* (Chambers & DeLeo, 2009). *S. aureus* can in addition to being a commensal of the human microbiota also become an opportunistic pathogen. As an opportunistic pathogen it can cause infections with varying severity, from superficial skin lesions (e.g., boils and styes) to invasive diseases, such as osteomyelitis, endocarditis, pneumonia, and sepsis (Foster, 1996; Gorwitz et al., 2008; Jenkins et al., 2015).

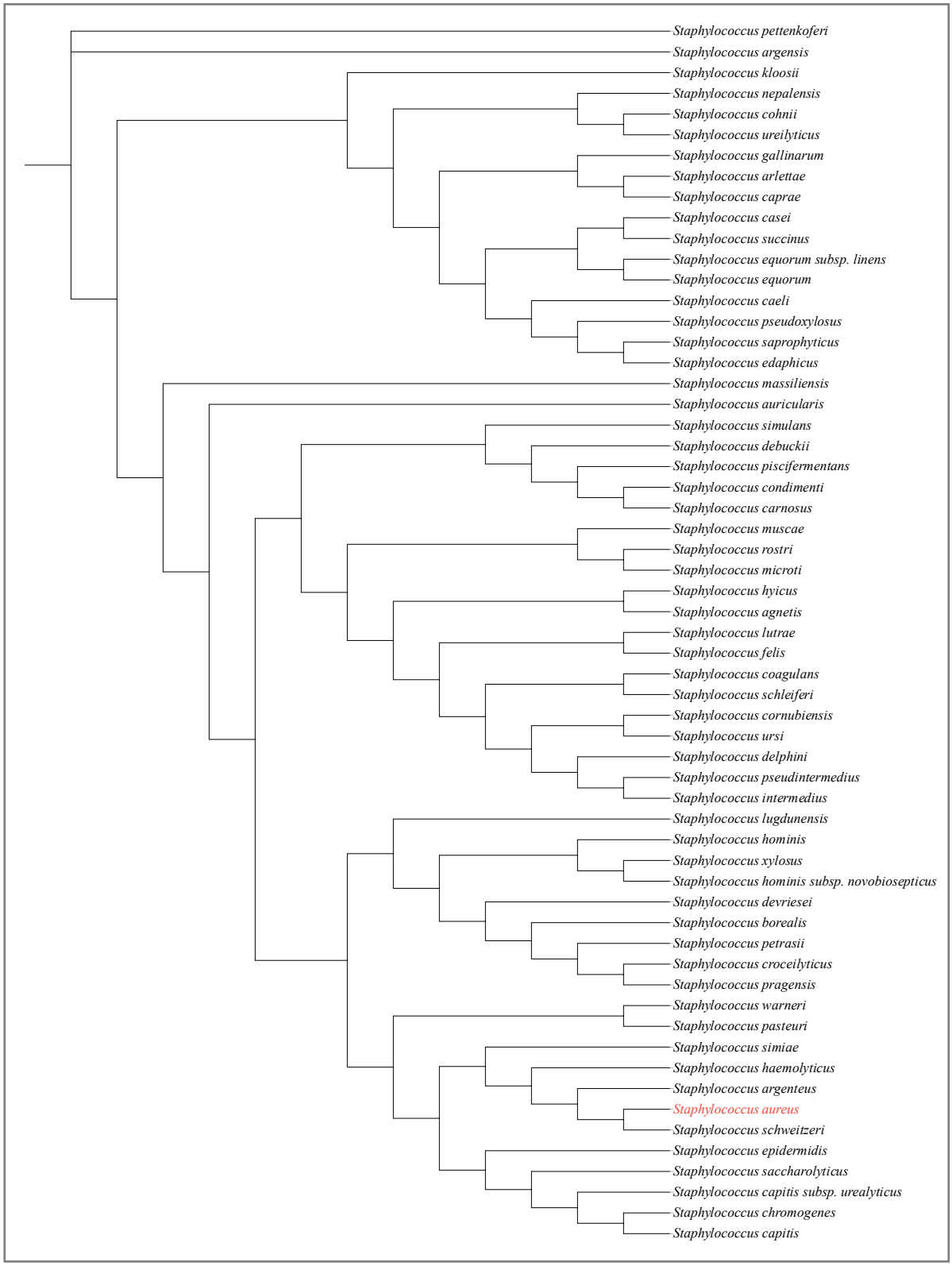

Figure 1.1 Phylogenetic tree depicting the relationship between the members of the *Staphylococcus* genus. The tree is based on sequence alignments (Clustal Omega) of 16S rRNA genes. Gene sequences were obtained from the "List of Prokaryotic names with Standing in Nomenclature" (LPSN) (Euzéby, 2021). A maximum likelihood phylogenetic tree was constructed with the sequence alignments using IQ-TREE. The phylogenetic tree was finally visualised and annotated using iTOL. *Staphylococcus aureus* is marked in red.

S. aureus infections can be divided into five stages: (1) colonisation, (2) local infection, (3) systemic dissemination and/or sepsis, (4) metastatic infections, and lastly (5) toxinosis. *S. aureus* can colonize mucous membranes and intact skin for months without causing an infection. However, prolonged hospitalisation, injection drug use, immune suppression, invasive medical devices (e.g., catheters and implants), and chronic metabolic diseases are factors that can predispose individuals to infections (Archer, 1998; Gnanamani, Periasamy, & Paul Satyaseela, 2017; Tong, Davis, Eichenberger, Holland, & Fowler, 2015). Local infections occur by inoculation of *S. aureus* from a site of carriage into the skin. The bacteria can then spread locally (e.g., cellulitis and impetigo) or to peripheral sites (e.g., endocarditis and osteomyelitis) via the blood (Archer, 1998). The extent to which the infection spreads depends on the complex interplay between *S. aureus*' virulence factors and the immune responses of the host (Lowy, 1998). *S. aureus* can also produce toxins with both local and systemic effects (e.g., toxic shock syndrome and foodborne gastroenteritis) (Archer, 1998). For instance, consumptions of enterotoxins produced by *S. aureus* can cause food poisoning (Argudín, Mendoza, & Rodicio, 2010).

1.1.2 Virulence factors

S. aureus' success as a human pathogen is partly due to its broad range of virulence mechanisms (van Belkum et al., 2009). It can express many different virulence factors, including adhesins, invasins, toxins, and immune evasins, and a majority of infections caused by *S. aureus* are multifactorial (Foster, 1996; Painter, Krishna, Wigneshweraraj, & Edwards, 2014). Many of the virulence factors are encoded on mobile genetic elements (MGE) obtained by horizontal gene transfer (HGT) between *S. aureus* strains (transduction, conjugation, or transformation) (Otto, 2014). Expression of the virulence factors are controlled by several overlapping, global regulatory systems, which ensures appropriate responses to changes in environmental conditions during infection (Painter et al., 2014). Two-component systems (TCSs) are important regulatory systems in *S. aureus*. They normally consist of a membrane-bound histidine kinase (HK) and a cytosolic response regulator protein that regulate expression of a large number of genes, including virulence factors, in response to defined signals from the host environment and the bacterial population. Most *S. aureus* strains have 16 TCSs (Haag & Bagnoli, 2017). The first identified regulatory system of virulence in *S. aureus* was the *agr* quorum-sensing (QS) system. Primary, it up-regulates secretion of toxins and exoenzymes responsible for cell lysis and destruction of tissue. Other important TCSs includes *sae*, *srr*, and *arl* (Balasubramanian, Harper, Shopsin, & Torres, 2017; R. P. Novick, 2003).

The idealistic bacterial growth cycle can be divided into four distinctive phases: lag, exponential (log), stationery, and death. *S. aureus* express vast different virulence factors during the four cell phases to sustain the infection. Initially, during the lag- and early exponential phase, cell wall-associated factors are mainly expressed (B. Wang & Muir, 2016). *S. aureus* can express up to 24 different cell wall-anchored (CWA) surface proteins (McCarthy & Lindsay, 2010). The CWA surface proteins enable attachment to the host tissue and evasion of the host's immune system, which in turn allow for accumulation and biofilm formation (B. Wang & Muir, 2016). Biofilms are complex microbial communities, enclosed in an extracellular matrix, that are attached to a surface or to other cells (Agarwal, Singh, & Jain, 2010). The complex teichoic acid (TA) polymers that are incorporated into the cell envelope of *S. aureus* also play an important role in colonisation, infection, and immune evasion. TAs can, for instance, mediate adhesion of *S. aureus* to nasal epithelial cells. They also play an important role in the first step of biofilm formation (Aly, Shinefield, Litz, & Maibach, 1980; Gross, Cramton, Götz, & Peschel, 2001; Xia, Kohler, & Peschel, 2010). The cell wall-associated factors are later down-regulated, during the late exponential phase, while expression of several extracellular proteins, including proteases and hemolysins, are up-regulated. These changes lead to dispersion of the biofilm, spread of bacteria, and lysis of the host cell (B. Wang & Muir, 2016).

1.1.3 Antibiotic resistance

S. aureus is naturally susceptible to most antibiotics, but it has an outstanding ability to rapidly acquire resistance to them. Antibiotic resistance is in most cases obtained by HGT, but other mechanisms also play an important role in acquired resistance, such as selective pressure and chromosomal mutations (Chambers & DeLeo, 2009). The genes coding for antibiotic resistance are primarily coded by plasmids, which facilitates the rapid spread of antibiotic resistance among *S. aureus* (Morris, Kellner, & Low, 1998). *S. aureus* has most notably obtained resistance to penicillin, methicillin, and vancomycin (**Figure 1.2**), however, different *S. aureus* strains have aquired resistance to a number of other antibiotics, including erythromycin, clindamycin, trimethoprim, and fusidic acid (Davey & Tong, 2019).

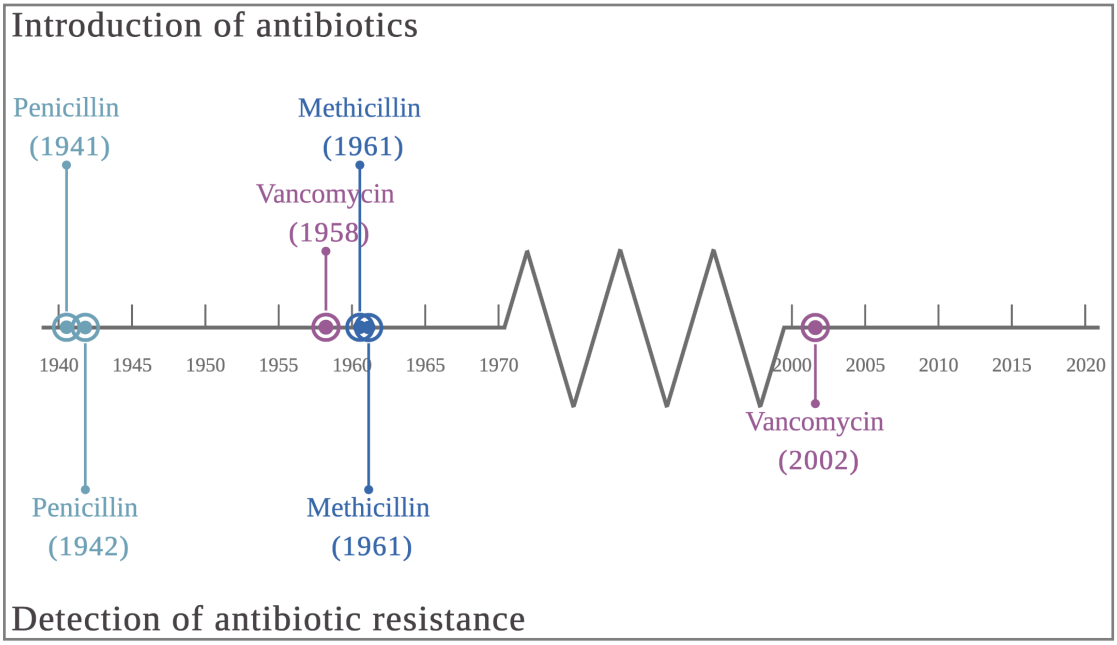

Figure 1.2 Timeline of introduction of, and subsequently development of resistance to, penicillin, methicillin, and vancomycin in *S. aureus*. The years for the development of theses antibiotics are shown on the top of the timeline, while the years when resistance to them were first observed in *S. aureus* are shown below. Created with BioRender.com.

1.1.3.1 Penicillin resistance

Prior to the introduction of antibiotics, bacteremia caused by *S. aureus* had a mortality rate of approximately 80% (Skinner & Keefer, 1941). This rate drastically improved with the introduction of penicillin for medical use in 1941. However, only one year later, in 1942, penicillin-resistant strains were observed in hospitals. These penicillin-resistant strains later spread to the community; a pattern observed with all the later waves of antibiotic resistant *S. aureus* strains (Lowy, 2003). By the mid-1960s, a high prevalence of resistance to penicillin was observed in both hospital-acquired (HA) and community-acquired (CA) *S. aureus* isolates (80-90% and 65-70%, respectively). The difference was that the HA isolates typically were resistant to several antibiotics, while the CA isolates usually only were resistant to penicillin (Chambers, 2001). Today, more than 90% of *S. aureus* isolates are resistant to penicillin, regardless of the clinical setting, and it is therefore no longer used to treat *S. aureus* infections. Resistance to penicillin is usually due to the production of β-lactamase (also known as penicillinase). This predominantly extracellular enzyme is encoded by *blaZ* (Lowy, 2003). Four different types of *blaZ* genes have been identified, three of which are typically located on plasmids that often encodes several other antimicrobial resistance genes (e.g., gentamicin and erythromycin), while the last type usually resides in the chromosome. β-lactamase inactivates penicillin by hydrolysing the β-lactam ring, which is found in all β-lactam antibiotics (including penicillin), before penicillin reaches its molecular target. Resistance to penicillin can also be

obtained by PBP2a encoded by *mecA*, described in **Section 1.1.3.2** (Olsen, Christensen, & Aarestrup, 2006).

1.1.3.2 Methicillin resistance

Methicillin was introduced in 1961 to target the *S. aureus* strains producing β-lactamase, and it thereby became the first semi-synthetic penicillinase-resistant penicillin. However, resistance to this antibiotic was found in S. *aureus* the same year. Resistance to methicillin occurs through the acquisition of the *mecA* gene, which is a part of a genetic mobile element called staphylococcal chromosomal cassette *mec* (SCC*mec*) (Schito, 2006). Eleven different SCC*mec* elements have been registered to date, with more expected to be found in the future (Keiichi Hiramatsu et al., 2013). *mecA* encodes the low-affinity penicillin-binding protein PBP2a. PBP2a is capable of substituting all four penicillin-binding proteins found in *S. aureus* (**Section 1.2.3.3**) in the presence of β-lactam antibiotics, given that PBP2a has low affinity to β-lactam antibiotics, and it confer resistance to β-lactam antibiotics in this way. PBP2a does, unlike β-lactamase, have a broad spectrum of activity, conferring resistance to most β-lactam antibiotics, including penicillins, cephalosporins, and carbapenems (Lowy, 2003). The first methicillin-resistant *S. aureus* (MRSA) strains to emerge never fully established in the community. They circulated in hospitals in Europe and USA, but largely disappeared by the 1980s. However, this did not mark the end of MRSA's prevalence. New and successful MRSA linages reached endemic levels by the mid-1980s. These linages later led to the worldwide pandemic of MRSA in hospitals that is still going on to this day (Chambers & DeLeo, 2009). MRSA was for a long time regarded as a nosocomial pathogen, but this perception has gradually changed over the last 25 years. Community-associated MRSA (CA-MRSA) have now also spread worldwide (DeLeo, Otto, Kreiswirth, & Chambers, 2010).

1.1.3.3 Vancomycin resistance

Vancomycin has been used to treat MRSA infections since its introduction in 1958. The increasing burden of MRSA infections led to increased use of vancomycin, which in turn led to acquisition of spontaneous adaptive mutations in MRSA (selective pressure) (Gardete & Tomasz, 2014). The first MRSA strains with reduced susceptibility to vancomycin were reported in 1997 (K Hiramatsu et al., 1997). These vancomycin intermediate-resistant *S. aureus* (VISA) strains were most likely a result of gradual mutation accumulation of VISA-associated genes, such as *walKR*, *graSR*, and *vraSR*, encoding TCSs. Mutations in these TCSs led to

alterations in peptidoglycan synthesis and degradation, resulting in irregular cell shapes, thicker cell wall, decreased cross-linking of peptidoglycan, alteration in TA structure or biosynthesis, and reduced autolytic activity (Cong, Yang, & Rao, 2020; Sieradzki & Tomasz, 2003). However, fully resistant strains were not observed until 2002, 44 years after the introduction of vancomycin. Resistance to vancomycin is mediated by the *vanA* gene cluster encoding five proteins essential for vancomycin resistance (VanS, VanR, VanH, VanA, and VanX). *vanA* was transferred to *S. aureus* from vancomycin-resistant *Enterococcus faecalis* via a plasmid. Vancomycin's target of action is the D-Ala-D-Ala terminus of the peptidoglycan precursor lipid II, and binding to it prevents their integration into peptidoglycan. The *vanA* genes modify the D-Ala-D-Ala to D-Ala-D-Lac which has almost 1000-fold decreased affinity to vancomycin. Infections caused by VRSA are, however, still relatively rare (Cong et al., 2020).

1.1.3.4 Prospects for the future

The mortality rate of individuals with *S. aureus* bacteremia is today approximately 20% (Guimaraes et al., 2018). *S. aureus* is the leading cause of nosocomial infections, but it is also becoming an increasing problem outside of hospitals (Klein, Smith, & Laxminarayan, 2007). Antibiotic treatment of these infections is becoming more ineffective with the development of antibiotic resistant strains, especially multi antibiotic resistant strains. The pharmaceutical industry has mainly been coping with this problem by modifying already existing antimicrobial agents. Very few new groups have been marketed in the last forty years. It is therefore critical to develop new treatment strategies, including vaccines and anti-infectives, and new classes of antibiotics, with novel targets and structures, to manage resistant *S. aureus* infections. Understanding the complex nature of *S. aureus* is necessary for this development (Balasubramanian et al., 2017; Belete, 2019; Chambers & DeLeo, 2009). Most of the clinically used antibiotics today target the biosynthesis of DNA, RNA, protein, or cell wall. Although the inhibition of bacterial cell division and teichoic acid biosynthesis have been recognised as promising strategies to counteract important pathogens with acquired resistance in recent years, better understanding of these mechanisms is thus highly important (L. W. Pasquina, Santa Maria, & Walker, 2013; Sass & Brötz-Oesterhelt, 2013).

1.2 Cell division in *S. aureus*

Cell division is a vital process by which a parental cell divides into two daughter cells. *S. aureus* does, like most bacterial cells, reproduce by binary fission. This type of asexual reproduction

is initiated by enlarging the cell wall, plasma membrane, and overall cell volume as new material is synthesised. The bacterial chromosome is replicated, and the two copies move towards opposite poles of the cell as the septum begins to form at midcell. Finally, the two daughter cells split, each with their own chromosome and other cellular cytoplasmic components. The time between each cell division is called the cell cycle, and this cycle can be divided into three phases: (1) the period of growth after cell splitting, (2) the chromosome replication and segregation period, and (3) the cytokinesis. However, unlike eucaryotic cells, bacteria does not follow the cell cycle phases sequentially, since cytokinesis begins before chromosome segregation is completed and new rounds of chromosome replication can be initiated before the cell split (Willey, Sherwood, & Woolverton, 2017c).

1.2.1 Chromosome replication and segregation

Replication of the bacterial chromosome begins at a single origin (*oriC*) and proceeds bidirectionally around the chromosome to the terminus (*ter*), located directly on the opposite side of *oriC* (J. D. Wang & Levin, 2009; Willey et al., 2017c). DnaA initiates DNA replication by binding to specific AT-rich sites at *oriC*, causing the DNA strands to unwind so that the two DNA synthesising machineries, called sister replisomes, can bind. DnaA is later inhibited to prevent over-initiation (J. D. Wang & Levin, 2009).

Several cellular mechanisms, both active and passive, ensure proper segregation of the replicated chromosomes. The structural maintenance of chromosomes (SMC) complex and the chromosome partitioning system ParABS are two of the most important active chromosome segregation systems found in bacteria (Pinho, Kjos, & Veening, 2013). SMC is involved in organisation and condensation of chromosomes, facilitating proper chromosome segregation in *S. aureus* and other bacteria where this protein has been studied (W. Yu, Herbert, Graumann, & Götz, 2010). The ParABS system consist of a Walker-like ATPase (ParA), a DNA-binding protein (ParB), and a chromosomal binding site (*parS*). ParB, also called SpoOJ in *S. aureus*, binds to the *parS* sites located near *oriC*, on the two daughter chromosomes (H. Chan, Söderström, & Skoglund, 2020; Willey et al., 2017c). Even though *S. aureus* lack a ParA homologue, SpoOJ alone have a function in chromosome segregation, but the exact mechanism is not known. In fact, SMC have been demonstrated to be recruited to *oriC*-proximal sites through interactions with ParB homologues in *Streptococcus pneumoniae* and *Bacillus subtilis*. Similar interactions have recently been found in *S. aureus*, and the absence of *smc* or *spoOJ* result in abnormal chromosome segregation (H. Chan et al., 2020). Both the SMC complex and

the ParABS system are non-essential in cocci, suggesting that passive processes also are important drivers of segregation. The passive processes that are believed to contribute to chromosomal segregation in cocci include DNA replication, transcription, and entropy. Both replication and transcription of DNA, performed by DNA polymerases and RNA polymerases, respectively, provide an extrusion force on the new DNA strands which might contribute to directing the chromosomal segregation. However, supportive experimental data is missing, specifically on *S. aureus*, and the importance of passive processes on chromosomal segregation vary between bacterial species (Pinho et al., 2013). A physical model, constructed by Jun and Mulder, propose that entropy alone can be the driving force for chromosome segregation. Under strong confining conditions, like in the cytoplasm, chromosome molecules will repel each other to maximize their total conformational entropy. Suggesting that duplicated chromosomes spontaneously demix as a result of entropic forces (Jun & Mulder, 2006; Jun & Wright, 2010). Chromosome segregation must be coordinated with cytokinesis for proper placement and timing of the septum, ensuring accurate inherence of genetic material. This proper spatial and temporal placement is mainly dependent on the regulation of FtsZ localisation (**Section 1.2.2.1**) (Veiga, Jorge, & Pinho, 2011).

1.2.2 Cytokinesis

Two identical daughter cells are formed by septal division of a parental cell during cytokinesis. Cytokinesis can be divided into the following four steps: (1) selection of the division site, (2) assembly of the Z ring, (3) assembly of the cell wall synthesizing machinery, and (4) constriction and closure of the division septum (Willey et al., 2017c).

1.2.2.1 Selection of division site

Proper selection of the division site is essential for coordination of cytokinesis and chromosome segregation, which in turn ensures formation of identical daughter cells. Two main mechanisms have been established for this selection in bacteria: (1) the Min-, and (2) nucleoid occlusion system. The Min system is not found in *S. aureus* (it lacks all the *min* genes), however, *S. aureus* does have a homolog to the nucleoid occlusion protein (Noc) found in *B. subtilis* (Pinho et al., 2013). Nucleoid occlusion prevents division through areas occupied by the nucleoid by binding Noc proteins, which acts as inhibitors of FtsZ polymerisation, at sites near *oriC*. The Z ring is thus only able to form at midcell after most of the daughter chromosomes have segregated and a Noc-free zone is generated, avoiding guillotining of the chromosomes. Other factors may also

contribute to division site selection, as mutants lacking both the Min- and nucleoid occlusion system still preferably assemble the Z ring at midcell (Veiga et al., 2011; Willey et al., 2017c).

S. aureus was up until very recently thought to divide in three alternating orthogonal planes over three consecutive division cycles. However, recent research has demonstrated that this is not always the case (Saraiva et al., 2020). Actually, a minority of staphylococcal cells display this mode of division. While the plane of division is always perpendicular to the previous division plane, it is not necessarily perpendicular to the penultimate one. The former theory of three perpendicular planes would infer that the cells needed a form of memory of the two previous division planes, but a mechanism to ensure such memory has never been identified. On the other hand, the new findings of division in two perpendicular planes do not require such memory. This mode of division only requires nucleoid occlusion and entropic forces. Two temporarily asymmetrical daughter cells, with different axis lengths, are formed after septal formation. Chromosome segregation will occur along the longer axis, which is parallel to the division septum, as this axis is favoured by entropy due to less spatial constraints. Only one possible division plane, that does not bisect the nucleoid containing Noc, is available during chromosome segregation. And this plane will inevitably be perpendicular to the previous division plane (Pinho et al., 2013; Saraiva et al., 2020).

1.2.2.2 Assembly of the Z ring and the divisome

The first protein to be recruited to the future division site is FtsZ. FtsZ is a tubulin-like protein that polymerises to form protofilaments in a GTP-dependent manner at midcell. These protofilaments organises into a dynamic structure known as the Z ring (Scheffers, de Wit, den Blaauwen, & Driessen, 2002). The curvature of the FtsZ polymers is referred to as the Z ring in this work, even though a recent study has revealed that FtsZ initially can assemble a D-shaped structure instead of a ring structure in staphylococcal cells (Saraiva et al., 2020). Proper Z ring assembly require attachment to the cytoplasmic membrane. FtsZ is a cytoplasmic protein with no intrinsic affinity for phospholipids. The FtsZ protofilaments are therefore anchored to the cytoplasmic membrane via interactions with FtsA, which binds directly to the membrane through a conserved membrane targeting sequence (Pichoff & Lutkenhaus, 2005). Several proteins are required for maintaining a stable Z ring in the early stages of cell division. SepF and EzrA have been found to be important division site regulators in Gram-positive bacteria (Hamoen, Meile, De Jong, Noirot, & Errington, 2006). EzrA is, for instance, a negative regulator of Z ring formation. It prevents inappropriate formation at other areas than midcell by

reducing GTP's affinity for FtsZ and enhancing the GTPase activity of FtsZ (Chung, Hsu, Yeh, & Chang, 2007). The fully assembled Z ring provides a scaffold for binding the late division proteins, including DivIB, DivIC, FtsL, GpsB, and PBPs in *S. aureus*, which are involved in cell wall synthesis (Booth & Lewis, 2019; Chaudhuri et al., 2009; Pinho et al., 2013). The large complex of proteins recruited by the Z ring is referred to as the divisome, and several of its proteins are conserved across bacterial species. The divisome facilitates the later steps during cytokinesis, which involves septal cell wall synthesis, closure of the septum, and finally splitting of daughter cells (**Section 1.2.3**) (Pinho et al., 2013).

1.2.2.3 Synthesis, constriction, and closure of the division septum

The final step of cytokinesis is constriction of the Z ring as the cell membrane invaginates, and the septal cell wall is synthesised (**Section 1.2.3.1-1.2.3.3**) (Willey et al., 2017c). The divisome controls the synthesis of new cell wall by localising the cell wall synthesis proteins to midcell, and the force needed for constrictions prior to cell splitting is generated by the Z ring as well as the activity of the peptidoglycan synthesis (Monteiro et al., 2018). The cell is lastly split into two daughter cells triggered by autolysins (**Section 1.2.3.4**) (Matias & Beveridge, 2007).

1.2.3 The cell wall of *S. aureus*

S. aureus is, as mentioned earlier, a Gram-positive bacterium. Gram-positive bacteria are encapsulated by a cytoplasmic membrane surrounded by a thick layer of peptidoglycan (Silhavy, Kahne, & Walker, 2010). Peptidoglycan is composed of glycan strands, made up of alternating *N*-acetylglucosamine (Glc*N*Ac) and *N*-acetylmuramic acid (Mur*N*Ac) residues linked by β-1→4 glycosidic bonds, crosslinked by short peptides into a mesh-like framework. The composition of the glycan strands are conserved among bacterial species, but their cross-linking is notably different in regard to their mode of cross-linkage, the amino acid composition of their interpeptide bridge, and their degree of cross-linkage. The glycan strands in the cell wall of *S. aureus* are connected through a pentaglycine bridge between the stem peptides attached to the MurNAc residue. The pentaglycine bridges extends from the amino group of the diamino acid at position 3 of one stem peptide to the carboxyl group of D-Ala at position 4 of another (Silhavy et al., 2010; Vollmer, Blanot, & De Pedro, 2008). *S. aureus* has a high degree of peptide cross-linkage. Between 74% and 92% of all peptides in *S. aureus* are present in cross-links. The length of the glycan strands also varies between species, and *S. aureus* has particularly short glycan strands. The average glycan strand in *S. aureus* (85-90%) is 6

disaccharides long, although glycan strands longer than 26 disaccharides are also observed. This is considerably shorter than the average *B. subtilis* glycan strand, which is longer than 500 disaccharides (Vollmer & Seligman, 2010). The short glycan strand found in *S. aureus* may be a result of high glucosaminidase activity. The staphylococcal membrane-associated *N*-acetylglucosaminidase SagB are found to cleave polymerised glycan strands to their final size (Y. G. Y. Chan, Frankel, Missiakas, & Schneewind, 2016).

In addition to a 20-30 nm thick mesh-like framework of peptidoglycan the staphylococcal cell wall also contains long anionic polymers, called teichoic acids (TAs) (**Section 1.3** describe teichoic acid biosynthesis) (Sharif, Singh, Kim, & Schaefer, 2009). TAs account for over 60 % of the mass of Gram-positive cell walls. Staphylococcal cell walls are, in addition, decorated with various proteins. Most surface proteins are covalently attached to the cell wall via stem peptides, but some are noncovalently attached to peptidoglycan or teichoic acids via ionic interactions. The surface proteins attached covalently to the cell wall contain an amino-terminal sequence for secretion through the membrane, and a carboxy-terminal pentapeptide cell wall sorting motif for incorporation into peptidoglycan. The composition of surface proteins in the cell wall depends on the environment of the particular *S. aureus* cell (Silhavy et al., 2010). The bacterial cell wall is required for survival, having a long list of functions. Some of its most important roles are to protect the cell from the environment, constrain the internal turgor pressure, maintain the cell shape, enable entry and efflux of molecules, and serve as a scaffold (Vollmer et al., 2008; Zerbib, 2017). Peptidoglycan is unique to bacteria making it a perfect target for antibiotics. Several classes of antibiotics target different aspects of the peptidoglycan synthesis, including β-lactams and glycopeptides (Otten, Brilli, Vollmer, Viollier, & Salje, 2018).

S. aureus mainly synthesises cell wall at the division septum, though slight elongation is also observed. Septation require synthesis of new peptidoglycan outside of the membrane. The divisome directs peptidoglycan synthesis to midcell and catalyses the synthesis (Reichmann et al., 2019). The synthesis of peptidoglycan can be divided into three main stages: (1) precursor synthesis, (2) assembly and flipping of lipid II, and (3) polymerisation and crosslinking of glycan strands (Typas, Banzhaf, Gross, & Vollmer, 2012). See **Figure 1.3** for all reactions and enzymes necessary in peptidoglycan synthesis.

1.2.3.1 Precursor synthesis

The peptidoglycan precursors are synthesised in the cytoplasm (**Figure 1.3**). The first step of this synthesis is the transfer of enolpyruvyl from phosphoenolpyruvate (PEP) to uridine diphosphate (UDP)-*N*-acetylglucosamine (GlcNAc). This reaction is catalysed by MurA, and it generates enolpyruvyl UDP-GlcNAc. Enolpyruvyl UDP-GlcNAc is then converted to UDP-MurNAc by MurB in a NADPH-dependent manner. A pentapeptide side chain (the stem peptide) is added onto UDP-MurNAc stepwise, catalysed by four Mur ligases (MurC, MurD, MurE, and MurF) (Lovering, Safadi, & Strynadka, 2012). The composition of the pentapeptide that is added differs between bacterial species, L-alanine-D-iso-glutamine-L-lysine-D-alanine-D-alanine is added in *S. aureus* (Kim, Singh, Preobrazhenskaya, & Schaefer, 2013).

1.2.3.2 Assembly and flipping of lipid II

The membrane protein MraY catalyses the transfer of UDP-MurNAc-pentapeptide from the cytoplasm to a undecaprenyl phosphate carrier, that is anchored on the cytoplasmic side of the membrane (**Figure 1.3**). This transfer generates the membrane-associated product referred to as lipid I. MurG catalyses the conversion of lipid I to lipid II by transferring GlcNAc from UDP-GlcNAc to lipid I (Lovering et al., 2012; Pinho et al., 2013). Lipid II is modified by a stepwise addition of five glycine residues at the third amino acid by FemX, FemA, and FemB. The lipid II-Gly_5 is then flipped to the external side of the cytoplasmic membrane by a flippase (Pinho et al., 2013). The flipping mechanism of lipid II-Gly_5 is poorly understood. FtsW was previously proposed to translocate lipid II across the membrane in *S. aureus*, however recent studies have demonstrated the MurJ more likely act as the lipid II flippase (Taguchi et al., 2019). MurJ is recruited to the divisome by the FtsL/DivIB/DivIC complex that ensures septum formation at midcell (Monteiro et al., 2018).

1.2.3.3 Polymerisation and crosslinking of glycan strands to form the division septum

The final stage of peptidoglycan synthesis include polymerisation and cross-linking of the glycan strands, catalysed mainly by PBPs and shape, elongation, division, and sporulation (SEDS) proteins. These proteins link glycan strands together (transglycosylation) and cross-link newly synthesised peptidoglycan strands (transpeptidation). Some PBPs also have the ability to hydrolyse peptide bonds in existing strands (endopeptidation), for insertions of new units, or to hydrolyse the last D-alanine of stem pentapeptides (DD-carboxypeptidation), to regulate the number of cross-links in the cell wall. The different PBPs can be divided into two

main groups: (1) high-molecular-mass (HMM) PBPs, and (2) low-molecular-mass (LMM) PBPs. The HMM PBPs can be further divided into: (1) class A PBPs, who are bifunctional with both transglycosylase and transpeptidase activity, and (2) class B PBPs, who are monofunctional with only transpeptidase activity. The LMM PBPs are usually DD-carboxypeptidases, although some possess transpeptidase activity (Pinho et al., 2013; Sauvage, Kerff, Terrak, Ayala, & Charlier, 2008). Four native PBPs are found in *S. aureus*: (1) PBP2 (class A HMM PBP), (2-3) PBP1 and PBP3 (class B HMM PBPs), and (4) PBP4 (LMM PBP with only transpeptidase activity) (Pinho et al., 2013).

Lipid II is polymerised into glycan strands by transglycosylases after translocation. How the activities of the different transglycosylases and transpeptidases are coordinated is not fully established yet. All PBPs in *S. aureus* have the ability to produce cross-links by performing transpeptidation, while only PBP2 have a transglycosylase activity. In addition to PBP2, however, there are several non-PBP transglycosylases that can catalyse the incorporation of new monomer to the growing glycan strands, including FtsW, RodA, Sgta, and SgtB (Emami et al., 2017; Reed, Veiga, Jorge, Terrak, & Pinho, 2011; Taguchi et al., 2019). The two transpeptidases PBP1 and PBP3 have been demonstrated to work in pairs with two non-PBP transglycosylase members of the SEDS protein family. Specifically, PBP1 has been shown to work together with FtsW, while PBP3 work together with RodA. PBP1 and FtsW are essential for the viability of *S. aureus*, while PBP3 and RodA are not. This is consistent with their functions, owing to the fact that elongation of *S. aureus* is mediated by RodA–PBP3, while inward incorporation of peptidoglycan at the septum is mediated by the FtsW–PBP1 pair. The FtsW–PBP1 pair does in addition stabilise the divisome by maintaining its localisation at midcell (Reichmann et al., 2019). The bifunctional PBP2 also play an essential role in *S. aureus* and is recruited to midcell by its affinity to lipid II (Monteiro et al., 2018). PBP4, on the other hand, is responsible for the high degree of peptide cross-linkage found in the *S. aureus* cell wall (Wyke, Ward, Hayes, & Curtis, 1981). It is recruited to the septum after PBP1 and PBP3 possibly to allow for insertion of proteins and polysaccharides before the highly cross-linked mesh-like framework is created (Pinho et al., 2013).

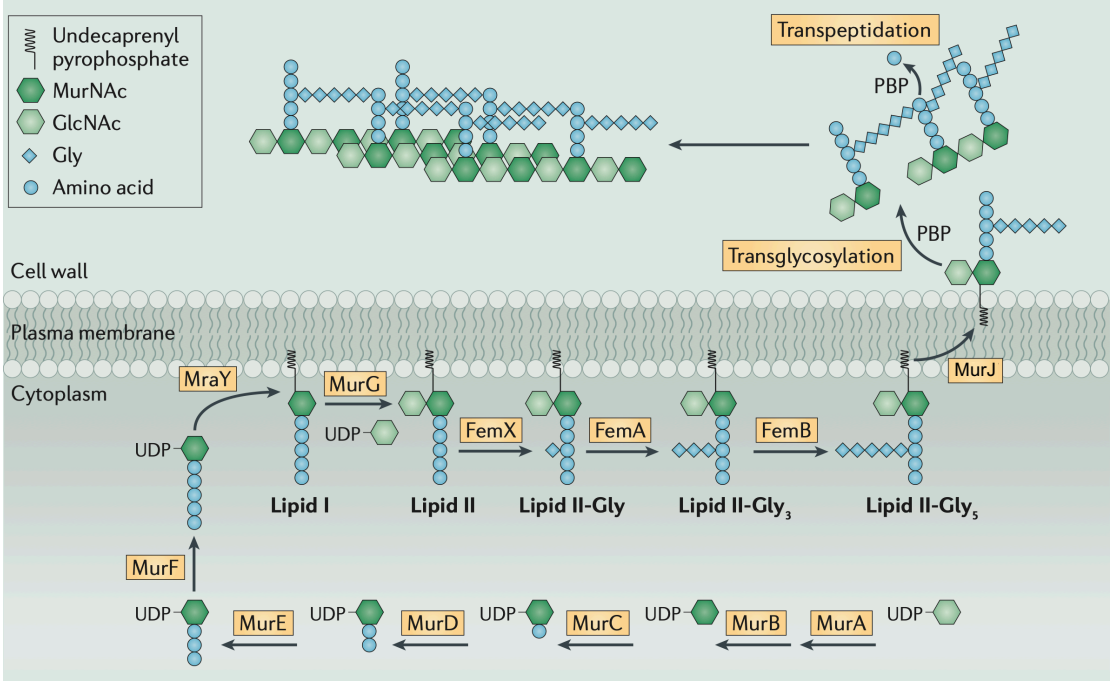

Figure 1.3 Peptidoglycan synthesis in Gram-positive bacteria, with all necessary reactions and enzymes. The figure is reproduced, with permission from Pinho et al., 2013.

1.2.3.4 The separation of daughter cells

Autolysins are required to split the newly synthesised septum (Pinho et al., 2013). The peptidoglycan layer of the outer cell wall presumably holds the septum together as it is synthesised, considering that the peptidoglycan layer is ~19 nm thick over most of the bacterium in contrast to the ~40 nm thick peptidoglycan layer found at the septum (the outer wall bridge) (Erickson, 2017). The septum is composed of two high-density zones (HDZs) separated by a low-density zone (LDZ). The HDZs correspond to the nascent cross walls, and their separation by the LDZ indicates that the septum forms independent structures before splitting. Autolysins likely trigger cell splitting by only degrading the outer wall bridge, not the entire septum (Matias & Beveridge, 2007). Atl is the best characterised autolysin important for hydrolysing peptidoglycan in *S. aureus*, although several other autolysins have also been demonstrated to play a role in the cleavage of the outer wall bridge, including Sle1, SceD, and IsaA (Kajimura et al., 2005; Stapleton et al., 2007). The bridge is not digested gradually; the separation is rather a result of an abrupt mechanical crack, initiated by perforation holes that are most likely created by a combination of mechanical stress and hydrolases, that propagates around the peripheral ring. The actual separation of daughter cells (popping) only takes ~1 millisecond. The cell growth of *S. aureus* has been found to happen continuously during cytokinesis, in contrary to the idea that their cell volume doubles after separation to cover the new hemisphere. Actually, the only period when the staphylococcal cell volume and surface

area decrease is initially after popping, when cells gradually convert their shape from hemi-ellipsoidal to ellipsoidal (Zhou et al., 2015). The glucosaminidases Atl, SagA, ScaH, and SagB have an essential role in remodelling the septum after popping. They decrease surface stiffness, by reducing the length of the glycan strands, which is vital for adapting the correct cell shape and increasing the cell volume (Wheeler et al., 2015).

1.3 Teichoic acid biosynthesis

Teichoic acids (TAs) are as stated earlier major constituents to the cell wall of *S. aureus* (**Section 1.2.3**). They are mainly composed of ribitol phosphate (Rbo-P) or glycerol phosphate (Gro-P) repeats. There are two main types of teichoic acids: (1) wall teichoic acids (WTAs), who are covalently linked to peptidoglycan, and (2) lipoteichoic acids (LTAs), who are anchored to the cytoplasmic membrane (**Figure 1.4A**) (Silhavy et al., 2010). Neither WTAs nor LTAs are essential, as deletion mutants of genes involved in either pathways are viable, but it is not possible to delete both pathways suggesting that they have overlapping essential functions in *S. aureus* (Oku et al., 2009). The levels of WTA and LTA are inversely regulated, meaning that production of WTA increases when LTA levels are low, and vice versa (Hesser et al., 2020). TAs have been found to play an important role in colonisation, infection, and immune evasion in *S. aureus*. TAs and enzymes required for TA biosynthesis are therefore attractive possible targets for antimicrobials (Xia et al., 2010). The synthesis of LTA is of primary interest in this work, as it is the relationship between this synthesis and the CozE proteins that is being studied.

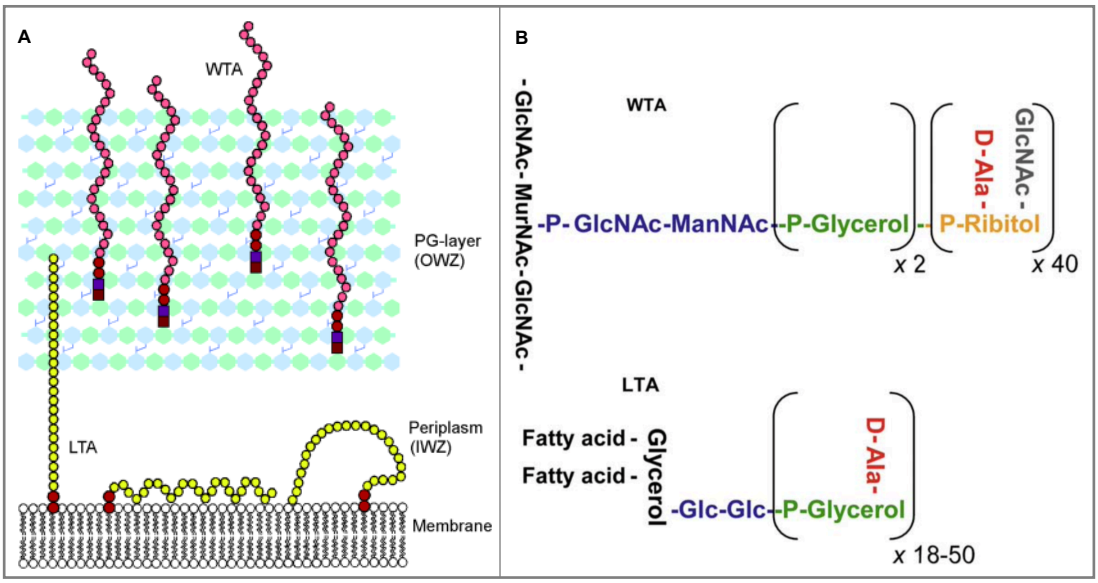

Figure 1.4 Depiction of *S. aureus* WTA and LTA localisation in the cell envelope (A) and structure (B): WTA = wall teichoic acid, LTA = lipoteichoic acid, OWZ = high-density outer wall zone, and IWZ = low-density inner wall zone. The figure is reproduced, with permission from Reichmann & Gründling, 2011 (**A**) and Xia et al., 2010 (**B**).

1.3.1 Wall teichoic acid (WTA) synthesis

WTAs are crucial for bacterial surface hydrophobicity, proper cell shape, and adhesion to the host (Oku et al., 2009). There are considerable structural variations between WTAs of different bacterial species, there are actually also often differences between WTAs of different bacterial clones from the same species. *S. aureus* produces WTAs that are covalently linked to the C6 hydroxyl of MurNAc of peptidoglycan via a (GlcNAc)-1-P and N-acetylmannosamine (ManNAc) disaccharide. This disaccharide is linked to two Gro-P units, which usually are linked to between 11 and 40 Rbo-P repeating units (**Figure 1.4B**), although *S. aureus* strains have been found to produce WTAs composed of only Gro-P repeating units and some strains appear to produce WTAs with both Rbo-P and Gro-P repeating units (Xia et al., 2010). WTAs are synthesised on undecaprenyl-phosphate (C_{55}-P) lipid carriers in the cytoplasmic membrane before being translocated to the extracellular surface of the membrane, by an ABC transporter, where they are attached to the C6 hydroxyl of MurNAc. 14 WTA biosynthetic proteins have been characterised for *S. aureus*. TagO, TagA, MnaA, TagB, TagF, TagD, TarL, TarI, and TarJ catalyses the intracellular synthesis of WTA polymers. TagG and TagH forms the two-component transporter that export WTA polymers to the extracellular surface. Finally, Msr, SA0908, and SA2101 from the LytR-CpsA-Psr (LCP) family are responsible for the final transfer of the WTA polymers to peptidoglycan. The "tag" proteins are involved in synthesis of both poly-Gro-P and poly-Rbo-P WTA, while the "tar" proteins only are involved in poly-Rbo-P WTA synthesis (Y. G.-Y. Chan, Kim, Schneewind, & Missiakas, 2014; Sewell & Brown, 2014; Xia et al., 2010).

1.3.2 Lipoteichoic acid (LTA) synthesis

LTAs have a different chemical composition and cellular compartmentation than WTAs, and therefore also employ a unique biosynthetic pathway (Walter et al., 2020). LTAs found in *S. aureus* consist of poly-Gro-P chains anchored to the cytoplasmic membrane via glycolipids (**Figure 1.4B**). The structure of *S. aureus*' LTAs are less complex than those of WTAs, and they are not surface exposed (**Figure 1.4A**). LTA synthesis, **Figure 1.5A**, begins in the cytoplasm with the production of the glycolipid anchor diglucosyl-diacylglycerol (Glc_2-DAG) by the glycosyltransferase UgtP (also called YpfP). UgtP transfers two glucose moieties from uridine diphosphate glucose (UDP-Glc) to DAG. A fraction of the synthesised Glc_2-DAGs is translocated to the outer leaflet of the membrane by the multi-membrane spanning protein LtaA. Lastly, the LTA synthase LtaS polymerases the poly-Gro-P backbone chain by transferring Gro-P units, derived from the head group of phosphatidylglycerol (Ptd-Gro), to the Glc_2-DAG,

on the outside surface of the membrane. Polymerisation using Ptd-Gro produces DAG as a by-product that is recycled back to Ptd-Gro by a separate pathway (Hesser et al., 2020; Reichmann & Gründling, 2011; Reichmann et al., 2014).

S. aureus cells with deletions of the genes required for glycolipid synthesis, *ugtP* or *ltaA*, are still viable, indicating that LtaS can initiate LTA synthesis on different lipids. The LTA backbones of Δ*ugtP* and Δ*ltaA* mutants are generally considered to be linked directly to DAGs, creating LTAs with simpler lipid anchors (Reichmann & Gründling, 2011), although Δ*ltaA* mutants have been demonstrated to produce a mixture of LTAs linked to both DAGs and Glc_2-DAGs, as a result of an unknown mechanism that can translocate Glc_2-DAG produced by UgtP to the outer leaflet of the membrane without LtaA (Hesser et al., 2020; Reichmann et al., 2014). Loss of *ugtP* or *ltaA* results in altered morphology and fitness. *S. aureus* Δ*ugtP* and Δ*ltaA* mutant cells are enlarged with division defects, including multiple and misplaced septa. The Δ*ugtP* mutant cells display more extreme defects than the Δ*ltaA* mutant cells. Absence of the Glc_2-DAG anchor yields abnormally long LTA polymers. The LTA polymers produced by Δ*ugtP* mutants are longer than those found in Δ*ltaA* mutants. The Δ*ugtP* and Δ*ltaA* mutants, with these long LTA polymers, are substantially more susceptible to enzymes that hydrolyses peptidoglycan, β-lactam antibiotics, and DltB inhibitors (**Section 1.3.2.1**) compared to wild-type. The defects observed in Δ*ugtP* and Δ*ltaA* can be correlated by reducing the length of the LTA polymers with mutation in *ltaS*, indicating that control of LTA length is important for the vitality of *S. aureus* cells (Hesser et al., 2020).

Deletion of *ltaS*, on the other hand, completely abolish LTA synthesis, which result in even more severe deficiencies in morphology and fitness. *S. aureus* Δ*ltaS* mutants are also enlarged with division defects, however, they can only grow in the present of a high sucrose or sodium chloride concentration. These defects suggest a link between synthesis of LTA and cell division. The three key proteins in LTA synthesis, UgtP, LtaA, and LtaS, have been shown to interact with each other and with multiple cell division proteins (EzrA, FtsA, FtsL, DivIB, and DivIC) and peptidoglycan synthesising proteins (FtsW, PBP1, PBP2, PBP3, and PBP4), forming a multi-enzyme complex (Reichmann et al., 2014). Consequently, LtaS has been demonstrated to mainly accumulate at the septum in *S. aureus*, indicating that LTA synthesis is primarily produced at the division site. However, UgtP and LtaA seem to be distributed more evenly around the membrane, indicating that the Glc_2-DAG anchor is not just synthesised at the division site. It is proposed that LTAs role in cell division is to ensure correct localisation of

Atl, which is responsible for hydrolysing peptidoglycan in the septum for separation of daughter cells, by serving as their receptors (Reichmann & Gründling, 2011; Reichmann et al., 2014).

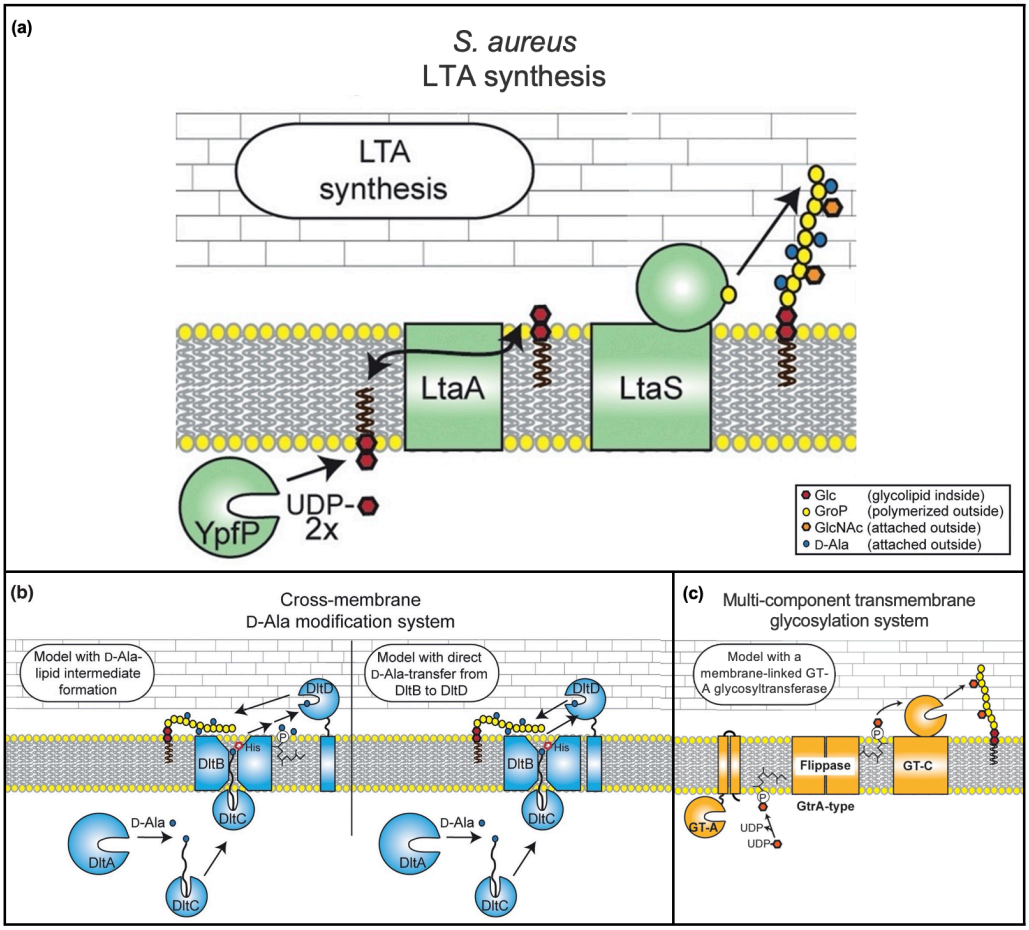

Figure 1.5 Schematic representation of *S. aureus* LTA synthesis (A), LTA D-alanine modification process (B), and LTA glycosylation modification process (C). The figure is reproduced, with permission from Rismondo et al., 2021.

1.3.2.1 Modification of LTA

LTA polymers are often further modified by d-alanylation (**Figure 1.5B**) and/or glycosylation (**Figure 1.5C**), which alters their properties and functions. WTA can also be modified, but is not described in this work. D-alanylation is catalysed by the DltABCD system, encoded in the *dlt* operon. Firstly, DltA loads the carrier protein DltC with D-alanine, and the DltC-D-Ala binds to the membrane bound protein DltB on the inner leaflet of the cytoplasmic membrane. The channel protein DltB will then either transfer the D-alanine to: (1) a lipid carrier (possible C_{55}-P or phosphatidylglycerol) that transfers the D-alanine to DltD, on the outside surface of the membrane, and subsequently to the LTA polymer, or (2) DltD directly which transfers it to the LTA polymer (Rismondo, Gillis, & Gründling, 2021). DltD have been demonstrated to interact with the three key proteins in LTA synthesis, UgtP, LtaA, and LtaS, indicating that

there is a coordination between synthesis and modification of LTA (Reichmann et al., 2014). LTA can also be decorated with GlcNAc. The membrane-linked glycosyltransferase protein CsbB (belonging to the GT-A family) transfers a GlcNAc moiety from UDP-GlcNAc to a C_{55}-P lipid carrier. The C_{55}-P-GlcNAc is then translocated to the outer leaflet of the cytoplasmic membrane by the flippase GtcA, and finally the GlcNAc moiety is added to the C2 hydroxyl of Gro-P in LTA by the glycosyltransferase YfhO (belonging to the GT-C family) (Kho & Meredith, 2018; Rismondo et al., 2021).

Modification of LTAs and WTAs can have great functional impact on bacteria. The extent of modification is dependent on both the strain and the environment (Swoboda, Campbell, Meredith, & Walker, 2010). Approximately 60-70% of all glycerol residues in staphylococcal LTAs are D-alanylated (Oku et al., 2009). Addition of D-alanine esters have been demonstrated to increase autolysin activity, help localise PBPs, and raise susceptibility to antibiotics (e.g. daptomycin), antimicrobial catalytic peptides, and lytic enzymes (Kho & Meredith, 2018). The functions of glycosyl modification on LTA is not defined yet, but it seems to impact the susceptibility of bacteria to stressful environmental condition (e.g. osmotic stress) (Rismondo et al., 2021).

1.4 The CozE proteins

The CozE (**c**oordinator **o**f **z**onal **e**longation) transmembrane protein was first discovered in *S. pneumoniae* (Fenton, El Mortaji, Lau, Rudner, & Bernhardt, 2016). CozE homologues are broadly distributed among various bacteria. They are, however, absent in the Mollicutes class lacking cell wall, indicating that they play a role in this mechanism. The CozE homologues found in *S. aureu*s, CozEa and CozEb, are important for proper cell division. They seem to be involved in the spatial and temporal coordination cell division and could therefore be interesting potential antimicrobial drug targets. Although better understanding of the molecular mode of action by which CozEa and CozEb work have to be obtained for this development to be possible (Fenton et al., 2016; Stamsås et al., 2018).

1.4.1 CozE and CozEb in *S. pneumoniae*

The CozE protein was discovered by Fenton et al. (2016) in *S. pneumoniae*. They revealed that it directs peptidoglycan synthesis to midcell for zonal elongation, hence the name. Inactivation of *cozE* was lethal in wild-type and in Δ*pbp2a* mutant *S. pneumoniae* strains, but not in Δ*pbp1a*,

suggesting that CozE work with the bifunctional class A PBP1a. Their results suggested that CozE work together with the protein MreC to control PBP1a localisation. This was supported by genetic assays, protein-protein interaction assays (bacterial two-hybrid analysis and a co-immunoprecipitation assay) demonstrating that CozE form a complex with MreC and PBP1a, and a microscopic analysis showing that GFP-CozE localisation to the septum was dependent on MreC. Furthermore, fluorescent labelling of PBP1a (with GFP) and peptidoglycan synthesis (with fluorescent D-amino acid TADA) in Δ*cozE* mutant cells revealed disturbance of the peptidoglycan synthesis (Ducret & Grangeasse, 2017; Fenton et al., 2016).

Recently Stamsås et al. (2020) discovered a CozE homolog in *S. pneumoniae*, named CozEb. This protein is a part of the same complex as CozE together with PBP1a. However, individual deletions of the genes encoding CozE and CozEb generated vast different morphologies. Δ*cozEb* mutant cells were smaller than wild-type, while Δ*cozE* were larger. Growth was also affected in the single deletion mutants, with the Δ*cozE* mutant cells displaying more severe effects. Cells with double deletion of both *cozE* genes were even more effected, they were hardly viable, indicating that CozE and CozEb have some overlapping functions. However, *cozEb* was not required for correct localisation of PBP1a. Nevertheless, overexpression of CozEb could compensate for deletion of *cozE*, supressing both growth and morphology defects, indicating that CozEb have the ability to localise PBP1a to midcell, even though it most likely is not directly responsible for this localisation under normal condition (Stamsås et al., 2020).

1.4.2 CozEa and CozEb in *S. aureus*

Two homologues to the CozE protein in *S. pneumoniae* have been found in *S. aureus*, named CozEa and CozEb. Although they do not appear to regulate the elongation of *S. aureus* cells, which is not surprising given that *S. aureus* have minimal elongation, only CozEa have been found to interact with MreCD, and neither CozEa nor CozEb interact with MreD or DivIVA, as was found in *S. pneumoniae*. Thus, the proteins probably fulfil different functions in *S. aureus*. However, both CozEa and CozEb, from *S. aureus*, can functionally complement the Δ*cozE* phenotype in *S. pneumoniae*, although CozEa and CozEb are only 31% and 30% identical to the CozE protein in *S. pneumoniae*, respectively. Both CozEa and CozEb are membrane proteins predicted to have 8 or 9 transmembrane segments. *cozEa* is monocistronic, while *cozEb* is polycistronic encoded by the same promotor as *glcT* and SAOUCHSC_01357 (*cozEb* is the last gene in this operon) (Stamsås et al., 2018).

Neither CozEa nor CozEb seem to be essential in wild-type *S. aureus*. Single deletions of the genes in the *S. aureus* SH1000 strain only result in slightly reduced cell size. However, cells with deletion of both genes could not be obtained in SH1000, indicating that CozEa and CozEb have overlapping functions that are essential to *S. aureus*. Depletion of CozEa or CozEb in respectively Δ*cozEb* or Δ*cozEa* (or depletion of both genes in wild-type) resulted in significantly reduced growth, variable cell shapes, increased clustering, frequent cell lysis, non-homogeneous DAPI staining pattern, and misplaced and aberrant septa in SH1000. In addition, the Δ*cozEa* cells displayed thicker cell walls than the wild-type in TEM microscopy. These changes were suggested to be caused by compromised timing and positioning of cell division and not alteration in the cell wall composition. CozEa and CozEb were found to interact with each other and with EzrA, which is an early cell division protein, in a bacterial two-hybrid analysis. The localisation of EzrA seems to be perturbed in the absent of the CozE proteins, and the SH1000 Δ*ezrA* phenotype is reminiscent of the phenotypes of SH1000 Δ*cozEa* and Δ*cozEb*. CozEa and CozEb might therefore mediate cell division control via their interaction with EzrA (Stamsås et al., 2018).

1.4.3 Potential link between CozE proteins and TA biosynthesis

In this work, we study the potential link between CozE proteins and TA biosynthesis. Interest in researching the CozE proteins in relation to the TA synthesis stems from the observation that the phenotypes of strain depleted of CozE proteins are reminiscent of mutants affecting TA synthesis and from a study performed by Corrigan et al. (2011) where *S. aureus* Δ*ltaS* strains acquired suppressor mutations in *cozEb*.

Corrigan et al. created five independently isolated SEJ1 Δ*ltaS* suppressor strains by cultivating the SEJ1 Δ*ltaS* mutant in medium without addition of sucrose or salt. All five strains still lacked LTAs afterwards, but they had obtained mutations in other genes (suppressor mutations) resulting in a morphology resembling the SEJ1 wild-type strain. Five genes containing potential suppressor mutations were identified, one of them being *cozEb*. In fact, four out of the five suppressor strains had obtained mutations in *cozEb*. These mutations could possible compensate for the lack of LTA, but further research must be conducted to determine their relationship (Corrigan et al., 2011).

1.5 The two-plasmid CRISPR interference (CRISPRi) system for *S. aureus*

The functionality of the genes of interest in this work (*cozEa*, *cozEb*, *ugtP*, *ltaA*, *ltaS*, and *dltA*) were studied through gene knockouts, which directly deletes/disrupts a gene, and through gene knockdown, which repress gene expression without destroying the gene. Gene knockout cannot be performed to study essential genes as bacteria depend on them to survive. Nonetheless, they are important to study as they play a key role in the bacteria and therefor can be potential targets for antibiotics (Zhao, Shu, & Sun, 2017).

A CRISPR (clustered regularly interspaced short palindromic repeats) interference (CRISPRi) system was employed to study the functionality of essential genes in this work. CRISPR systems are naturally found in ~40% of all bacteria, where they provide acquired immunity against viruses and plasmid by targeting and cleaving foreign DNA in a sequence specific manner. One of the simplest CRISPR system is the type II system found in *Streptococcus pyogenes*. It consists of a single gene encoding a Cas9 protein and two RNAs, CRISPR RNA (crRNA) and trans-acting RNA (tracrRNA) (Horvath & Barrangou, 2010; Qi et al., 2013). tracrRNA:crRNA complexes guide the Cas9 endonucleases to their targets, known as protospacers, where they cut the double stranded DNA and thereby thwarts the infection. In addition to the protospacers Cas9 also requires the presence of protospacer-adjacent motifs (PAMs) downstream of the protospacers (Bikard et al., 2013).

The CRISPR-Cas9 system have been repurposed to enable efficient genome editing in both eukaryotes and prokaryotes. This gene editing tool consist of a catalytically inactive Cas9 protein (dCas9) and a single guide RNA (sgRNA). The sgRNA contains all the essential components of the crRNA and tracrRNA, found in the naturally occurring CRISPR system, (Bikard et al., 2013; Guzzo, Castro, Reisch, Guo, & Laub, 2020). It is designed to target the gene of interest (with a 20 nucleotide long base pairing region) in addition to binding the dCas9 (with a Cas9-handle region), that lacks endonuclease activity due to mutations introduced in the catalytic residues (H840A and D10A) of the gene encoding Cas9. The dCas9-sgRNA complex binds to the target gene, but it does not cleave it, instead it blocks RNA polymerase from proceeding with the transcription of the gene resulting in down-regulation of transcription (Stamsås et al., 2018; Zhao et al., 2017).

1.6 Aim of the study

The emergence of *S. aureus* strains with reduced susceptibility to current antibiotics complicates treatment of infections and demands the development of new therapeutic strategies, with novel targets and mechanisms of action, to counteract these (multi) antibiotic resistant strains. Inhibition of the bacterial cell division and teichoic acid biosynthesis have been recognised as promising strategies for antibiotic attack. To be able to develop such antibiotics a greater understanding of the genes and processes underlying these mechanisms are needed (Sass & Brötz-Oesterhelt, 2013). The CozE proteins found in *S. aureus*, CozEa and CozEb, are involved in the spatiotemporal coordination of cell division and they are also potential links to the teichoic acid biosynthesis (Corrigan et al., 2011; Stamsås et al., 2018).

In this work, the functions of the conserved membrane proteins CozEa and CozEb in *S. aureus* are further investigated in order to get deeper insight into their function. The aims of this project are:

- To characterise and investigate the functions of CozE proteins in different *S. aureus* strains.
- To study whether CozE proteins affect peptidoglycan synthesis in *S. aureus*.
- To investigate the presence of a hypothesised functional link between CozE proteins and biosynthesis of TA.

2 Materials

2.1 Strains

The parental strains used in this work are listed in **Table 2.1**, while the mutant strains are listed in **Table A1.1** in **Appendix A1**. Their growth and storage conditions are described in **Section 3.1**.

Table 2.1 Parental strains used in this work.

Strain	Genotype and characteristics	Reference
S. aureus		
NCTC8325-4	NCTC8325 cured of phages φ11, φ12 and φ13	(R. Novick, 1967)
SH1000	*rbsU*+ derivative of strain NCTC8325-4	(Horsburgh et al., 2002)
JE2	USA300 LAC derivative cured of plasmids p01 and p03	(Fey et al., 2013)
COL	Clinical MRSA strain expressing *pls*	(Gill et al., 2005)
E. coli		
IM08B	DH10B, Δ*dcm*, P_{help}-*hsdMS*, P_{N25}-*hsdS* (strain expressing the *S. aureus* CC8 specific methylation genes)	(Monk, Tree, Howden, Stinear, & Foster, 2015)
DH5α	F- *endA1 glnV44 thi-1 recA1 relA1 gyrA96 deoR nupG purB20* φ80*dlacZ*Δ*M15* Δ(*lacZYA-argF*)U169, *hsdR17*(r_K^- m_K^+), λ^-	(Chen, Li, Zhang, & Wang, 2018)

2.2 Plasmids

All plasmids used in this work (**Table 2.2**) were purified using the E.Z.N.A.® Plasmid Mini Kit I (Omega Bio-tek), as described in **Section 3.3**, and stored in elution buffer at -20 ºC.

Table 2.2 Plasmids used in this work.

Plasmid	Description	Variants of the plasmid used in this work	Reference
pLOW	Low copy number shuttle vector for IPTG-inducible expression of proteins in *S. aureus*, amp^r (*E. coli*), ery^r (*S. aureus*)	pLOW-dCas9_extra_*lacO*, pLOW-dCas9_aad9, pLOW-m(sf)*gfp*-SA1477, and pLOW- *gfp_ugtP*	(Liew et al., 2011)
pCG248	*E.* coli/S. *aureus* shuttle vector, amp^r (*E. coli*), cam^r (*S. aureus*)	pCG248-sgRNA(*cozEa*), pCG248-sgRNA(*cozEb*), pCG248-sgRNA(*cozEa*+*cozEb*), pCG248-sgRNA(*luc*), pCG248-sgRNA(*cozEb*+*ugtP-ltaA*), pCG248-sgRNA(*cozEb*+*ltaS*), and pCG248-sgRNA(*cozEb*+*dltA*).	(Helle et al., 2011)
pVL2336	*E. coli*/*S. aureus* shuttle vector, amp^r (*E. coli*), cam^r (*S. aureus*)	pVL2336-sgRNA(*ugtP-ltaA*), pVL2336-sgRNA(*ltaS*), pVL2336-sgRNA(*dltA*), and pVL2336-sgRNA(*luc*)	Unpublished

pMAD	Low copy number shuttle vector for allelic replacement in Gram-positive bacteria, amp^r (*E. coli*), ery^r (*S. aureus*)	pMAD-Δ*cozEa*::*cam*, pMAD-I-SceI, pMAD-ori_*parS*, pMAD-*gfp_ugtP*::*spc*, and pMAD-Δ*ugtP*::*spc*	(Arnaud, Chastanet, & Débarbouillé, 2004)
pRAB11	*E.* coli/S. *aureus* shuttle vector, amp^r (*E. coli*), cam^r (*S. aureus*)	pRAB11-*cozEa*, pRAB11-*cozEb*, and pRAB11-*lacA*	(Helle et al., 2011)
pCN55	*E. coli*/*S. aureus* shuttle vector	pCN55	(Charpentier et al., 2004)

2.3 Primers

The primers used in this work, listed in **Table A2.1** in **Appendix A2**, were shipped and received in lyophilised state. Master stocks (100 µM) were prepared for each primer by diluting the lyophilised primers in dH_2O. Every master stock where further diluted to a 10 µM working stock. Both master stocks and working stocks were stored at -20 ºC.

2.4 Inducers of protein expression

Stock solutions for the inducers of protein expression used in this work (**Table 2.3**) were sterile filtered and stored at -20 ºC. The inducer stock solutions were added to liquid media before use. IPTG was used to induce *S. aureus* mutants carrying pLOW plasmids, while aTc was used to induce *S. aureus* mutants carrying pRAB11 plasmids.

Table 2.3 Inducers of protein expression used in this work.

Inducer	Formula	Stock concentration	Working concentration	Product number	Supplier
Isopropyl β-D-1-thiogalactopyranoside (IPTG)	$C_9H_{18}O_5S$	1 M	500 µM[a]	A1008	PanReac AppliChem
Anhydrotetracycline hydrochloride (aTc)	$C_{22}H_{22}N_2O_7 \cdot HCl$	1 mg/mL	0.004 µg/mL	37919	Sigma-Aldrich

a. *S. aureus* strains carrying pLOW- *gfp_ugtP* were only induced with 50 µM IPTG.

2.5 Antibiotics

Stock solutions for the antibiotics used in this work (**Table 2.4**) were sterile filtered and stored at -20 ºC. The antibiotic stock solutions were added to liquid media before use and to solid media at ~55 ºC before solidification.

Table 2.4 Antibiotics used in this work.

Antibiotic	Dissolved in	Stock concentration (mg/mL)	Working concentration (µg/mL)	Product number	Supplier
Ampicillin (amp)	dH_20	100	100	A9251	Sigma-Aldrich
Chloramphenicol (cam)	Ethanol	10	10	C0378	Sigma-Aldrich
Daptomycin (dap)	Ethanol	1	5 (MIC assay)	D2446	Sigma-Aldrich
Erythromycin (ery)	Ethanol	10	5	E6376	Sigma-Aldrich
Oxacillin (oxa)	dH_20	10	4 (MIC assay)	O1002	Sigma-Aldrich
Spectinomycin (spc)	dH_20	100	100	S9007	Sigma-Aldrich
Vancomycin (van)	dH_20	10	20 (MIC assay)	V2002	Sigma-Aldrich

2.6 Enzymes, molecular weight standards and nucleotides

Table 2.5 Enzymes, molecular weight standards, and nucleotides used in this work.

Name	Stock solution	Product number	Supplier
1 kb DNA ladder	500 µg/mL	N3232	New England Biolabs
Alkaline Phosphatase, Calf Intestinal (CIP)	10 000 U/mL	M0290	New England Biolabs
BamHI	20 000 U/mL	R0136	New England Biolabs
BamHI-HF	20 000 U/mL	R3136	New England Biolabs
BglII	10 000 U/mL	R0144	New England Biolabs
Color Prestained Protein Standard	-	P7719	New England Biolabs
dNTPs	10 mM	N0447	New England Biolabs
EcoRI	20 000 U/mL	R0101	New England Biolabs
EcoRI-HF	20 000 U/mL	R3101	New England Biolabs
GFP antibody rabbit polyclonal	-	PABG1	ChromoTek GmbH
Lysostaphin from *Staphylococcus simulans*	10 mg/mL	L9043	Sigma-Aldrich
Lysozyme human	100 mg/mL	L1667	Sigma-Aldrich
MagicMark™ XP Western Protein Standard	-	LC5603	Thermo Fisher Scientific
NcoI-HF	20 000 U/mL	R3193	New England Biolabs
Phusion® High Fidelity DNA polymerase	2000 U/mL	M0530	New England Biolabs
Proteinase K	-	BIO-37037	Bioline
PstI	20 000 U/mL	R0140	New England Biolabs
RNase A from bovine pancreas	-	R6513	Sigma-Aldrich
Red Taq DNA Polymerase 2x Master Mix	-	5200300	VWR International
SalI-HF	20 000 U/mL	R3138	New England Biolabs
T4 DNA Ligase	400 000 U/mL	M0202	New England Biolabs

2.7 Kits

Table 2.6 Kits used in this work.

Kit name	Purpose	Product number	Supplier
SuperSignal™ West Pico PLUS Chemiluminescent Substrate	Detect immunoreactive LTA polymers/GFP-tagged proteins from different mutants visualised by immunoblot analysis.	34580	Thermo Fisher Scientific
E.Z.N.A.® Plasmid Mini Kit I, (V-spin)	Isolate plasmid DNA from overnight bacterial cultures.	D6943	Omega Bio-tek
NucleoSpin® Gel and PCR Clean-up	Purify DNA fragments from enzymatic reactions and agarose gels.	740609	Macherey-Nagel

2.8 Chemicals

All chemicals used in this work are listed in **Table A3.1** in **Appendix A3**.

2.9 Growth media

2.9.1 Media for growth and maintenance of *S. aureus* strains

Brain Heart Infusion (BHI) medium. BHI powder (37 g/L) was dissolved in dH_2O and sterilised by autoclaving. For solid medium, 15 g/L agar was added before autoclaving.
(Used most frequently.)

Tryptic Soy Broth (TSB) medium. TSB powder (30 g/L) was dissolved in dH_2O and sterilised by autoclaving. For solid medium, 15 g/L was agar added before autoclaving.
(Used for Western blot cell harvesting and for gene replacement with the pMAD vector.)

Tryptic Soy Broth (TSB) medium with 0.5 M sucrose. Equal parts of sterilised 2x TSB medium (60 g/L TSB powder) and 1 M Sucrose (342.3 g/L Sucrose) were mixed.
(Used to help cells recover after electroporation.)

Mueller-Hinton (MH) medium. Three different MH medium variations were used in this work: (**1**) **MH medium with 25 mg/L Ca^{2+} and 12.5 mg/L Mg^{2+}**, used for MIC assays with vancomycin, (**2**) **MH medium with 50 mg/L Ca^{2+} and 12.5 mg/L Mg^{2+}**, used for MIC assays with daptomycin, and (**3**) **MH medium with 25 mg/L Ca^{2+}, 12.5 mg/L Mg^{2+}, and 2% Sodium chloride**, used for MIC assays with oxacillin.
For all three MH media MH broth (21 g/L) was dissolved in dH_2O and sterilised by autoclaving, although for variation (**3**) Sodium chloride (40 g/L) was also added before autoclaving. The

MH media were then chilled to 2-8 °C followed by cation-adjustments. All three variations were cation-adjusted with sterilised 10 mg/mL Ca^{2+} stock solution (36.8 g /L Calcium chloride dihydrate) and 10 mg/mL Mg^{2+} stock solution (8.36 mg/L Magnesium chloride hexahydrate). Variation (**1**) and (**3**) were added 22.34 mg/L Ca^{2+} and 8.34 mg/L Mg^{2+}, while variation (**2**) was added 47.34 mg/L Ca^{2+} and 8.34 mg/L Mg^{2+}. The pH of the media were then adjusted to 7.2-7.4 and they were stored at 4 ºC.

2.9.1 Media for growth and maintenance of *E. coli* strains

Lysogeny Broth (LB) medium. Tryptone (10 g/L), Yeast extract (5 g/L), and Sodium chloride (10 g/L) were dissolved in dH_2O and sterilised by autoclaving. For solid medium, 10 g/L agar was added before autoclaving.
(Used most frequently.)

Super Optimal broth with Catabolite repression (SOC) medium. Tryptone (20 g/L), Yeast extract (5 g/L), Sodium chloride (10 mM), and Potassium chloride (2.5 mM) were dissolved in dH_2O and sterilised by autoclaving. After autoclaving, Magnesium chloride (20 mM) and Glucose (20 mM) was added to the solution, using a sterilised 1 M Magnesium chloride stock solution (203.3 g/L Magnesium chloride hexahydrate) and a sterilised 2 M Glucose stock solution (360.31 g/L Glucose).
(Used to help cells recover after heat shock.)

2.10 Solutions and buffers

2.10.1 Premade solutions and buffers

Table 2.7 Premade solutions and buffers used in this work.

Compound	Product number	Supplier
5x Phusion® High Fidelity Reaction Buffer	B0518S	New England Biolabs
10x CutSmart® Buffer	B7204S	New England Biolabs
10x NEBuffer™ 3.1	B7203S	New England Biolabs
10x T4 Ligase Reaction Buffer	B0202A	New England Biolabs
Nuclei Lysis Solution	A7941	Promega
Protein Precipitation Solution	A795A	Promega

2.10.2 Solutions and buffers for polymerase chain reaction (PCR)

Staphylococcal lysis buffer I. Sodium hydroxide (40 mM) and Sodium dodecyl sulfate (SDS) (0.2% v/v).

2.10.3 Solutions and buffers for agarose gel electrophoresis

50x Tris acetate EDTA (TAE). Tris base (424 g/L), Acetic acid (5.7% v/v), and Ethylenediaminetetraacetic acid (EDTA) with pH 8.0 (0.05 M) were dissolved in dH_2O.

1% Agarose gel with peqGREEN. Agarose (0.5 g) was dissolved in TAE buffer (50 mL) by heating the agarose solution in a microwave. peqGEEN (1 µL) was added to the solution after cooling to ~55 ºC, to enable visualisation of DNA bands, before it was poured into a gel tray with well combs.

6x Gel loading buffer. Tris hydrochloride with pH 8.0 (10 mM), EDTA (1 mM), Sucrose (40 % v/v), and Bromophenol blue (0.01% v/v).

1 kb DNA ladder (50 mg/ml). 1 kb ladder (50 µL), 10x Gel loading buffer (200 µL), and dH_2O (750 µL).

2.10.4 Solutions and buffers for SDS-PAGE and immunoblotting

Phosphate Buffered Saline Tween-20 (PBST). Sodium chloride (8 g/L), Potassium chloride (0.2 g/L), Disodium hydrogen phosphate (1.44 g/L), Potassium dihydrogen phosphate (0.24 g/L), and Tween-20 (0.2 % v/v) were dissolved in dH_20. The pH was lastly adjusted to 7.4.

5% skimmed milk. Skim milk powder (50 g/L) was dissolved in PBST.

2.10.4.1 Solutions and buffers for lipoteichoic acid detection with anti-LTA antibodies

Staphylococcal lysis buffer II. Tris hydrochloride with pH 7.4 (50 mM), Sodium chloride (150 mM), and Lysostaphin (200 µg/mL).

4x SDS loading buffer. Tris hydrochloride with pH 6,8 (200 mM), Dithiothreitol (DTT) (20 mM), Sodium dodecyl sulfate (SDS) (8% v/v), Bromophenol blue (0,4% v/v), and Glycerol (40% v/v).

Running buffer I. Tris base (5 g/L), Glycine (15 g/L), and Sodium dodecyl sulfate (SDS) (1 g/L) were dissolved in dH_20.

Transfer buffer I. Tris base (3 g/L), Glycine (14.4 g/L), and Methanol (20% v/v) were dissolved in dH_20. The solution was stored at 4 ºC.

2.10.4.2 Solutions and buffers for detection of the relative expression of CozEa and CozEb with anti-GFP antibodies

2x SDS loading buffer. Tris hydrochloride with pH 6.8 (100 mM), Dithiothreitol (DTT) (10 mM), Sodium dodecyl sulfate (SDS) (4% v/v), Bromophenol blue (0.2% v/v), and Glycerol (20% v/v).

PAGE gel (12% separation gel and 4% stacking gel). The separation gel (12%) was prepared first, by mixing the following together: ddH_20 (4.3 mL), 1.5 M Tris hydrochloride with pH 8.8 (2.5 mL), 10% Sodium dodecyl sulfate (SDS) (0.1 mL), 40% Acrylamide + 0.8% Bis-acrylamide (3 mL), 10% Ammonium persulfate (APS) (0.1 mL), and Tetramethylethylenediamine (TEMED) (0.005 mL). 10% APS and TEMED were added last as they solidify the gel. This mixture (3.2 mL) was pipetted into an assembled Mini-PROTEAN cassette. Immediately followed by addition of dH_20. The separation gel was allowed to polymerize for ~45 minutes.

The dH_20 was then removed, and the stacking gel (4%) was prepared by mixing the following together: ddH_20 (3.14 mL), 0.5 M Tris hydrochloride with pH 6.8 (1.25 mL), 10% Sodium dodecyl sulfate (SDS) (0.05 mL), 40% Acrylamide + 0.8% Bis-acrylamide (0.5 mL), 10% Ammonium persulfate (APS) (0.05 mL), Tetramethylethylenediamine (TEMED) (0.005 mL), and Bromophenol blue (0.05 mL). This mixture (2.5 mL) was pipetted on top of the solidified separation gel, and a well comb was placed in the cassette. The stacking gel was allowed to polymerize for ~30 minutes.

Running buffer II. Tris base (25 mM), Glycine (192 mM), and Sodium dodecyl sulfate (SDS) (3.5 mM).

Transfer buffer II. Tris base (3 g/L), Glycine (14.4 g/L), and Methanol (20% v/v) were dissolved in dH_20. The solution was stored at 4 ºC.

2.10.5 Solutions and buffers for preparation of competent cells

15% glycerol with 0.1 M calcium chloride. Equal parts of 30% Glycerol and 0.2 M Calcium chloride (29.402 g/L Calcium chloride dihydrate) were mixed.

10% glycerol with 0.5 M sucrose. Equal parts of 20% Glycerol and 1 M Sucrose (342.3 g/L Sucrose) were mixed.

2.10.6 Solutions and buffers for microscopy

Phosphate-Buffered Saline (PBS). Sodium chloride (8 g/L), Potassium chloride (0.2 g/L), Disodium hydrogen phosphate (1.44 g/L), and Potassium dihydrogen phosphate (0.24 g/L) were dissolved in dH_20. The pH was lastly adjusted to 7.4.

Agarose gel (1.2%) for microscopy. Certified molecular biology agarose (0.24 g) was dissolved in PBS (20 mL) by heating the agarose solution in a microwave.

Tris buffered saline (TBS). Tris hydrochloride with pH 7.5 (50 mM) and Sodium chloride (100 mM).

Electron microscopy (EM) fixation solution. Paraformaldehyde (2% v/v), Cacodylate buffer (0.1 M), and Glutaraldehyde solution (grade I) (1.25% v/v). A 0.4 M Cacodylate buffer (85.61 g/L Sodium cacodylate trihydrate) was used in this work.

2.10.7 Other solutions and buffers

1 M Tris hydrochloride buffers. Tris base (15.15 g/L) was dissolved in dH_2O. The tris hydrochloride buffers were adjusted to the desired pH by addition of either Sodium hydroxide or Hydrochloride.

1 M Ethylenediaminetetraacetic acid (EDTA), pH 8.0. Ethylenediaminetetraacetic acid (EDTA) (186 g/L) was dissolved dH_2O. The pH was lastly adjusted to 8.0.

2.11 Equipment

Table 2.8 Equipment used in this work.

Equipment	Purpose	Model	Supplier
Electroporator I	Transform *S. aureus* cells by applying an electrical field that increases their permeability, allowing for plasmids to be introduced into the cells.	Gene pulser™	Bio-Rad Laboratories
Electroporator II	"	MicroPulser™	Bio-Rad Laboratories
Gel electrophoresis system I	Separate DNA fragments in an electric field through an agarose gel matrix.	Mini-Sub Cell GT Cell	Bio-Rad Laboratories
Gel electrophoresis system II	Separate proteins/LTA polymers in an electric field through a polyacrylamide gel matrix.	Mini-PROTEAN Tetra Cell	Bio-Rad Laboratories
Gel imager I	Visualise DNA in agarose gels after electrophoresis, by exposing them to UV light.	Gel Doc™ XR+ Imager	Bio-Rad Laboratories
Gel Imager II	Visualise antibody bound proteins/LTA polymers after immunoblotting.	Azure Imager c400	Azure Biosystems
Mechanical homogeniser	Lyse bacterial cells.	FastPrep-24™	MP Biomedicals
Microplate reader I	Monitor bacterial proliferation in time by measuring OD_{600}.	Hidex Sense	Hidex Oy
Microplate reader II	"	Synergy™ H1 Hybrid Multi-Mode Reader	BioTek Instruments
Microscope I	Visualise bacterial cells with phase contrast microscopy and fluorescence microscopy.	LSM 700	Zeiss
Microscope II	Visualise bacterial cells with transmission electron microscopy.	Morgagni™ 268	FEI Company
Microscope camera I	Capture images of bacteria visualised in LSM 700.	ORCA-Flash4.0 V3 Digital CMOS camera	Hamamatsu Photonics K.K.
Microscope camera II	Capture images of bacteria visualised in Morgagni™ 268.	Veleta CCD camera	Olympus Corporation
Spectrophotometer I	Measure the DNA concentration of different samples (PCR products, isolated gDNA, and isolated plasmids).	NanoDrop™ 2000	Thermo Fisher Scientific
Spectrophotometer II	Measure OD_{600} of bacterial cultures in test tubes and cuvettes.	GENESYS™ 30	Thermo Fisher Scientific
Spectrophotometer III	"	Novaspec® II	Pharmacia Biotech
Thermal cycler	Amplify specific DNA sequences.	ProFlex™ PCR System	Thermo Fisher Scientific
Immunoblotting transfer system	Transfer proteins/LTA polymers separated by SDS-PAGE to an immobilising membrane, using an electric field.	Trans-Blot Turbo System	Bio-Rad Laboratories

a. Additional standard laboratory equipment, not listed in this table, were also used in this work.

3 Methods

3.1 Growth and storage of bacteria

3.1.1 Growth of *S. aureus*

All *S. aureus* strains used in this work (**Table A1.1**) were grown under aerobic conditions at 37 ºC, with the exception of bacterial cells transformed with the temperature sensitive pMAD vector which were first grown at 30 ºC and later at 42-44 ºC (**Section 3.11.3**). Brain Heart Infusion (BHI), Tryptic Soy Broth (TSB), or Mueller-Hinton (MH) medium was used for cultivation of *S. aureus* strains. They were either grown in liquid medium with vigorous shaking (~200 rpm), or on agar plates without shaking. Some strains required antibiotics and/or inducers of protein expression (**Table A1.1**), concentration of such is outlined in **Table 2.4 and 2.3**. IPTG was the inducer of protein expression for *S. aureus* mutants carrying pLOW plasmids, while aTc was used to induce mutants carrying pRAB11 plasmids.

3.1.2 Growth of *E. coli*

All *E.* coli strains in this work (**Table A1.1**) were grown under aerobic conditions at 37 ºC in/on Lysogeny Broth (LB) medium with 100 µg/mL ampicillin, with the exception of the final step of transformation where Super Optimal broth with Catabolite repression (SOC) medium was used to obtain maximal transformation efficiency. Growth in liquid media was performed at ~200 rpm, while growth on solid media was performed without shaking.

3.1.3 Storage of *S. aureus* and *E. coli*

For short-term storage, the bacterial tubes/plates were kept at 4°C. Frozen stocks were prepared for long term storage of the bacterial strains, by adding glycerol to bacterial overnight cultures to a final concentration of ~15% glycerol. The frozen stocks were stored at -80 ºC.

3.2 Isolation of genomic DNA (gDNA)

Genomic DNA (gDNA) refers to the chromosomal DNA found in an organism. *S. aureus* cells have a single, circular chromosome made up of ~2.7-2.8 Mb (Młynarczyk, Młynarczyk, & Jeljaszewicz, 1998). In this work, gDNA was isolated from the MDB1 mutant, for use as template DNA in several PCR reactions (**Section 3.6**).

Many different methods have been created for isolation of bacterial gDNA, and a version of the Promega Quick method was used in this work. Firstly, 5 mL overnight culture was centrifuged at maximum speed for 2 minutes to pellet the cells. The cell pellet was resuspended in 100 µL ethylenediaminetetraacetic acid (EDTA) (50 mM), 5 µl lysozyme (100 mg/mL), and 1 µl lysostaphin (10 mg/mL) and incubated at 37 ºC for 30 minutes. After incubation, 600 µl Nuclei Lysis Solution was added and mixed by gently pipetting. The solution was then incubated at 80 ºC for 5 minutes, before it was cooled to room-temperature and added 5 µl RNase A (10 mg/mL). The RNase was mixed with the solution, by inversion of the tube, to degrade the RNA. The solution was then incubated at 37 ºC for another 30 minutes and later cooled to room-temperature. Next, 200 µl Protein Precipitation Solution was added and mixed by vortexing, followed by 5 minutes incubation on ice. The precipitated protein was then removed by centrifugation at maximum speed for 3 minutes. The supernatant (~1 mL), containing the DNA, was transferred to a 1.5 mL microcentrifuge tube containing 600 µL isopropanol for DNA precipitation. The supernatant was mixed with the isopropanol by inversion until thread-like strands of DNA were visible, it was then centrifuged at maximum speed for 2 minutes. The supernatant was aspirated and the gDNA pellet was washed with 600 µl 70% ethanol. The solution was centrifuged at maximum speed, for another 2 minutes, and the supernatant was once again aspirated. It is important that all the ethanol evaporates before proceeding with the extraction, the gDNA pellet was therefore air-dried at 30 ºC for approximately 20 minutes. The gDNA pellet was then rehydrated, by adding 50 µl dH_2O, and incubated at 60 ºC for 15-30 minutes. The isolated gDNA was verified with agarose gel electrophoresis (**Section 3.7**), and the concentration was determined using the NanoDrop™ 2000 (**Section 3.5**). The isolated gDNA was stored at -20 ºC.

3.3 Plasmid isolation

Plasmids are small, double-stranded molecules with typically relatively few genes (< 30) (Willey, Sherwood, & Woolverton, 2017b). They are quite easy to isolate and modify genetically and are therefore frequently used as cloning vectors in recombinant DNA technology, which was done in this work (**Section 3.10.2 and 3.11.2**).

Plasmids were isolated from *E. coli* strains, using the E.Z.N.A.® Plasmid Mini Kit I (Omega Bio-tek), in this work. The foundation of this method is the HiBind® matrix that can bind DNA reversibly under optimised conditions. Firstly, cells were harvested from 2.5 mL overnight

culture by centrifugation at 4 000 x g for 5 minutes. The supernatant was then discarded, and the cell pellet was resuspended in 250 µl Solution I (with RNase A). The dissolved pellet was transferred to a clean 1.5 mL microcentrifuge tube. The cells were further lysed by addition of 250 µl Solution II, mixed by gently inverting the tube until it was clear. Solution III (350 µl) was then added to neutralize the pH and to precipitate cellular debris. The gDNA is trapped in this precipitate, while the plasmid DNA remains in the solution. The precipitate was removed by centrifugation at maximum speed for 10 minutes. The HiBind® DNA Mini Column was equilibrated, while the tube was centrifuged, by addition of 50 µl Equilibrium Buffer. The clear supernatant (~700 µL) was transferred to the equilibrated HiBind® DNA Mini Column, which in turn was centrifuged at maximum speed for 1 minute. The filtrate was discarded, and the column was added 500 µL HCB Buffer, for binding of plasmid DNA to the matrix. The DNA was then washed with 700 µL DNA Wash Buffer (x2). The column was dried by centrifugation for 2 minutes at maximum speed. It is important that the column is completely dry, because ethanol can disturb the following eluation process. The column was transferred to a clean 1.5 mL microcentrifuge tube, and the plasmid was eluated by adding 30 µL Eluation Buffer (warmed to ~55 ºC). The tube was incubated at room temperature for 5 minutes, before it was centrifuged at maximum speed for 1 minute. The concentrations of the isolated plasmid was determined using the NanoDrop™ 2000 (**Section 3.5**), and it was stored at -20 ºC.

3.4 Precipitation of DNA

A few of the isolated plasmids had relatively low DNA concentration. Approximately 700-1000 ng isolated plasmid DNA is required for transformation of competent cells (**Section 3.11.2**), and to avoid using a large volume of isolated plasmid, the DNA was precipitated and redissolved in a smaller volume to increase the concentration. Pellet Paint® Co-Precipitant (EMD Biosciences) was used to precipitate DNA in this work. It is a fluorescent dye-labelled carrier for alcohol precipitation of both DNA and RNA (EMD Biosciences, 2003). Pellet Paint was added to the DNA sample (2 µL regardless of the sample volume), followed by 0.1 volume (10% of the sample volume) 3 M sodium acetate. The sodium acetate neutralizes the negatively charged phosphate groups of the DNA, making it less hydrophilic. Two volumes 96% ethanol was then added, and the solution was incubated at room temperature for 2 minutes. The ethanol has a lower dielectric constant than water making it easier for the Na^+ ions to interact with the phosphate groups. The precipitated DNA was then separated from the rest of the solution by centrifugation at 14 000-16 000 x g for 5 minutes. The pink DNA pellet was washed with

several volumes of 70% ethanol and centrifuged at 14 000-16 000 x g for 5 minutes. Afterwards, it was washed with 96% ethanol and once again centrifuged at 14 000-16 000 x g for 5 minutes. The pellet was air-dried at 30 ºC for approximately 20 minutes after washing to evaporate residual ethanol. Finally, it was resuspended in dH_2O and stored at -20 ºC.

3.5 Quantification of DNA

It is necessary to quantify the amount of DNA present in a sample for an array of methods, for instance overlap extension PCR (**Section 3.6.2**), restriction digestion (**Section 3.9.1**), and Sanger sequencing (**Section 3.14.1**). Various quantification methods have been developed to perform this important step (Linacero, Rueda, & Vázquez, 1998). Spectrophotometric determination is employed in this work. The ultraviolet (UV) spectroscopy method measures the UV absorbance at 260 nm. The more light absorbed by the sample at this wavelength, the higher the DNA concentration. Spectrophotometric absorbance was determined using the NanoDrop™ 2000 (Thermo Fisher Scientific). The sample (2 µl) was simply pipetted directly onto the pedestal of this instrument, and the measurement took less than 5 seconds. In addition to DNA quantity, the UV spectroscopy method also gives information concerning the purity of the sample. The 260/280 ratio and the 260/230 ratio are important indicators of the quality of the DNA sample.

3.6 The Polymerase Chain Reaction (PCR)

The polymerase chain reaction (PCR) is a method for amplification of a specific DNA sequences from a sample *in vitro*, and it has become the "golden standard" assay in microbiology since its development in 1985 (Saiki et al., 1985). A single reaction can produce millions of amplicons in only a few hours. The amplicons can then be used in further applications, such as plasmid construction (**Section 3.9**) and DNA sequencing (**Section 3.14**) (Hollister, Brooks, & Gentry, 2015). Only a few components are required in a PCR: template DNA, primers, reaction buffer, nucleotides, DNA polymerase, salt, and water (Analytical Methods Committee, AMCTB No. 59, 2014).

PCR consist of three major temperature-specific steps: (1) denaturation, (2) primer annealing and, (3) elongation. These steps encompass a single PCR cycle, and they are often repeated 25-40 times during a PCR. The number of amplicons doubles with each repetition. The first step is usually carried out at 94-95 ºC, since it relies on heat to separate the antiparallel DNA strands

in the helix into two single molecules by breaking the hydrogen bonds between the individual nucleobases on opposite strands. In the second step, usually carried out at 45-60 ºC, two different single-stranded DNA primers (~18-22 nucleotides long) anneal to the ends of the DNA target. More specifically they bind to the 3' ends of the separated antiparallel strands. The temperature at which this step is carried out is highly dependent on the composition of the primers. It should ideally be 2-4 ºC below the primers melting temperature (T_m). The T_m depends on the GC content and the length of the primer. In the final step, usually carried out at 72 ºC, DNA polymerases synthesises new DNA strands from the annealed primers in a 5' to 3' direction. The duration of this step is therefore dependent on the length of the DNA target, as well as the type of DNA polymerase used. In addition to the PCR cycles, the PCR often begins with an initial melting step at ~95 ºC and ends with a final elongation step at ~72 ºC (**Table 3.1**) (Analytical Methods Committee, AMCTB No. 59, 2014; Hollister et al., 2015).

Table 3.1 Standard thermocycling conditions for Phusion® High Fidelity PCR and Red Taq PCR.

Step	**Temperature (Phusion HF/Red Taq)**	**Time (Phusion HF/Red Taq)**	**Cycles**
Initial denaturation	98 ºC / 95 ºC	3 minutes	1x
Denaturation	98 ºC / 95 ºC	30 seconds	
Primer annealing	58 ºC[a]	30 seconds	25-35x
Elongation	72 ºC	30 seconds/kilobase / 1 minute/kilobase	
Final extension	72 ºC	10 minutes / 5 minutes	1 x
Hold	4 ºC	∞	

a. The primers used in this work were designed to have a melting temperature of ~60 ºC.

As stated earlier, several different DNA polymerases are available and they vary greatly with regards to speed, accuracy, sensitivity, and optimal temperature (Hollister et al., 2015). In this work, two different DNA polymerases were used: Red Taq DNA Polymerase (VWR International) and Phusion® High Fidelity (HF) DNA polymerase (New England Biolabs). The thermocycler conditions for these DNA polymerases are listed in **Table 3.1**. The Phusion® HF DNA Polymerase has higher fidelity and speed than the Red Taq DNA Polymerase, due to a fusion with a novel *Pyrococcus*-like proofreading polymerase. The error-rate of the Phusion® HF DNA Polymerase is approximately 50-fold lower than that of Taq DNA polymerase (Dolgova & Stukolova, 2017). Phusion® HF DNA Polymerase was therefore used when high fidelity of the PCR product was important, which includes sequencing and cloning. Red Taq DNA Polymerase, on the other hand, was used when fidelity was less important, like when

screening colonies. Red Taq DNA Polymerase comes in a ready-to-use master mix where only template DNA, primers, and dH_2O needs to be added, see **Table 3.2** for volumes and concentrations. The master mix contains Taq polymerase, dNTPs, reaction buffer with $MgCl_2$, and red dye, and the PCR product can therefore be loaded directly onto an agarose gel after the PCR (VWR, 2013). The Phusion® HF DNA Polymerase does not come in a master mix, and therefore requires the addition of dNTPs and 5x Phusion® HF buffer in addition to template DNA, primers, and dH_2O before the amplification, and addition of loading dye after, see **Table 3.3** for volumes and concentrations (New England Biolabs, 2021).

Table 3.2 Components of the Red Taq PCR reaction mixture.

Component	10 µL volume	Final concentration
Red Taq DNA Polymerase 2x Master Mix[a]	5 µL	1x
10 µM forward primer	0.2 µL	0.2 µM
10 µM reverse primer	0.2 µL	0.2 µM
DNA template	X µL	Genomic DNA: 50 ng (10-500 ng) Plasmid DNA: 0.5 ng (0.1-1 ng) Bacterial DNA: 5 ng (1-10 ng)
dH_2O	X µL	-

a. The Master Mix contains: (1) 2x Red Taq Reaction Buffer (Tris-HCl with pH 8.5, $(NH_4)_2SO_4$, 3.0 mM $MgCl_2$, and 0.2% Tween® 20), (2) 0.4 mM of each dNTP, (3) 0.2 U/µL VWR Taq polymerase, (4) Stabilizer, and (5) 2x Red dye.

Table 3.3 Components of the Phusion® High Fidelity PCR reaction mixture.

Component	50 µL volume	Final concentration
5x Phusion® High Fidelity Reaction Buffer	10 µL	1x
10 mM dNTPs	1 µL	200 µM
10 µM forward primer	2.5 µL	0.5 µM
10 µM reverse primer	2.5 µL	0.5 µM
DNA template	X µL	Genomic DNA: 50-250 ng Plasmid or viral DNA: 0.001-10 ng
Magnesium chloride solution (optional)	1 µL	1 mM[a]
Phusion® High Fidelity DNA polymerase	0.5 µL	0.1 units/50 µl PCR
dH_2O	X µL	-

a. The Reaction Buffer already contains 1.5 mM $MgCl_2$, so the addition of 1 mM gives a final concentration of 2.5 mM $MgCl_2$.

3.6.1 Colony PCR

Colony PCR is a method for rapid screening of bacterial colonies, to check for the presence of a specific DNA sequence. It is therefore important to choose a primer pair that only anneals to the targeted DNA sequence, to avoid false positives. Primers that anneal to sites flanking the insert are standard, such primers are used when screening mutants to check for uptake of the

desired plasmid in this work (**Section 3.10**). The size of the PCR product gives great information with such primers, and furthermore they can be used to screen other mutants created with the same backbone. Colony PCR does not usually require isolation of genomic DNA, which can be both time-consuming and call for large amounts of material (Cao, Fu, Guo, & Pan, 2009). Bacteria from single colonies on agar plates or from overnight cultures can instead be used directly in the PCR where they will be lysed during the initial denaturation step. The PCR products produced in the colony PCR are lastly visualised using agarose gel electrophoresis (**Section 3.7**).

Red Taq DNA Polymerase was used to screen potential transformants in this work. For *E. coli*, a toothpick touched with a colony or 2 µL overnight culture were mixed with, respectively, 10 µL or 8 µL PCR master mix, see **Table 3.2** for volumes and concentrations. Additional lysis steps were required when screening *S. aureus* cells, due to their difficulty to lyse. *S. aureus* has been found to be completely resistant to the hydrolytic activity of lysozyme, due to modification of its peptidoglycan, by an O acetylation at the C6 position of the *N*-acetyl muramic acid (MurNAc), modifications to its wall teichoic acids, and high degree of cross-linking (Bera et al., 2007). *S. aureus* cells were therefore treated with Staphylococcal lysis buffer I (**Section 2.10.2** for recipe) before setting up the PCR reaction. A colony picked with a toothpick or 3 µL overnight culture were resuspended in 20 µL lysis buffer I. The solution was then incubated at 98 ºC for 5 minutes, followed by cooling on ice for another 5 minutes. It was then diluted in 200 µL dH_2O, and 2 µL of this dilution was used in a 10 µL Red Taq PCR reaction (**Table 3.2**). However, not all *S. aureus* strains were lysed with this chemical treatment and had to be lysed mechanically with glass beads. In these cases, 2 mL overnight culture was centrifuged at maximum speed for 2 minutes. The supernatant was aspirated, and the cell pellet was resuspended in 250 µL dH_2O. The dissolved pellet was then transferred to a 2 mL Lysing Matrix tube with 0.5 g ≤ 106 µm glass beads. The cells were homogenised in the FastPrep-24™ (MP Biomedicals) for 20 seconds at 4 m/s (x3), with 30 seconds incubation between each cycle. After lysis, the tube was cooled on ice followed by centrifugation at maximum speed for 2 minutes, to allow the beads to settle. The supernatant was lastly transferred to a 1.5 mL microcentrifuge tube, and 1 µl of this solution was used in a 10 µL Red Taq PCR reaction (**Table 3.2**). A few *S. aureus* screenings did, however, not give any bands even after glass bead-beating, but all screenings were successful after purifying DNA from the lysed cells with the E.Z.N.A.® Plasmid Mini Kit I (Omega Bio-tek). See **section 3.3** for the purification protocol with this kit (the final volume with solution I and lysed cells should be 250 µL).

3.6.2 Overlap extension PCR

Overlap extension PCR (OE-PCR) is a method used to introduce mutations into a DNA sequence or to fuse different DNA fragments together (Hilgarth & Lanigan, 2020). In this work, OE-PCR was used to construct two different pMAD inserts by splicing different PCR products. Phusion® HF DNA Polymerase was used to amplify DNA fragments in OE-PCR and to fuse them. The components of the PCR reaction mixture are presented in **Table 3.3**. It is important to design primers that only anneals one place in the template and that have a 5' overhang which is complementary to the 3' end of the fragment it is going to be spliced with, when performing OE-PCR (Zarghampoor et al., 2020).

3.6.2.1 Construction of the pMAD-*gfp_ugtP*::*spc* insert

pMAD-*gfp_ugtP*::*spc* was constructed to allow integration of *gfp-ugtP* into the chromosome of *S. aureus*. The OE-PCR steps performed to construct this plasmid insert, including the fragments and primers used, are illustrated in **Figure 3.1**. The first step of the OE-PCR was to amplify the four DNA fragments that the pMAD-*gfp_ugtP*::*spc* construct consist of: (1) the DNA sequence upstream of the target gene (ori_up), (2) the *ugtP*-promotor (P_{ugtP}), (3) the *ugtP* sequence marked with green fluorescent protein (gfp_ugtP), and (4) a spectinomycin resistance cassette spliced with the DNA sequence downstream of the target gene (spc+ori_down) (**Figure 3.1A**). Both ori_up and P_{ugtP} were amplified using genomic MDB1 DNA as template, while purified pLOW-*gfp_ugtP* and pMAD-ori-*parS* were used as template DNA for amplification of gfp_ugtP and spc+ori_down, respectively. ori_up was amplified using the MDB3 and MDB4 primers (see **Table A2.1** for all primers). MDB3 introduces an EcoRI restriction site upstream of ori_up. P_{ugtP} was amplified using MDB5 and MDB6, both of these primers introduce overhangs. MDB5 introduces an overhang to ori_up, while MDB6 introduces an overhang to gfp_ugtP. gfp_ugtP was amplified using MK48 and MDB7. MDB7 introduces an overhang which is complementary to spc. spc+ori_down was amplified using MK188 and MDB8. MDB8 introduces a SalI restriction site to the end of the fragment. MDB3 and MDB8 introduce restriction sites to the ends of the construct that were utilised in the cloning of the fragment (**Section 3.9**). All PCR products were separated using gel electrophoresis and purified using NucleoSpin® Gel and PCR Clean-up (**Section 3.7**).

The second step of the OE-PCR was to fuse ori_up together with P_{ugtP}, and gfp_ugtP together with spc+ori_down, separately (**Figure 3.1B**). The fragments were combined in approximately equimolar amounts (molar ratio of ~1:1), with ~50 ng used of the largest PCR fragment. The overlapping complementary sequences that were introduced in the first PCR allow for hybridisation of the two fragments under optimal conditions. The two primers used in the second OE-PCR reactions flank the outer parts of the desired PCR product as in a normal PCR (MDB3 and MDB6 for splicing ori_up and P_{ugtP}, and MK48 and MDB8 for splicing gfp_ugtP and spc+ori_down). The PCR products produced in the second PCR step were also separated and purified from an agarose gel (**Section 3.7**) to remove non-specific side products.

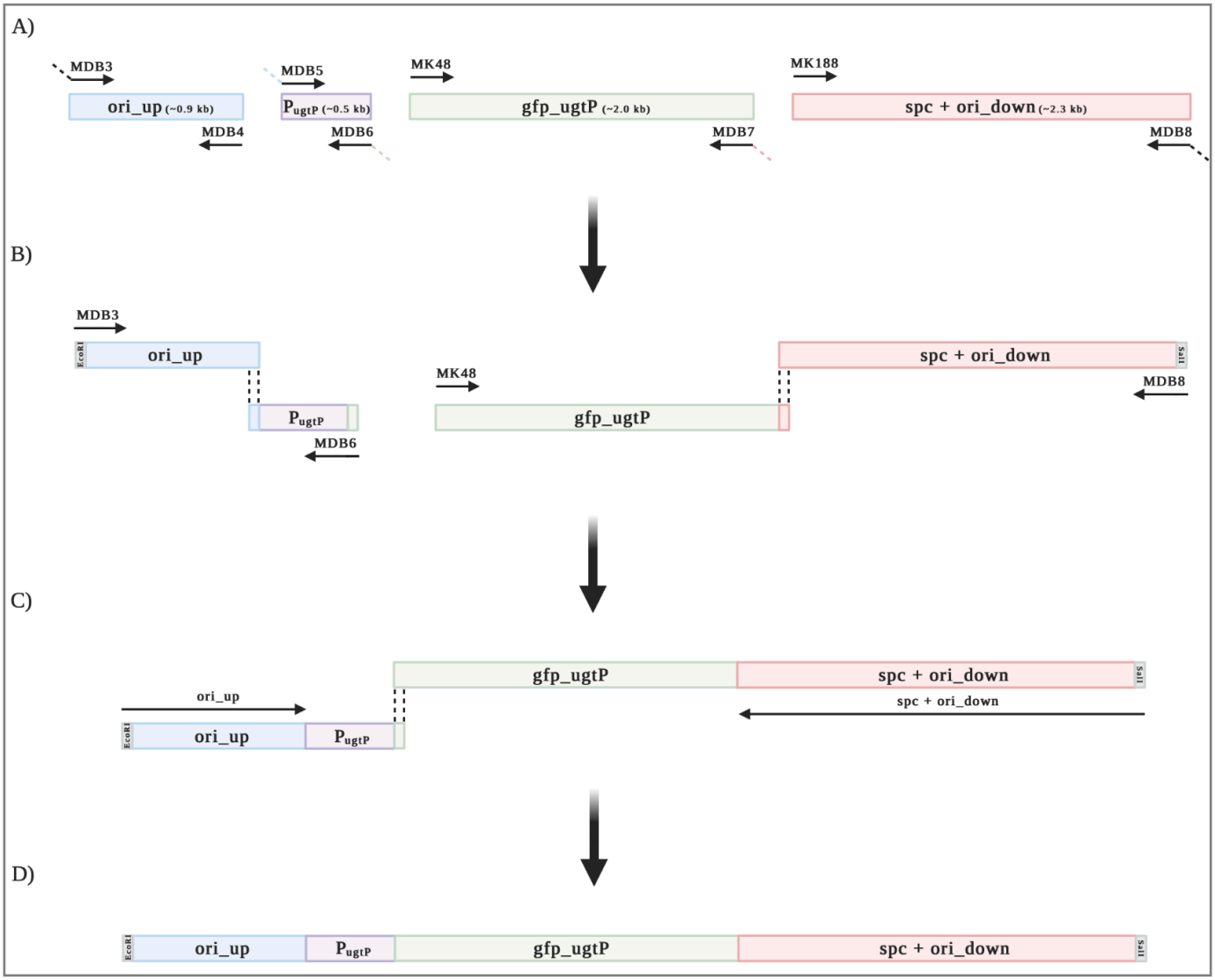

Figure 3.1 Schematic representation of the steps performed to construct the pMAD-*gfp_ugtP*::*spc* insert using overlap extension (OE) PCR. The differently coloured boxes represent DNA sequences, while the arrows represent primers pointing in in a 5' to 3' direction. Primers with overhang are illustrated with dotted lines. The colour of the dotted lines corresponds to their complementary sequence (the primers with black dotted lines introduce restriction sites). (**A**) The first step of the OE-PCR consisted of individual amplifications of the four DNA fragments that were to be spliced (ori_up, P_{ugtP}, gfp_ugtP, and spc+ori_down). (**B**) The second step of the OE-PCR consisted of two separate PCR reactions: (1) ori_up was fused together with P_{ugtP}, and (2) gfp_ugtP was fused together with spc+ori_down. (**C**) The Last step of the OE-PCR consisted of splicing the two PCR-products from the second OE-PCR step (ori_up+P_{ugtP} and gfp_ugtP+spc+ori_down) together giving the final pMAD-*gfp_ugtP*::*spc* insert (**D**). Created with BioRender.com.

ori_up+P_{ugtP} was fused together with gfp_ugtP+spc+ori_down in final OE-PCR step (**Figure 3.1C**). The PCR master mix was prepared as described earlier (**Table 3.3**), except without the addition of primers. The PCR reaction was run with the annealing temperature of the homologue region for 10 PCR cycles without primers. After these 10 PCR cycles, 4 µl of both the ori_up and the spc+ori_down PCR products were added, followed by another 30 cycles with the annealing temperature of the "primers" (for a total of 40 cycles). The final PCR product was separated and purified from an agarose gel (**Section 3.7**).

3.6.2.2 Construction of the pMAD-Δ*ugtP*::*spc* insert

pMAD-Δ*ugtP*::*spc* was constructed to allow deletion of *ugtP* from the chromosome of *S. aureus*. The first step of the OE-PCR was to amplify the three DNA fragments that the pMAD-Δ*ugtP*::*spc* construct consist of: (1) the DNA sequence directly upstream of *ugtP* (ugtP_up), (2) a spectinomycin resistance cassette (spc), and (3) the DNA sequence directly downstream of *ugtP* (ugtP_down) (**Figure 3.2A**). gDNA from the MDB1 strain was the template DNA for amplification of both ugtP_up and ugtP_down, while purified pCN55 was the template for spc. ugtP_up was amplified using the MK501 and MK502 primers (see **Table A2.1** for all primers), MK502 introduces an overhang to spc. spc was amplified using MK503 and MK504. Lastly, ugtP_down was amplified using MK505 and MK506. MK505 introduces an overhang to spc while MK506 introduces a BamHI restriction site to the end of the fragment. No restriction site is introduced upstream of ugtP_up with MK501, because the ugtP_up PCR product naturally have a NcoI restriction site near its 5' end (marked in **Figure 3.2**). All PCR products were separated using gel electrophoresis and purified using NucleoSpin® Gel and PCR Clean-up as described in **Section 3.7**.

ugtP_up and spc were fused together in the second OE-PCR step, with MK501 and MK504 (**Figure 3.2B**). Both fragments were combined in approximately equimolar amounts, with ~50 ng of the largest PCR fragment. These PCR products were separated and purified from an agarose gel (**Section 3.7**). In the last step, **Figure 3.2C**, ugtP_up+spc was combined with ugtP_down in a PCR reaction mix without primers (**Table 3.3**). The PCR reaction mixture was run with the annealing temperature of the homologue region for 20 PCR cycles (without primers). After these 20 PCR cycles, MK501 and MK506 were added, followed by another 30 cycles with the annealing temperature of the primers (for a total of 50 cycles). The final PCR product was also separated and purified from an agarose gel (**Section 3.7**).

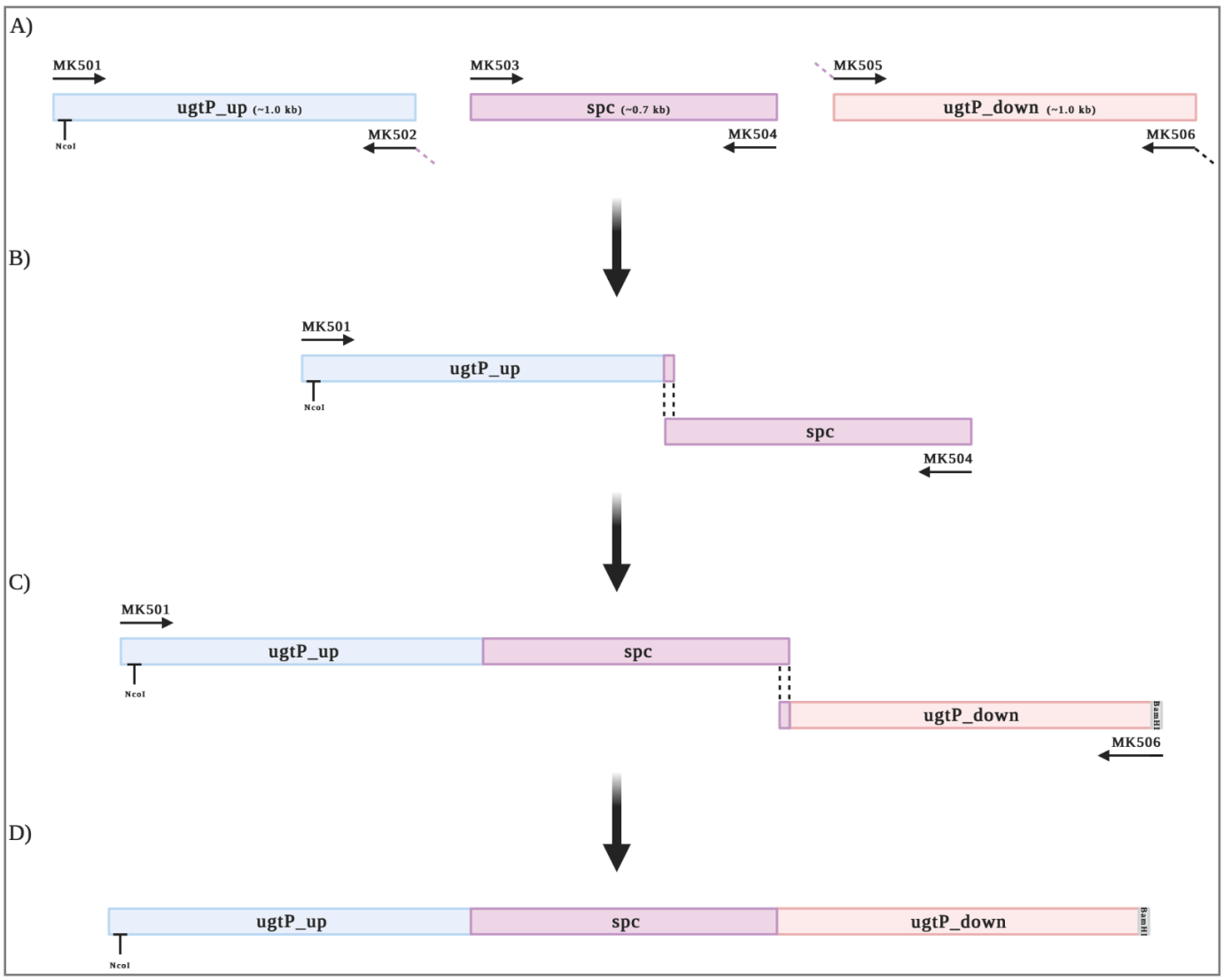

Figure 3.2 Schematic representation of the steps performed to construct the pMAD-Δ*ugtP*::*spc* insert using overlap extension (OE) PCR. The differently coloured boxes represent DNA sequences, while the arrows represent primers pointing in in a 5' to 3' direction. Primers with overhang are illustrated with dotted lines. The colour of the dotted lines corresponds to their complementary sequence (the primers with black dotted lines introduce restriction sites). (**A**) The first step of the OE-PCR consisted of individual amplifications of the three DNA fragments that were to be spliced (ugtP_up, spc, and ugtP_down). (**B**) The second step of the OE-PCR consisted of fusing ugtP_up together with spc. (**C**) The Last step of the OE-PCR consisted of splicing the PCR-products from the second OE-PCR step (ugtP_up+spc) together with ugtP_down giving the final pMAD-Δ*ugtP*::*spc* insert (**D**). Created with BioRender.com.

3.7 Agarose gel electrophoresis

Agarose gel electrophoresis is a simple method for separation, identification, and purification of DNA fragments (from 100 bp to 25 kb). Linear DNA molecules in a sample are separated from each other according to size, when placed in an electric field, through the porous agarose gel matrix. DNA is separated when subjected to an electrical field because it is negatively charged, and therefore migrates through the gel toward the positive pole (anode) when loaded at the negative pole (cathode). The distance each DNA molecule travels inversely relates to their size (molecular weight); large molecules have more difficulty passing through the porous

gel and thus migrate slower than smaller DNA molecules. However, DNA is not only separated based on size, as shape and topological properties also can play a role in the separation. A circular DNA molecule, for instance, travels slower than an equally sized linear molecule, while supercoiled DNA molecules migrates faster. The DNA molecules are visualised after the electrophoresis is completed by adding a fluorescent dye to the agarose gel before casting. PeqGREEN was used in this work, it fluoresces under UV-light when bound to DNA (both single and double stranded) (Lee, Costumbrado, Hsu, & Kim, 2012; Watson et al., 2013).

The rate of migration is determined by several factors, with one of them being the concentration of agarose in the gel. Gels with 1% agarose was used in this work, see **Section 2.10.3** for the recipe. The agarose gel was placed in the electrophoresis chamber with TAE buffer after solidification, and the well combs were removed. Loading buffer has to be added to the samples before they are loaded into the wells, because it allows them to sink (glycerol makes the samples denser than the running buffer) and allows for tracking of their migration (bromophenol blue provides colour to the samples). The Red Taq Master Mix contains a 2x red loading dye and PCR products amplified with Red Taq PCR could therefore be loaded directly into the gel after amplification. PCR products amplified by the Phusion® HF DNA Polymerase, on the other hand, had to be mixed with a loading buffer before electrophoresis. A 6x gel loading buffer was used in this work, it was mixed with the samples to a final concentration of 1x. A 1 kb DNA ladder, with DNA fragments ranging from 0.5 kb to 10 kb, was also loaded into the gel (5 µL). This ladder allows for determination of the approximate size of the DNA molecules in the samples and their approximate mass. The gel electrophoresis was run with a voltage of 90 for 20-40 minutes in the Mini-Sub Cell GT Cell (Bio-Rad Laboratories). The gel was visualised after the electrophoresis was completed in the Gel Doc™ XR+ Imager (Bio-Rad Laboratories) by exposure to UV light.

3.7.1 Extraction of DNA from agarose gels

The NucleoSpin® Gel and PCR Clean-up kit (Macherey-Nagel) was used to purify DNA fragments from the agarose gels after separation with gel electrophoresis. The purified DNA can be directly used in further applications, such as PCR (**Section 3.6**), restriction digestion (**Section 3.9.1**), and sequencing (**Section 3.14**).

The band containing the desired DNA fragment was cut from the gel with a scalpel and dissolved in NTI buffer (200 µL NTI buffer per 100 mg agarose gel) at 55 ºC. The gel should

be exposed to as little UV light as possible, since prolonged exposure can damage the DNA. The sample was loaded onto a NucleoSpin® Gel and PCR Clean-up Column placed in a 2 mL Collection Tube, when the gel was completely dissolved, followed by centrifugation of the tube at 11 000 x g for 30 seconds. The NTI buffer ensures optimal conditions for binding of DNA to the silica membrane of the column. The flow-through was discarded and the silica membrane was washed with 700 µL ethanolic NT3 buffer for 30 seconds at 11 000 x g (x2). After washing, the silica membrane was dried by centrifugation at 11 000 x g for 1 minute, to remove residual ethanol from the NT3 buffer that can inhibit later enzymatic reactions. The NucleoSpin® Gel and PCR Clean-up Column was then placed in a clean 1.5 mL microcentrifuge tube. NE buffer (15-40 µL) warmed to ~55 ºC was applied to the silica membrane, and the tube was incubated at room temperature for 5 minutes. The slightly alkaline NE buffer (pH 8.5) solubilises and releases the DNA from the column. The DNA was lastly eluated by centrifugation at 11 000 x g for 1 minute. The concentrations of the eluated DNA was determined using the NanoDrop™ 2000 (**Section 3.5**), and it was stored at -20 ºC.

3.8 SDS-PAGE and immunoblotting

Proteins can be separated and visualised on the basis of mass and charge by migration in an electric field similarly to DNA. Electrophoresis of proteins are usually carried out in polyacrylamide gels. Polyacrylamide have smaller pore size than agarose and is therefore suitable for the separation of the majority of proteins and smaller DNA molecules. The mobility of proteins through these pores depends on both mass and shape. Higher mass tends to decrease mobility, while higher compactness tends to increase it. Proteins are therefore often denatured before electrophoresis to eliminate the effect shape has on mobility. Sodium dodecyl sulphate (SDS) was used to denature proteins in this work. A protein binds 1.4 times its weight of SDS, which equal almost one SDS molecule per amino acid monomer. SDS is a negatively charged detergent and therefore renders the intrinsic charge of the protein insignificant when bound to it in addition to unfolding the protein. Carrying out SDS-PAGE thus separates proteins almost completely on the basis of molecular weight (Lesk, 2016; Nelson & Cox, 2017a).

The results of the SDS-PAGEs were visualised by immunoblotting, a method used to identify the presence of a target antigen in a sample with a mixture of many different antigens. The separated proteins are firstly transferred onto an immobilising membrane, either a nitrocellulose or polyvinylidene fluoride (PVDF) membrane, using an electric field oriented perpendicular to

the gel surface. The negatively charged proteins travels from the gel to the membrane placed closer the anode. The membrane has to be blocked after blotting to prevent nonspecific binding of the antibodies to the surface of the membrane. After blocking, the membrane is incubated with antibodies specific to the protein of interest. The protein is typically probed with a combination of antibodies: (1) an antibody that recognises and binds the protein of interest (primary antibody), and (2) an antibody that binds the primary antibody (secondary antibody). The secondary antibody is normally conjugated with a signal molecule which allows for detection of the antigen. Unbound antibodies are washed away leaving only the bound antibodies which can be detected using the appropriate substrate. In this work the SuperSignal™ West Pico PLUS Chemiluminescent Substrate (Thermo Fisher Scientific) that detects horseradish peroxidase (HRP) using a CCD imager was employed (Mahmood & Yang, 2012; H.-W. Yu, Halonen, & Pepper, 2015).

3.8.1 Lipoteichoic acid detection with anti-LTA antibodies

The degree of polymerisation of LTA from different *S. aureus* strains was compared based on their migration in an SDS-polyacrylamide gel electrophoresis (PAGE) visualised by immunoblotting, in this work.

3.8.1.1 Sample preparation

The *S. aureus* strains to be analysed were firstly grown overnight at 37 ºC in 5 mL TSB medium containing the appropriate antibiotics. The following day, they were diluted 1:1000 in 5 mL TSB medium containing the appropriate antibiotics and inducers of protein expression. The bacterial dilutions were incubated at 37 ºC until they reached an OD_{600} between 0.6 and 0.8, with the exception of MDB45 which was only grown to an OD_{600} = 0.28 due to a slow growth rate and a high degree of cell lysis. The bacterial cultures were cooled on ice when they reached the desired OD_{600} to stop growth. When cooled, the cultures were normalised to an OD_{600} = 0.6 with the following formula: Bacterial culture ($\frac{0.6 * 500\ \mu L}{\text{Measured OD}}$ = x) + TSB (500 µL – x). The normalised cultures were harvested by centrifugation at 7 500 rpm for 3 minutes at 4 ºC. The pellets were resuspended in 50 µL Staphylococcal lysis buffer II (**Section 2.10.4.1**) and incubated at 37 ºC for 10 minutes for chemical lysis. The suspensions were then added 50 µL 4x SDS loading buffer and boiled at 95 ºC for 30 minutes. The cell lysates were then centrifuged at 16 000 x g for 10 minutes to pellet cellular debris. The supernatants (60 µL) were transferred

to clean 1.5 mL microcentrifuge tubes containing 60 µL dH_2O. The diluted suspensions were lastly added 0.5 µL proteinase K (20 mg/mL) and incubated at 50 ºC for 2 hours.

3.8.1.2 SDS-PAGE

4–20% Mini-PROTEAN® TGX™ Precast Protein Gels were used for separation of LTA in this work. One of these gradient gels was placed in the electrophoresis chamber with running buffer I (**Section 2.10.4.1**). The comb was removed, and the wells were rinsed with running buffer before the samples, containing the extracted LTAs, (20 µL) were loaded into the wells in the polyacrylamide gel. MagicMark™ XP Western Protein Standard, with nine recombinant proteins ranging from 20 kDa to 220 kDA, was also loaded into the gel (5 µL). Each protein in the standard contains an immunoglobulin G (IgG) binding site which binds the secondary antibody, allowing for visualisation of the ladder together with the LTAs. The gel was run at 200 V, in the Mini-PROTEAN Tetra Cell (Bio-Rad Laboratories), for ~3 minutes after the front of the blue stained samples had migrated out of the gel.

3.8.1.3 Immunoblotting

The LTAs in the polyacrylamide gel were subsequently transferred to a PVDF membrane. First, the membrane was activated in methanol for 1 minute. The membrane was then washed with dH_20 (x3), before being soaked in cold (~4 ºC) transfer buffer I (**Section 2.10.4.1**) together with the gel and two filter papers. They were then stacked on the anode plate of the Trans-Blot Turbo System (Bio-Rad Laboratories): a filter paper first followed by the membrane, the gel and lastly the second filter paper. The blotting was performed at 25 V (and 2.5 A) for 7 minutes. The membrane was then blocked in 5% skimmed milk (**Section 2.10.4.1**) for one hour at room temperature on a mixing table, followed by blocking at 4 ºC overnight.

The blocking solution was poured off the next day, and the membrane was washed with PBST twice. The membrane was then incubated for one hour with the anti-LTA primary antibody (diluted 1:4000 in PBST) at room temperature on a mixing table. All the following incubation steps were performed on a mixing table at room temperature. Three PBST washing steps were performed to remove unbound antibodies. The membrane was incubated for 10 minutes between each washing step. The membrane was the incubated for another hour with the anti-Mouse secondary antibody (diluted 1:5000 in PBST). The secondary antibody binds both the primary antibody and the protein standard, and it is conjugated with horseradish peroxidase

(HRP) which produces light when treated with the chemiluminescent substrate. After incubation, unbound antibodies were removed by washing the membrane 3 times in PBST for 10 minutes. Detection was performed using the SuperSignal™ West Pico PLUS Chemiluminescent Substrate kit. Equal parts of Stable Peroxide Solution and Luminol/Enhancer Solution were mixed (2.5 mL of each), and the membrane was incubated in this solution for ~5 minutes. Images of the membrane were captured using the Azure Imager c400 (Azure Biosystems), with an exposure ranging from 20 seconds to 30 minutes.

3.8.2 Detection of the relative expression of CozEa and CozEb with anti-GFP antibodies

Immunoblotting can both indicate the presence, size, and relative quantity of the target protein. The gene for green fluorescent protein was fused to the 3' end of gene for CozEa and the gene for CozEb in the NCTC8325-4 *S. aureus* strain, for comparison of the relative expression of the two CozE proteins in this strain. The proteins of these mutants were separated with SDS-PAGE, followed by visualisation with immunoblotting using an anti-GFP antibody.

3.8.2.1 Sample preparation

The bacterial strains with the *cozE-gfp* fusions, MK1582 and MK1584, were first grown overnight at 37 ºC in 5 mL TSB medium with 100 µg/ml spectinomycin. The overnight cultures were diluted 1:100 in 10 mL TSB medium with spectinomycin (100 µg/ml) the following day. The diluted bacterial cultures were incubated at 37 ºC until they reached an OD_{600} = ~0.4, followed by cooling on ice to stop the bacterial growth. When cooled, the cultures were normalised to an OD_{600} = 0.4 with the following formula: Bacterial culture ($\frac{0.4 * 500\ \mu L}{\text{Measured OD}} = x$) + TSB (500 µL – x). The normalised cultures were harvested by centrifugation at 4 000 x g for 1 minute at 4 ºC, and the pellets were resuspended in 500 µL TBS buffer. The bacterial cells were lysed mechanically in the FastPrep-24™ (MP Biomedicals). The suspensions were transferred to 2 mL Lysing Matrix tubes with 0.5 g ≤ 106 µm glass beads before being homogenised for 20 seconds at a speed of 6 m/s (x3), with 1 minute incubation on ice between each cycle. After lysis, the tubes were cooled on ice followed by centrifugation at maximum speed for 2 minutes, to allow the beads to settle. The supernatants were mixed with equal volume 2x SDS loading buffer (1:1) (**Section 2.10.4.2**), followed by heating at 95 ºC for 5 minutes.

3.8.2.2 SDS-PAGE

The proteins in the two cell lysates were separated using SDS-PAGE. The polyacrylamide gel used in this work consisted of a 12% separation gel with at 4% stacking gel on top, see **Section 2.10.4.2** for the recipe. The gel was placed in the electrophoresis chamber with running buffer II (**Section 2.10.4.2**) after solidification. The comb was removed, and the wells were rinsed with running buffer before the lysed mixtures (10 µL) were loaded into two different wells in the polyacrylamide gel. MagicMark™ XP Western Protein Standard and Color Prestained Protein Standard were also loaded into the gel (5 µL of each). The gel was run at 90 V, in the Mini-PROTEAN Tetra Cell (Bio-Rad Laboratories), until the front of the blue stained samples aligned in the separation gel. The gel was thereafter run at 200 V until the front of the blue stained samples had migrated out of the gel.

3.8.2.3 Immunoblotting

The separated proteins in the polyacrylamide gel were transferred to a PVDF membrane and visualised using immunoblotting, as described in **Section 3.8.1.3**, with the following exceptions: (1) transfer buffer II was employed instead of transfer buffer I (**Section 2.10.4.2**), (2) the anti-GFP primary antibody (diluted 1:4000 in PBST) was used instead of the anti-LTA primary antibody (diluted 1:4000 in PBST), (3) the anti-Rabbit secondary antibody (diluted 1:5000 in PBST) was used instead of the anti-Mouse secondary antibody (diluted 1:5000 in PBST), and (4) 4 washing steps were performed after incubation with the secondary antibody instead of 3.

3.9 Plasmid construction

DNA cloning is dependent on the ability to construct recombinant DNA molecules that can be taken up and maintained in the host cells. These molecules consist of genetic elements (often genes) inserted into cloning vectors for propagation. Cloning vectors typically share three important characteristics: (1) An origin of replication (*ori*) that allows for replication independently of the host chromosome, (2) A selectable marker that allows for identification of the transformants (e.g., antibiotic resistance genes), and (3) Unique restriction sites that allows for specific insertion of the DNA fragment into the vector. Plasmids are the most frequently used cloning vector, they are often designed with many different restriction sites clustered in a region appointed the multicloning site (MCS). All plasmids used in this work are shuttle vectors. Shuttle vectors have two origins of replication which are recognised by different host

organisms, in this work *E. coli* and *S. aureus*, facilitating transfer ("shuttle") from one host to another. This allow for manipulation of the plasmid in *E. coli* cells before being transformed into the *S. aureus* strain of interest (Watson et al., 2013; Willey, Sherwood, & Woolverton, 2017d). Six different plasmids were constructed in this work: (1) pCG248-sgRNA(*cozEb*+*ugtP*-*ltaA*), (2) pCG248-sgRNA(*cozEb*+*ltaS*), (3) pCG248-sgRNA(*cozEb*+*dltA*), (4) pLOW-*gfp_ugtP*, (5) pMAD-*gfp_ugtP*::*spc*, and (6) pMAD-Δ*ugtP*::*spc*.

3.9.1 Restriction digestion and ligation

Inserting a DNA fragment into a plasmid is a relatively simple process, if the DNA fragment is flanked on both sides with the appropriate restriction sites. Firstly, the DNA fragment to be inserted into the plasmid (insert) and the plasmid (backbone) are cut with compatible restriction enzymes in two individual reactions (**Figure 3.3**). Restriction enzymes are naturally occurring endonucleases that cleave double stranded DNA at particular sites by recognising specific sequences, generating either blunt or sticky ends. Restriction enzymes used in restriction digestion usually recognize short palindromic target sequences (4-8 bp) and cut at a defined position within this sequence leaving behind sticky ends. Some restriction enzymes generate identical stick ends, for instance BamHI and BglII used to construct the double sgRNA plasmids. They recognise different sequences (BamHI; 5'-GGATCC-3', and BglII; 5'-AGATCT), but generate the same overhang (5'-GATC-3'). It is important that the insert and backbone are treated with restriction enzymes that generates compatible sticky ends and only cut one place in the insert/backbone (Watson et al., 2013; Willey et al., 2017d).

The insert and backbone to be digested were mixed with their respective 10x restriction buffer, two different restriction enzymes, and dH_2O. The components in the different restriction digestions, in this work, are presented in **Table 3.5**, and the final concentration/volumes of these components are presented in **Table 3.4**. The restriction digestion reaction mixture was incubated at optimal temperature for 1-2 hours. In this work, all restriction digestions were carried out at 37 ºC in a thermal cycler. For restriction digestion of the pMAD-I-SceI 1 µL CIP (Alkaline Phosphatase, Calf Intestinal) was added to the reaction after 80 minutes of incubation, with 40 minutes remaining. CIP non-specifically catalyses the dephosphorylation of the 5' and 3' ends of DNA phosphomonoesters to prevent re-ligation of the cut plasmids. After incubation, the digested DNA was either: (1) separated using gel electrophoresis and purified using NucleoSpin® Gel and PCR Clean-up (**Section 3.7.1**), or (2) verified using agarose gel

Table 3.4 Components of the restriction digestion reaction mixture.

Component	50 µL volume	Final concentration
DNA	X µL	1 µg
10x restriction buffer[a]	5 µL	1x
Restriction enzyme 1	1 µL	Genomic DNA: 10-20 units Plasmid or viral DNA: 5-10 units
Restriction enzyme 2	1 µL	Genomic DNA: 10-20 units Plasmid or viral DNA: 5-10 units
Alkaline Phosphatase, Calf Intestinal (CIP)[b]	1 µL	10 unit
dH2O	X µL	-

a. 10x NEBuffer™ 3.1 (containing 1000 mM NaCl, 500 mM Tris-HCl, 100 mM $MgCl_2$, and 1000 µg/ml BSA) or 10x CutSmart® Buffer (containing 500 mM CH_3CO_2K, 200 mM Tris-acetate, 100 mM $C_4H_6MgO_4$, and 1000 µg/ml BSA) were used in this work.
b. Only added when digesting the pMAD-I-SceI vector.

Table 3.5 Overview of the components (backbone, insert, restriction enzymes, and restriction buffer) used to construct the six plasmids in this work.

Complete plasmid	Backbone	Insert	Restriction enzymes	Restriction buffer
pCG248-sgRNA(*cozEb*+*ugtP*-*ltaA*)	pCG248-sgRNA(*cozEb*)	pVL2336-sgRNA(*ugtP*-*ltaA*)	BglII and PstI (backbone), and BamHI and PstI (insert)	10x NEBuffer™ 3.1
pCG248-sgRNA(*cozEb*+*ltaS*)	pCG248-sgRNA(*cozEb*)	pVL2336-sgRNA(*ltaS*)	BglII and PstI (backbone), and BamHI and PstI (insert)	10x NEBuffer™ 3.1
pCG248-sgRNA(*cozEb*+*dltA*)	pCG248-sgRNA(*cozEb*)	pVL2336-sgRNA(*dltA*)	BglII and PstI (backbone), and BamHI and PstI (insert)	10x NEBuffer™ 3.1
pLOW-*gfp_ugtP*	pLOW-m(sf)*gfp*-SA1477	The PCR-product from Phusion® HF PCR with SH1000 gDNA and the MDB9 and MDB2 primers	BamHI and EcoRI (backbone), and BamHI-HF and EcoRI-HF (insert)	10x NEBuffer™ 3.1 (backbone), and 10x CutSmart® Buffer (insert)
pMAD-*gfp_ugtP*::*spc*	pMAD-I-SceI	See **section 3.6.2.1**	EcoRI-HF and SalI-HF	10x CutSmart® Buffer
pMAD-Δ*ugtP*::*spc*	pMAD-I-SceI	See **section 3.6.2.2**	NcoI-HF and BamHI-HF	10x CutSmart® Buffer

electrophoresis (3 µL sample + 1 µL 6x Gel LD) and purified directly from the digestion reaction using NucleoSpin® Gel and PCR Clean-up. In direct purification 1 volume of sample was mixed with 2 volumes of NTI Buffer, but the subsequent steps were identical to the gel purification protocol (**Section 3.7.1**). Only the pLOW-*gfp_ugtP*, pMAD-*gfp_ugtP*::*spc* and pMAD-Δ*ugtP*::*spc* inserts were purified directly, since they only generated small unwanted DNA fragments that could easily be removed with the NucleoSpin® Gel and PCR Clean-up kit.

The purified digested inserts and plasmids were mixed with ligase buffer, dH_2O, and ligase (**Table 3.6**). The insert and backbone were mixed with a molar ratio of 1:3 backbone to insert. The digested plasmids are mixed with an excess of inserts to ensure that a majority of the plasmids are resealed with the incorporation of the insert. The ligation mixtures were incubated at 16 ºC overnight in a thermal cycler or water bath. The sticky ends of the digested inserts and plasmids hybridises under these conditions and are joined by DNA ligase that generates hydrogen bonds and phosphodiester bonds between the compatible sticky ends. The restriction enzymes were heat inactivated the next day at 65 ºC for 10 minutes to increase the transformation efficiency. The ligated plasmids were then either stored at -20 ºC or chilled on ice before being transformed into the desired host, being competent IM08B *E. coli* cells in this work (**Section 3.10.2**).

Table 3.6 Components of the ligation reaction mixture.

Component	20 µL volume	Final concentration
10x T4 Ligase Buffer[a]	2 µL	1x
Vector DNA	X µL	0.020 pmol
Insert DNA	X µL	0.060 pmol
dH_2O	X µL	-
T4 DNA Ligase	1 µL	400 units

a. The 10x T4 Ligase Buffer contains: (1) 500 mM Tris-HCl, (2) 100 mM $MgCl_2$, (3) 10 mM ATP, and (4) 100 mM DTT.

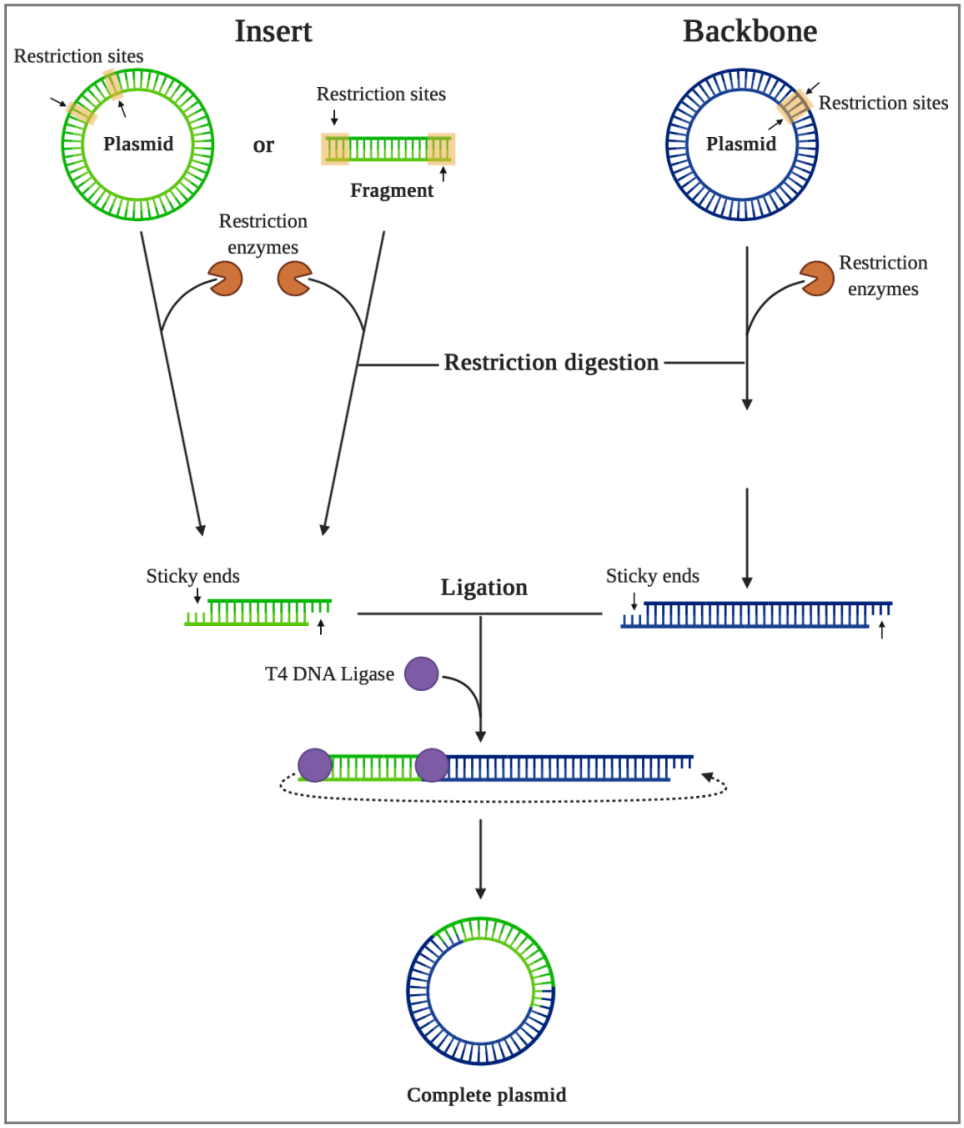

Figure 3.3 Schematic representation of the steps performed to construct plasmids with restriction digestion and ligation. The insert and backbone were firstly cut with restriction enzymes that generates compatible sticky ends. After digestion, the insert and backbone were purified followed by ligation. The T4 DNA Ligase produce the complete ligated plasmid by joining the compatible sticky ends from the insert and backbone together. Created with BioRender.com.

3.10 Transformation of *E. coli*

All plasmids constructed in this work were transformed into competent IM08B *E. coli* cells for propagation. I addition, all plasmids isolated in this work were propagated in IM08B, except for pCN55. The IM08B strain mimic the type I adenine methylation profiles of *S. aureus* strains, enabling high efficiency transformation of plasmids isolated from IM08B into *S. aureus* cells. Plasmids lacking the specific methylation profile of the host are recognised as foreign and subsequently degraded (Monk et al., 2015). The following *E. coli* mutants were constructed in this work: MDB22, MDB23, MDB24, MDB53, MDB72, and MDB73 (**Table A1.1**).

3.10.1 Preparation of competent *E. coli* cells using calcium chloride treatment

Bacteria that naturally can take up DNA from the environment are said to have genetic competence. *E. coli*, however, cannot and therefore have to be rendered competent for DNA uptake by calcium chloride treatment. The exact mechanism of how Ca^{2+} ions enable DNA uptake is not known, though Ca^{2+} ions most likely shield the negative charge of the DNA, allowing it to penetrate the membrane (Watson et al., 2013). In addition, Ca^{2+} ions have been demonstrated to increase the permeability of the membrane by disrupting it (Liu, Liu, & Shergill, 2006).

The IM08B cells to be rendered competent were first grown overnight in 5 mL LB medium at 37 ºC. The overnight culture was diluted 1:1000 in new LB medium to a final volume of 100 mL in an Erlenmeyer flask the next day. The diluted bacterial culture was then incubated at 37 ºC until it reached an OD_{600} = ~0.4, followed by cooling on ice. All subsequent steps were carried out at 4 ºC or on ice. After ~20 minutes, the cells were harvested by centrifugation at 6000 rpm for 5 minutes in two nunc 50 mL centrifuge tubes. The supernatants were discarded, and the pellets were resuspended in 0.5 volume cold 0.1 M calcium chloride. The resuspended cells were incubated on ice for 2 hours, followed by centrifugation at 4000 rpm for 5 minutes. The final pellet was resuspended in ~5 mL cold 15% glycerol with 0.1 M calcium chloride, and aliquoted in 1.5 mL microcentrifuge tubes stored at -80 ºC.

3.10.2 Heath shock transformation

Recombinant plasmids are introduced into *E. coli* cells by chemical transformation. The chemically competent *E. coli* IM08B cells are transformed by heat shocking the cells in a solution containing the plasmid. Transformation is a relative ineffective process, considering only a small fraction of the competent cells take up the plasmid. It is therefore necessary to use a selection with antibiotic, in this work ampicillin, that only allows for growth of the cells transformed with the plasmid. Unfortunately, ligation is never 100% efficient, so one must distinguish between colonies that carries plasmids with the insert from those who carries plasmids without the desired insert. This distinction is achieved by choosing primers flanking the insert when PCR screening the colonies and by sequencing the plasmids (Watson et al., 2013).

Firstly, the competent IM08B cells were thawed on ice. The competent cells (50 µL) were then mixed with 2-10 µL ligation mix (or isolated plasmid), depending on the concentration. This

mixture was incubated on ice for 30 minutes, before being heat shocked at 37 ºC for 5 minutes. After 5 minutes, the mixture was put on ice and immediately added 250 µL SOC medium. The bacterial cultures were then incubated at 37 ºC for 1 hour. Following incubation, the solution was plated on LB agar plates with 100 µg/mL ampicillin. The transformants were verified by colony PCR (**Section 3.6.1**) the following day, and by sequencing the plasmid insert (**Section 3.14.1**).

3.11 Construction of *S. aureus* mutants

The *S. aureus* mutants in this work were constructed by transforming plasmids isolated form IM08B *E. coli* cells into different *S. aureus* strains. Studying the phenotype of these *S. aureus* mutants is fundamental for understanding the function of different genes. Identifying the cellular processes the mutation effect provides a window into the biological role of the gene (Alberts et al., 2002). The 50 *S. aureus* mutants constructed in this work are listed in **Table A1.1**.

3.11.1 Preparation of competent *S. aureus* cells

S. aureus is not naturally competent and therefore have to be rendered competent for DNA uptake by electroporation. Electrocompetent cells are prepared by removing salt and charged chemicals that can interfere with the applied electrical current leading to cell lysis. The *S. aureus* cells to be rendered competent were firstly grown overnight in 5 mL BHI medium with the respective antibiotics at 37 ºC. The overnight culture was diluted 1:100-1:1000 in new BHI medium with antibiotics to a final volume of 100 mL in an Erlenmeyer flask, and incubated at 37 ºC until it reached an OD_{600} between 0.4 and 0.6. The bacterial culture was then cooled on ice for 10 minutes. All subsequent steps were carried out at 4 ºC or on ice. The cells were harvested by centrifugation at 4000 rpm for 10 minutes in two nunc 50 mL centrifuge tubes. The supernatants were discarded, and the pellets were washed with 35 mL cold dH_2O (x2), 5 minutes centrifugation is sufficient for the washing steps. The pellets were subsequently washed with 25 mL cold 10% glycerol (x3). The final pellets were combined and resuspended in ~2.5 mL cold 10% glycerol with 0.5 M sucrose. The electrocompetent cells were lastly aliquoted in 1.5 mL microcentrifuge tubes and stored at -80 ºC.

3.11.2 Electroporation

Competent *S. aureus* cells were transformed with electroporation in this work. The cells to be transformed were mixed with the plasmid followed by a brief pulse of high-voltage electricity. The electrical pulse makes the membrane temporarily permeable by creating pores that allows for penetration of the plasmid into some of the cells (Willey et al., 2017d). Only a small percentage of the competent cells take up the plasmid, antibiotic selection is therefore necessary.

The electrocompetent *S. aureus* cells where thawed on ice, and 50 µL of the cells were subsequently mixed with between 750 and 1000 ng isolated plasmid. This mixture was transferred to a 1 mm cuvette that was electroporated at 2.1 volt, 100 ohm and 25 µF. TSB medium with 0.5 M sucrose (950 µL) was added to the cells immediately after electroporation to help cells recover following the electric pulse. Most bacterial cultures were then incubated at 37 ºC for 2 hours before being plated on BHI plates with the appropriate selective antibiotics. These plates were incubated overnight at 37 ºC and the transformants were verified by colony PCR (**Section 3.6.1**) the following day, and by sequencing the plasmid insert (**Section 3.14.1**). However, cells transformed with one of the pMAD plasmids (pMAD-Δ*cozEa*::*cam*, pMAD-*gfp_ugtP*::*spc*, or pMAD-Δ*ugtP*::*spc*) were treated differently given that pMAD only replicate at 30 ºC, see **Section 3.11.3** for their protocol.

3.11.3 Gene replacement using the pMAD vector

Most of the mutants constructed in this work were transformed with plasmids that replicates independently of the host's chromosome, though mutants with chromosomal mutations were also constructed using the pMAD vector. pMAD is a temperature sensitive shuttle vector for allelic replacement in naturally nontransformable Gram-positive bacteria (with low GC-content), like *S. aureus*. The pMAD vector contains the *bgaB* gene (from *Bacillus stearothermophilus*) that encodes for the thermostable β-galactosidase enzyme that allows for screening of transformants on plates with X-gal (Arnaud et al., 2004). β-galactosidase can cleave X-gal into galactose and 5-bromo-4-chloro-3-hydroxyindole. 5-bromo-4-chloro-3-hydroxyindole is the indigo-coloured insoluble compound that allows for identification of the clones containing the recombinant DNA. Cells with the inserted DNA will form white colonies on X-gal, while cells without the inserted DNA will produce blue colonies since they produce β-galactosidase that cleaves X-gal (Hollister et al., 2015). The pMAD vectors constructed in this work (pMAD-Δ*cozEa*::*cam*, pMAD-Δ*ugtP*::*spc*, and pMAD-*gfp_ugtP*::*spc*) all carry the

upstream part of the target gene, an antibiotic cassette, and the downstream part of the target gene. pMAD-*gfp_ugtP*::*spc* does in addition carry a *gfp-ugtP* fusion and a promotor for the expression of this fluorescent protein. pMAD-Δ*cozEa*::*cam* and pMAD-Δ*ugtP*::*spc* were constructed to produce deletion mutants where the gene of interest (*cozEa* and *ugtP*) is exchanged with an antibiotic resistance marker (chloramphenicol and spectinomycin). While pMAD-*gfp_ugtP*::*spc* was constructed to produce a mutant for localisation of UgtP with fluorescent microscopy.

The pMAD vectors were firstly transformed into competent IM08B *E. coli* cells, as described in **Section 3.10.2**, and then isolated as described in **Section 3.3**. The isolated plasmids were transformed into the desired *S. aureus* strain as described in **Section 3.11.2**, but instead of incubating the bacterial culture at 37 ºC for 2 hours it was incubated at 30 ºC for 3.5 hours. After incubation, the culture was plated on TSA plates with erythromycin (5 µg/mL) and X-gal (50 µg/mL). 50 µL 40 mg/mL X-gal was plated out on each TSA agar plate (with erythromycin) approximately 30 minutes before the bacterial culture, allowing the X-gal to dry. The plates were incubated at 30 ºC for 2 days (in the dark). Four blue colonies were PCR screened with relevant primers (**Section 3.6.1**) and incubated overnight at 30 ºC in TSB medium, considering that the blue colour indicates that the cells have taken up the pMAD vector. One of the positive colonies was re-streaked on a TSA plate with erythromycin and X-gal (50 µg/mL) the following day. This plate was incubated at 30 ºC for 2 days (in the dark). After incubation, one blue colony from this plate was picked and grown in TSB medium without antibiotic at 30 ºC for 2 hours, followed by incubation at 42-44 ºC for 6 hours. After 6 hours, the culture was diluted 1:1000 in TSB and incubated overnight at 42-44 ºC. The bacterial culture was serial diluted the next day. Undiluted, 10^{-1} diluted, and 10^{-2} diluted cultures were plated on TSA plates with chloramphenicol (10 µg/mL)/spectinomycin (100 µg/mL) and X-gal (50 µg/mL) and incubated at 42-44 ºC for 1-2 days (in the dark). The pMAD vector does not replicate at this temperature so only clones with integration of the plasmid should be able to grow on plates with antibiotic selection. After incubation, most colonies are blue or pale blue though some are hopefully also white. The white colonies are most likely a result of a double crossover event and loss of the vector, while blue and pale blue colonies likely are a result of a single crossover event. Approximately 20 white colonies were screened for chloramphenicol resistance and erythromycin sensitivity (pMAD-Δ*cozEa*::*cam*), or spectinomycin resistance and erythromycin sensitivity (pMAD-Δ*ugtP*::*spc* and pMAD-*gfp_ugtP*::*spc*). The colonies with the desired susceptibility properties were selected for colony PCR (**Section 3.6.1**) using primers that check

if the insert has correct placement and orientation in the bacterial chromosome and if the target gene is deleted. One of the positive colonies was lastly verified by sequencing (**Section 3.14.1**).

3.12 Bacterial growth assay (optical density)

A great deal of our understanding of bacterial life cycles stems from monitoring their proliferation in time, and one of the most common techniques for this monitorisation is to measure optical density (OD). A spectrophotometer measuring the OD at 600 nm (OD_{600}) is employed when looking at microbial growth. The more light absorbed by the sample at this wavelength, the higher the bacterial concentration (Stevenson, McVey, Clark, Swain, & Pilizota, 2016). OD measurements were used to characterize the growth of different mutants and to study their sensitivity to different antibiotics in this work, using either the Hidex Sense (Hidex Oy) or the Synergy™ H1 Hybrid Multi-Mode Reader (BioTek Instruments) microplate reader.

The bacterial strains to be monitored were firstly grown overnight in BHI medium with the respective antibiotics. They were then diluted 1:1000 in new BHI medium with the respective antibiotics and inducers of growth. Each bacterial dilution was applied to three separate wells (300 µL x3) in a 96-well microtiter plate. It is important to include a well with only medium. This blank is used to normalize the OD_{600} values of the various bacterial cultures in the plate by subtracting any possible absorption contributed by the media. The plates were incubated in a microplate reader at 37 ºC for 18-20 hours. OD_{600} measurements were taken every 10 minutes. The plate was shaken for 2-5 seconds before every measurement to obtain the most accurate OD_{600} possible. Individual growth curves for each strain were generated using the OD_{600} values. All growth curves in this work are the mean value of three replicate measurements performed in separate wells on the same plate, with the exception of the MIC assays (**Section 3.12.1**).

3.12.1 Minimum Inhibitory Concentration (MIC) assay

Minimum inhibitory concentrations (MICs) are the lowest concentration of an antimicrobial that inhibit visible growth of an organism grown overnight. In this work, MIC assays were performed to determine different strains (MDB1, MDB2, MDB3, and MDB11) sensitivity to the same antibiotics (daptomycin, oxacillin, and vancomycin). To determine the MIC of these antibiotics, they were serially diluted in MH medium with the respective bacterial strains.

Firstly, the bacterial strains were grown overnight in MH medium with the selective antibiotics. They were diluted 1:100 in cold MH medium with selective antibiotics and inducers of growth the following day. MDB11 was induced with three different concentration of IPTG (10 µL, 50 µL, and 100 µL). The diluted cultures were incubated until they reached a OD_{600} between 0.4 and 0.6. They were then re-diluted in 1:1000 in cold MH medium (extra Ca^{2+} for daptomycin and 2% sodium chloride for oxacillin, see **Section 2.9.1**) with selective antibiotics, inducers of growth, and a 2-fold dilution of the antibiotic (from 5 µg/mL for daptomycin, from 4 µg/mL for oxacillin, and from 20 µg/mL for vancomycin). In addition to the wells with the serial diluted antibiotic cultures each strain was grown without antibiotic and a blank was included for normalisation of the cultures. Two parallels were prepared for the MIC assays of MDB1, MDB2, and MDB3 (no parallels for MDB11). The plates were incubated in a microplate reader at 37 ºC for ~18 hours. OD_{600} measurements were taken every 10 minutes. The plates were shaken for 5 seconds before every measurement to obtain the most accurate OD_{600} possible. The MIC values for the different strains were set as the lowest concentration where no growth was observed ($OD_{600} < 0.1$) using the OD_{600} values.

3.13 Microscopy

The invention of the microscope can be dated far back, nonetheless it continues to be one of the most important method for studying microorganisms today. Two different microscopes were used in this work: The LSM 700 (Zeiss) laser scanning confocal microscope with a light microscope system and the Morgagni™ 268 (FEI Company) transmission electron microscope (TEM).

Bacterial cells were immobilised on agarose before imaging with the LSM 700 to prevent movement, this is especially important when doing multichannel fluorescent microscopy. A thin, flat layer of 1.2% agarose gel were cast on microscope slides with reaction wells, see **Section 2.10.6** for the recipe. 0.4 µL of each bacterial sample were applied to the individual wells. The cells were trapped in the porous matrix of the agarose gel and secured with a cover glass. This form of immobilising does not kill the cells, as fixation does, and thus enables live imaging which is necessary for time-lapse microscopy.

3.13.1 Phase contrast microscopy

Light microscopes consist of multiple lenses (ocular, objective, and condenser) which can be varied to obtain different types of microscopy: bright field, dark field, phase contrast, differential interference, and fluorescence. Both phase contrast microscopy and fluorescence microscopy were employed in this work. Phase contrast microscopy takes advantage of the different densities of cell components to provide a high-contrast image. Light passing through the cell structures (deviated light waves) will be diffracted and slowed more than the light only passing through the surrounding medium (undeviated light waves). A condenser annulus and a phase plate in the microscope allow for manipulation of the undeviated light followed by recombination of the undeviated light with the deviated light to form an image of the dark bacteria against a lighter background (Roane & Pepper, 2015; Willey, Sherwood, & Woolverton, 2017a).

Phase contrast microscopy was used to study the morphology of the different *S. aureus* strains in this work. The strains to be studied were first grown overnight in BHI medium with the respective antibiotics. The overnight cultures were diluted 1:1000 in new BHI medium with the respective antibiotics and inducers of growth the next day. The diluted bacterial cultures were then incubated until they reached an OD_{600} = ~0.4, followed by cooling on ice to stop the bacterial growth. When cooled, the bacterial cultures were either: (1) directly applied to the wells on the slides with agarose gel, or (2) concentrated by centrifuging 1 mL of the bacterial cultures at 8 000 x g for 2 minutes at 4 ºC and resuspending them in 200 µl PBS, before being applied to the wells on the slides. The bacteria were viewed with the 100x phase contrast objective, and the pictures were captured using the ORCA-Flash4.0 V3 Digital CMOS camera (Hamamatsu Photonics K.K.) with an exposure time of ~260 ms (using the TL channel).

3.13.2 Fluorescence microscopy

Fluorescence microscopy utilizes a UV light source to excite fluorochromes instead of passing light through the bacteria. The fluorochromes absorbs light at a certain wavelength and fluoresces. The emitted fluorescent light is used to form the image. Many different fluorochromes have been developed, each with its own emission and excitation spectrum (Willey et al., 2017a). 4′,6-diamidino-2-phenylindole (DAPI), BODIPY FL vancomycin (VanFL), green fluorescent protein (GFP), and 7-hydroxycoumarincarbonylamino-D-alanine (HADA) were used in this work.

3.13.2.1 Labelling cell structures (cell wall and DNA)

Bacterial cell wall and DNA was labelled with VanFL and DAPI respectively. VanFL is a green-fluorescent dye containing a single BODIPY dye per vancomycin molecule. It is used to detect the binding sites for vancomycin in bacteria, which are the D-alanyl-D-alanine residues present in the carboxyl-terminal of the peptidoglycan precursors. These precursors are incorporated into the bacterial cell wall via a transpeptidation reaction which results in crosslinking of the precursors, catalysed by PBPs. The D-Ala-D-Ala bond is cleaved in the crosslinking and the terminal D-Ala is released. VanFL is known to label nascent cell wall in various Gram-positive bacteria, owing to the fact that the D-Ala-D-Ala bond is hydrolysed by carboxypeptidases. However, VanFL label the entire cell wall and septum of *S. aureus* cells, because they have a high number of residues with the D-Ala-D-Ala bond (Pinho & Errington, 2003). DAPI, on the other hand, is a blue-fluorescent dye which binds to DNA, preferably to AT base pairs in the minor groove. Bound DAPI fluorescens very strongly compared to unbound DAPI, there is more than a 20-fold difference between the two. DAPI can also bind to RNA, but this complex results in a much weaker fluorescence (Kapuscinski, 1995).

The *S. aureus* cells labelled with these fluorochromes were prepared in the same manner as the cells visualised with phase contrast microscopy (**Section 3.13.1**), except for the addition of VanFL (0.8 µg/mL) and DAPI (7.5 µg/mL) before being applied to the slides with agarose gel. Images of the bacteria were captured using the ORCA-Flash4.0 V3 Digital CMOS camera (Hamamatsu Photonics K.K.) with an exposure time of ~80 ms for DAPI (using the DAPI channel) and ~600 for VanFL (using the BODIPY FL channel).

3.13.2.2 Labelling target proteins with GFP

Another important use of fluorescence microscopy is to find the localisation of specific proteins within the bacteria. Some organisms produce naturally fluorescent proteins that can be used in such applications. Most notably the green fluorescent protein (GFP) originally isolated from the jellyfish *Aequorea victoria* (Chalfie, Tu, Euskirchen, Ward, & Prasher, 1994; Willey et al., 2017a). Unlike DAPI and VanF, GFP was not added to the bacterial cultures after growth, the gene for GFP was rather fused to the gene of interest when constructing the mutant. GFP labelling was used to localise CozEa and CozEb in the NCTC8325-4 wild-type (constructed by Dr. Morten Kjos) and to localise UgtP in the NCTC8325-4 wild-type, Δ*cozEa*, and Δ*cozEb*. The localisation of UgtP was determined using two different strategies: (1) the pLOW-*gfp_ugtP* and (2) the pMAD-*gfp_ugtP*::*spc*. Expressing proteins from the pLOW plasmid is faster and

easier than integrating the genes of interest into the host chromosome using the pMAD plasmid (**Section 3.11.3**). However, integration of the target genes is preferable as one overcomes plasmid-based overexpression and genetic instability with this technique. Overexpression of plasmid-based genes have been found to lead to diversion of cellular resources, such as ribosomes. In addition, selective pressure is necessary for cultivation of strains with extrachromosomal plasmids (Saleski et al., 2021).

The strains with GFP fusions and the strains carrying the pLOW-*gfp_ugtP* plasmid were firstly grown overnight in BHI medium with the respective antibiotics. The overnight cultures were diluted 1:100 (GFP-UgtP)/1:500 (CozE-GFP) in new BHI medium with the respective antibiotics and inducers of growth the next day. The strains carrying the pLOW plasmid (MDB64, MDB65, and MDB66) were induced with 50 µM IPTG instead of 500 µM, since induction with high IPTG consecrations resulted in oversaturated signals (**Figure 4.24**). The diluted bacterial cultures were incubated until they reached an OD_{600} = ~0.5 (GFP-UgtP)/ ~0.3 (CozE-GFP), followed by cooling on ice to stop the bacterial growth. When cooled, the bacterial cultures were directly applied to the wells on the slides with agarose gel. Images of the bacteria were captured using the ORCA-Flash4.0 V3 Digital CMOS camera (Hamamatsu Photonics K.K.) using the superfolder GFP channel. Time-lapse (TL) images were taken in addition to the standard images of the bacteria. For the TL images a picture was taken of the cells every fourth second for 36 seconds (GFP-UgtP)/every third second for 27 seconds (CozE-GFP).

3.13.2.3 Labelling newly synthesised peptidoglycan with HADA

HADA labelling enables real-time spatiotemporal tracking of peptidoglycan biosynthesis in live bacterial cells. HADA is a blue fluorescently modified D-amino acids, and as stated in **Section 1.2.3**, the cell wall of *S. aureus* consists of glycan strands that are cross-linked by short D-amino acid-containing peptide chains. Incorporation of HADA into peptidoglycan therefore visualises the sites of peptidoglycan synthesis and thereby also distinguish sites of active growth from older cell wall. HADA is non-toxic to bacteria and should therefore not affect cell morphology nor growth (at least not with a concentration below ~500 µM to 1 mM) (Kuru, Tekkam, Hall, Brun, & Van Nieuwenhze, 2015).

The labelling procedure with HADA is simple. HADA is directly added to the actively growing bacterial cells for a desired labelling duration. The labelling duration in this work was short,

lasting only for 2 minutes. The strains to be labelled were first grown overnight in BHI medium with the respective antibiotics. The overnight cultures were diluted 1:250 in new BHI medium with the respective antibiotics and inducers of growth the next day. The diluted bacterial cultures were then incubated until they reached an OD_{600} = ~0.4, with the exception of MDB11 without IPTG that was grown until it reached an OD_{600} of ~1.4. Each culture (50 µL) was transferred to a 1.5 mL microcentrifuge tube containing 4 µL HADA (1 mg/mL), giving a final HADA concentration of 250 µM. It is important to keep HADA in the dark, as light can degrade the solution. The cultures containing HADA were incubated at 37 ºC in a water bath for 2 minutes. After incubation, the tubes were immediately put on ice to stop bacterial growth. The bacteria were pelleted by centrifugation at maximum speed for 1 minute at 4 ºC when cooled, and the pellets were resuspended in 50 µL cold PBS to remove any excess and unbound dye. The cells were then washed again by centrifugation at maximum speed for 1 minute at 4 ºC and the final pellets were resuspended in 25 µL cold PBS. These samples were applied to the wells on a slide with agarose gel. Images of the bacteria were captured using the ORCA-Flash4.0 V3 Digital CMOS camera (Hamamatsu Photonics K.K.) using the same channel as for DAPI.

3.13.3 Transmission electron microscopy (TEM)

Electron microscopes (EMs) produces high resolution images of microorganisms by using electrons instead of light. The best light microscopes have a resolution limit of ~0.2 µm, while EMs often can distinguish points closer than 0.5 nm. Resolution increases with decreasing wavelength, and the wavelength of the electron beam is approximately 100 000 times shorter than that of visible light, and it therefore has a much higher resolving power. The electron beam in EMs is aimed at the sample which is placed in a vacuum chamber (air molecules deflect electrons when they collide). Intricate grayscale images of the fine structures and details of the microorganisms in the sample are obtained by focusing the beam using a series of electromagnets. These electromagnets, called magnetic lenses, are doughnut shaped since electrons cannot pass through glass (Roane & Pepper, 2015; Willey et al., 2017a).

Different types of EMs have been developed, with transmission electron microscopes (TEMs) being one of them. TEMs produces images of microorganisms by passing electrons through the sample. Dense regions of the organisms (electron dense regions) scatter the most electrons and therefore appear darker in the image than electron-transparent regions. The organisms have to be thin sectioned (20-100 nm) to allow passage of electrons. The electrons are easily absorbed or scattered if the sections are too thick. The selective absorption of electrons in the sections

make TEM especially useful when studying fine internal cell structures (Roane & Pepper, 2015; Willey et al., 2017a).

The bacterial strains to be visualised by TEM (MDB19, MDB45, MDB46, and MDB57 ± IPTG) were firstly harvested. Overnight bacterial cultures cultivated in BHI medium with the respective antibiotics were diluted 1:1000 in BHI with the respective antibiotics and with/without IPTG. The diluted bacterial cultures were incubated at 37 ºC until they reached a OD_{600} = ~0.3. Each of the bacterial cultures (10 mL) were mixed with 10 mL EM fixation solution (**Section 2.10.6**) by inversion of the tubes. The tubes were incubated at room temperature for 1 hour, followed by incubation at 4 ºC overnight. The next day, the cells were washed with 5 mL PBP, pH 7.4, and centrifuged at 5000 x g (x3). The final pellets were dissolved in 2 mL PBS and transferred to 2 mL microcentrifuge tubes.

Sample preparation for TEM is quite extensive. In this work, sample preparation was performed by Lene Cecilie Hermansen at the Imaging Centre. The cells were firstly fixed with chemicals to stabilize the cell structures. Following fixation, the cells were dehydrated with organic solvents. Dehydration is important because the medium used to embed the cells is hydrophobic. The cells were then embedded in a medium consisting of unpolymerised, liquid epoxy plastic that was cured causing the medium to polymerize and harden. The medium formed a solid block around the cells when cured. This block was cut into 60 nm section using a microtome equipped with a diamond knife. Poor contrast can be a problem when microscoping bacteria, they were therefore stained with uranyl acetate. The heavy uranium ions bind to the cell membrane, nucleic acid, and nucleic acids containing protein complexes, providing electron density to the cells which enhances their contrast (Roane & Pepper, 2015; Willey et al., 2017a). The stained sections were lastly mounded on copper grinds and viewed in the Morgagni™ 268 microscope (FEI Company). Images of the bacteria were captured using a Veleta CCD camera (Olympus Corporation) with an exposure time of ~1000 ms.

3.13.4 Analysis of the microscopic pictures using MicrobeJ

The distribution of cell sizes among different *S. aureus* strains were determined using MicrobeJ. A stack of phase contrast images of the strain to be analysed were run in MicrobeJ, where the bacterial cells are detected. Several specifications (e.g., area, length, and width) can be adjusted to make this detection more accurate. The default values of these specifications are [0-max], though some were adjusted in this work, see **Table 3.7**. In addition, the "Exclude on Edges",

"Shape descriptors", "Segmentation", and "Intensity" option boxes were checked. Every cell was manually examined after the MicrobeJ run, and detection continued by manually marking cells that had been omitted, splitting cells that were divided, and discarding cells that were incorrectly marked.

Table 3.7 The value intervals for the specifications used to detect bacterial cells in MicrobeJ.

Specification	Value interval
Area [p^2]	0.7-2.5
Length [p]	0-2
Circularity [0-1]	0.7-max
Curvature [0-max]	0-1

a. MicrobeJ include several other specifications, though they were not adjusted and are therefore not included in this table.

In addition to analysing cell sizes, the cell cycle of the bacteria was also analysed by manual counting the different cell phases (phase 1, 2 or 3) of 100-150 random cells from each strain based on VanFL staining.

3.14 DNA sequencing

DNA sequencing is a technique used to determine the order of nucleotides in DNA. It was introduced for the first time in 1977 with the development of two DNA sequencing methods, one by Allan Maxam and Walter Gilbert and the other by Frederick Sanger. The Sanger method, often referred to as the chain-termination DNA sequencing method, became the most commonly used. It was notably used to sequence the first human genom in 2001. Although, Sanger sequencing have two major limitations, it is expensive and time consuming. The human genome project (HGP) cost ~300 million dollars and took nearly a decade to finish. Several new techniques solving these problems have been developed the last ~15 years, called next-generation sequencing (NGS). Sequencing a human genome using NGS only takes 1-2 days, and a bacterial genome can be sequenced in just a few hours. The key change with the NGS techniques is multiplexing, which allows for treating millions to billions of immobilised templates with a single reagent (Mardis, 2017; Willey, Sherwood, & Woolverton, 2017e). Sanger sequencing was performed to verify plasmids and mutants in this work.

3.14.1 Targeted gene sequencing

Target gene sequencing was performed to verify that the constructed plasmids and transformants were correct. The DNA to be sequenced was sent to GATC (Eurofins Genomics) for Sanger sequencing. The Sanger method depends upon synthesis of a new DNA strand using the DNA to be sequenced as template. The single stranded DNA template is mixed with DNA polymerase, a primer immediately flanking the region of interest, deoxyribonucleotide triphosphates (dNTPs), and dideoxynucleoside triphosphates (ddNTPs). ddNTPs are nucleotide analogues that interrupt DNA synthesis when added to the template strand because they lack the 3'-OH group needed to attack the 5'-PO_4 of the next dNTP. The ddNTPs in Sanger sequencing are labelled with different coloured fluorescent dyes, which allows for introduction of all four ddNTPs (ddGTP, ddATP, ddTTP and ddCTP) into a single reaction. A small fraction of the synthesised strands is prematurity terminated each round of primer extension by incorporation of a fluorescently labelled ddNTP, resulting in mixture of coloured DNA fragments of varying lengths, where fragments terminating in the same nucleotide have the same colour. The resulting DNA fragments are separated by electrophoresis in a capillary tube. A laser beam detects the identity of the ddNTPs of the different bands in the gel by their fluorescent colour. Software translates this information into a DNA sequence in the form of a chromatogram where the amplitude of each spike represents the fluorescent intensity of each nucleotide (Nelson & Cox, 2017b; Shendure & Ji, 2008; Willey et al., 2017e).

The DNA to be sequenced was mixed with a primer and dH_2O. Each DNA target was prepared in two different tubes, one with the forward primer immediately flanking the region of interest and the other with the reverse primer. When sequencing plasmids 5 µL purified plasmid DNA (80-100 ng/µL) was mixed with 2.5 µL primer (10 µM) and 2.5 µL dH_2O, and when sequencing transformants 5 µL purified PCR product (2 ng/µL for 150-300 bp, 12 ng/µL for 300-1000 bp, and 25 ng/µL for >1000 bp) was mixed with 2.5 µL primer (10 µM) and 2.5 µL dH_2O. The automated Sanger system can accurately read ~1000 bp in a single run, so multiple primers were used to completely cover the sequence for genes larger than a 1000 bp. The premixed samples were lastly sent to GATC (Eurofins Genomics) for sequencing. The sequences were analysed using Benchling.

4 Results

4.1 Phylogenetic distribution of CozE proteins among bacteria in the *Staphylococcaceae* family.

CozE proteins are distributed in Bacteria (Fenton et al., 2016). In order to investigate the distribution of CozE proteins within the *Staphylococcaceae* family, a phylogenetic analysis was performed. The *Staphylococcaceae* family consist of Gram-positive bacteria belonging to the genera *Staphylococcus*, *Macrococcus*, *Jeotgalicoccus*, *Salinicoccus*, and *Nosocomiicoccus* (Lory, 2014). Strains from the *Staphylococcus* genus are of primary interest in this work, and a majority of the strains in the phylogenetic analysis therefore belong to this genus. Strains from the other four genera are also included, since they provide an insight into how common the functions of the CozE proteins in *Staphylococcus* are among other bacteria.

Homology searches were performed using the protein sequence of CozEa from *S. aureus* as the query against 28 strains belonging to the *Staphylococcaceae* family with BLASTP. Two homologues were found in each strain. The homologue with the highest identity percentage to the query corresponds to CozEa, coloured blue in **Figure 4.1**, while the other homologue corresponds to CozEb, coloured red in **Figure 4.1**. Sequence alignments were performed using Clustal Omega. A maximum likelihood phylogenetic tree was constructed with the sequence alignments, from Clustal Omega, using IQ-TREE. The phylogenetic tree was finally visualised and annotated using iTOL, generating the tree seen in **Figure 4.1**. The CozE proteins from species belonging to the genus *Staphylococcus* (labelled with dark blue and dark red in **Figure 4.1**) generated two separate subgroups, while the CozE proteins from the other genera (labelled with light blue and light red in **Figure 4.1**) are clustered together independent of CozE type, with the exception of the *Macrococcus* strains. This indicates that the function of CozEa and CozEb are conserved among *Staphylococcus* and *Macrococcus*. The cluster containing the *Jeotgalicoccus*, *Salinicoccus*, and *Nosocomiicoccus* strains are closer to the CozEa subgroup than the CozEb subgroup, suggesting that CozEb have a unique function in *Staphylococcus* and *Macrococcus*.

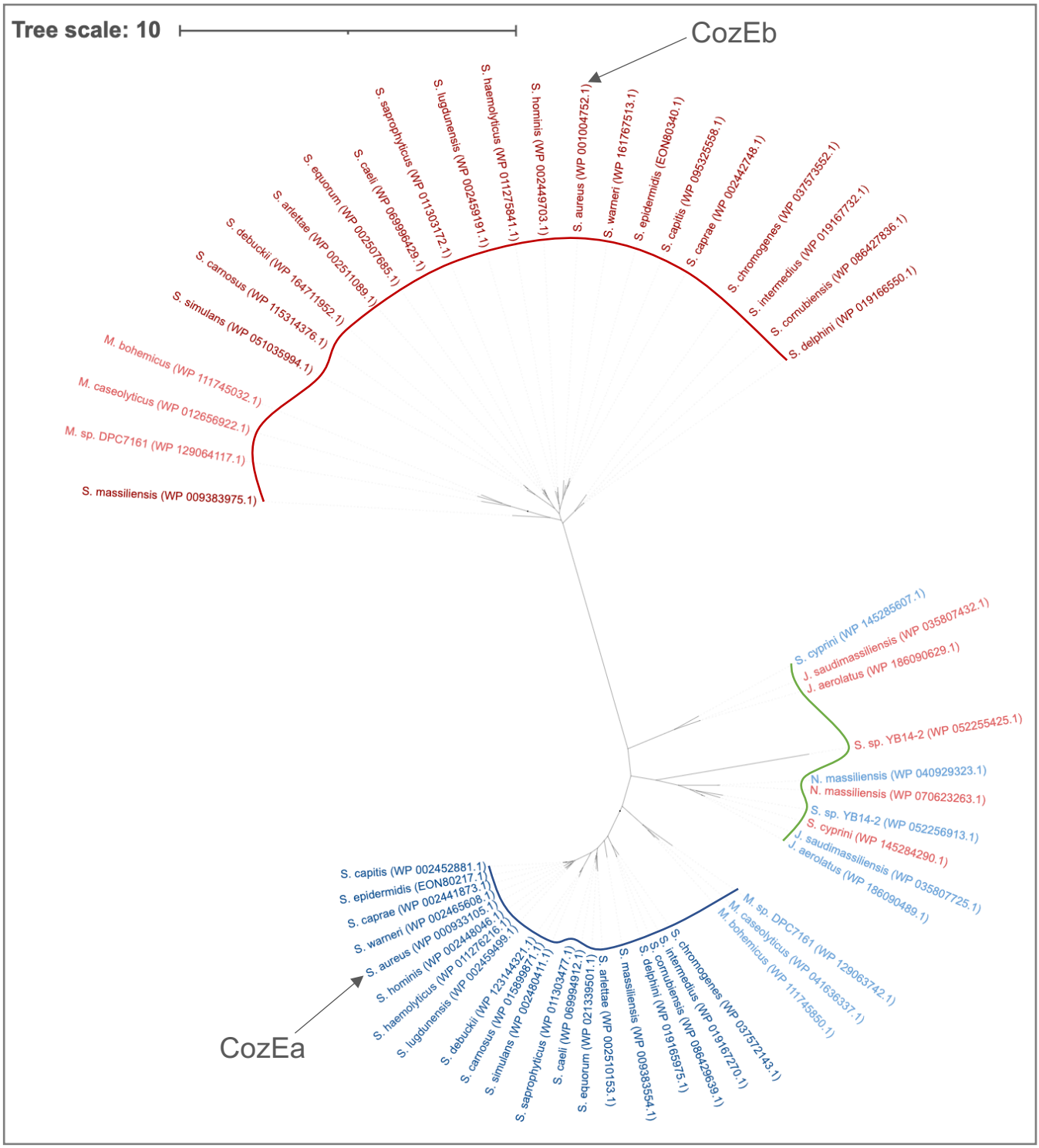

Figure 4.1 Phylogenetic distribution of CozE proteins in the *Staphylococcaceae* family (consisting of the *Staphylococcus*, *Macrococcus*, *Jeotgalicoccus*, *Salinicoccus*, and *Nosocomiicoccus* genera). The colour of the leaves distinguishes the CozEa proteins (blue) from the CozEb proteins (red) found in every strain. The CozEa proteins belonging to the *Staphylococcus* genus are dark blue, while the CozEa proteins belonging to the other genera are light blue. Likewise, the CozEb proteins belonging to the *Staphylococcus* genus are dark red in contrast to the light red CozEb proteins belonging to the other genera. The subgroups formed in the phylogenetic tree are labelled with different colours (CozEa from *Staphylococcus* and *Macrococcus* = blue, CozEb from *Staphylococcus* and *Macrococcus* = red, and CozEa and CozEb from *Jeotgalicoccus*, *Salinicoccus*, and *Nosocomiicoccus* = green). In addition, the CozE proteins found in *S. aureus* are pointed to by grey arrows.

4.2 Single deletions of *cozEa* and *cozEb* only have minor effect on growth and cell division in different *S. aureus* strains.

To investigate if the results obtained by single deletions of *cozEa* and *cozEb* in the *S. aureus* SH1000 strain by Stamsås et al. (**Section 1.4.2**) are conserved among other *S. aureus* strains, both genes were deleted individually in the methicillin-susceptible S. *aureus* (MSSA) strain NCTC8325-4 and the community-acquired MRSA strain JE2. Growth assays and microscopy were performed on the NCTC8325-4 and JE2 cells with single deletions of the *cozE* genes, where *cozEa* or *cozEb* had been replaced with an antibiotic resistance cassette. Individual deletions of *cozEa* and *cozEb* in NCTC8325-4 did not result in any growth defects compared to wild-type (**Figure 4.2A**). The JE2 Δ*cozEa* and Δ*cozEb* mutant strains, on the other hand, did exhibit a longer lag- and log phase than their respective wild-type (**Figure 4.2C**). Even so, neither the NCTC8325-4 mutants nor the JE2 mutants displayed any obvious differences in cell shape (phase contrast), cell wall labelling- (VanFL) or nucleoid staining pattern (DAPI) compared to their wild-type (**Figure 4.2E**). All strains displayed spherical cells almost entirely filled by the nucleoid, as visualised by DAPI staining. VanFL binds to the cell wall surrounding all cells, in addition to the septum of dividing cells. Micrographs of the VanFL labelled cells were used to determine the distribution of cell cycle phases among the strains with single deletions of the *cozE* genes (**Figure 4.3**). Cells in phase 1 are in the initial cell cycle phase before initiation of septum formation. Cells in phase 2 have initiated synthesis of the division septum, and the cells in the final cell cycle stage (phase 3) have a complete septum. Based on the manual cell cycle analysis (**Figure 4.3**), absence of CozE did not appear to disturb the cell cycle of *S. aureus* cells sustainably. Cell sizes and circularity was measured using MicrobeJ. Cell size analysis demonstrated that single deletions of *cozEa* and *cozEb* did not notably affect the size of the cells (**Fig 4.2B and D**). There were no significant differences between the area means ± standard deviations of the mutants, compared to their respective wild-type cells (MDB2 = 1.19 ± 0.26 and MDB3 = 1.18 ± 0.26 compared to MDB1 = 1.24 ± 0.27, and MDB38 = 1.01 ± 0.22 and MDB10 = 1.09 ± 0.24 compared to MDB37 =1.09 ± 0.22). In addition, all strains exhibited the same mean circularity score, 0.98 ± 0.01, where the value 1 represents a completely circular cell. Thus, the cell shapes of the mutants are similar to their respective wild-types. These results are consistent with those obtained by Stamsås et al. in the *S. aureus* SH1000 strain, suggesting that single deletions of the *cozE* genes does not have a clear effect on cell morphology in *S. aureus*.

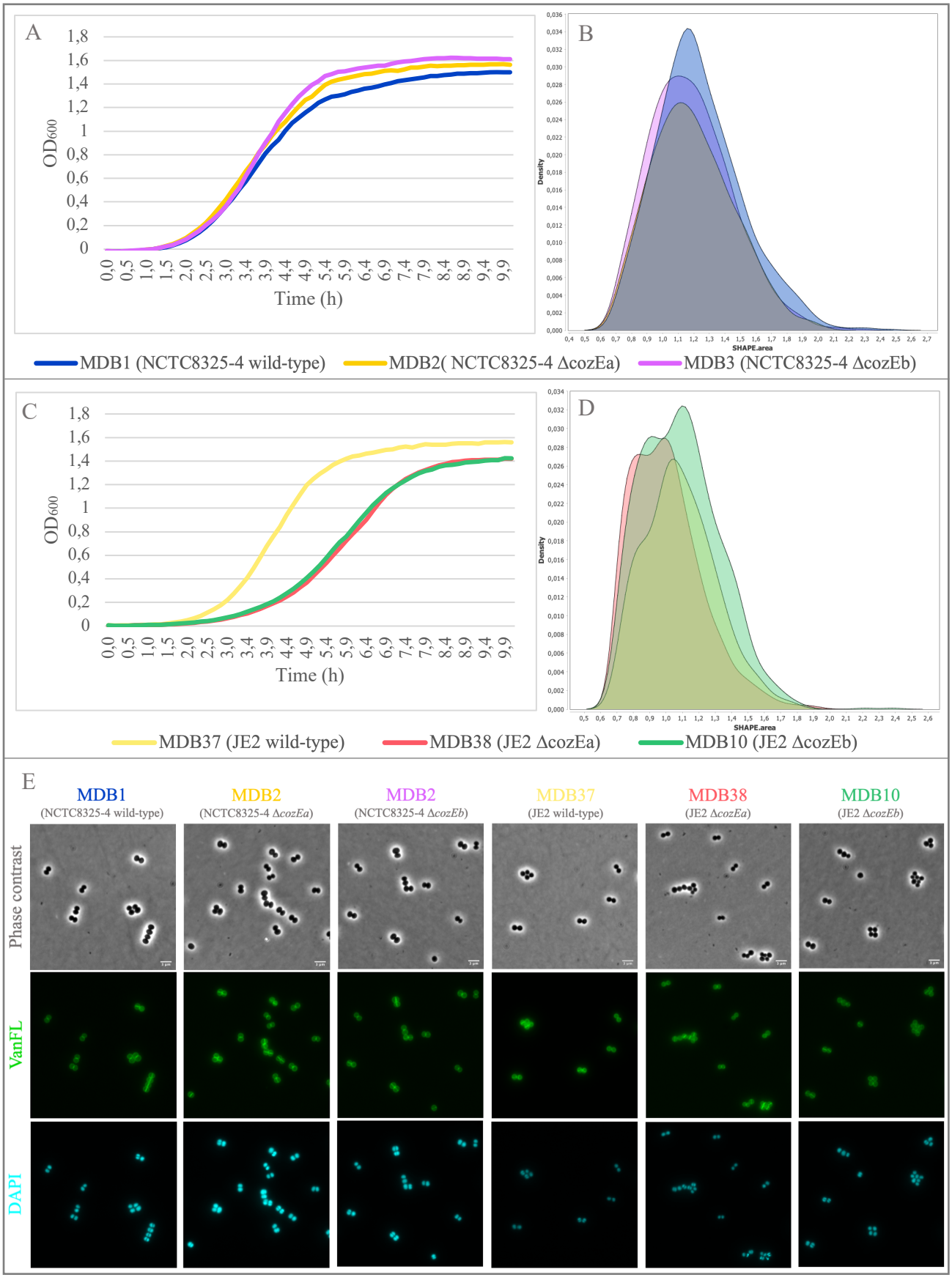

Figure 4.2 Single deletions of *cozEa* and *cozEb* in *S. aureus* NCTC8325-4 and JE2.
A. Growth curves for NCTC8325-4 (MDB1, MDB2, and MDB3).
B. Density plot of the cell areas of MDB1 (n =1 401), MDB2 (n = 1078), and MDB3 (n = 1092) determined using MicrobeJ.
C. Growth curves for JE2 (MDB37, MDB38, and MDB10).
D. Density plot of the cell areas of MDB37 (n = 671), MDB38 (n = 1426), and MDB10 (n = 1211) determined using MicrobeJ.
E. Phase contrast, VanFL staining and DAPI staining micrographs of both NCTC8325-4 (MDB1, MDB2, and MDB3) and JE2 (MDB37, MDB38, and MDB10). The scale bars on the phase contrast images represents 3 µm.

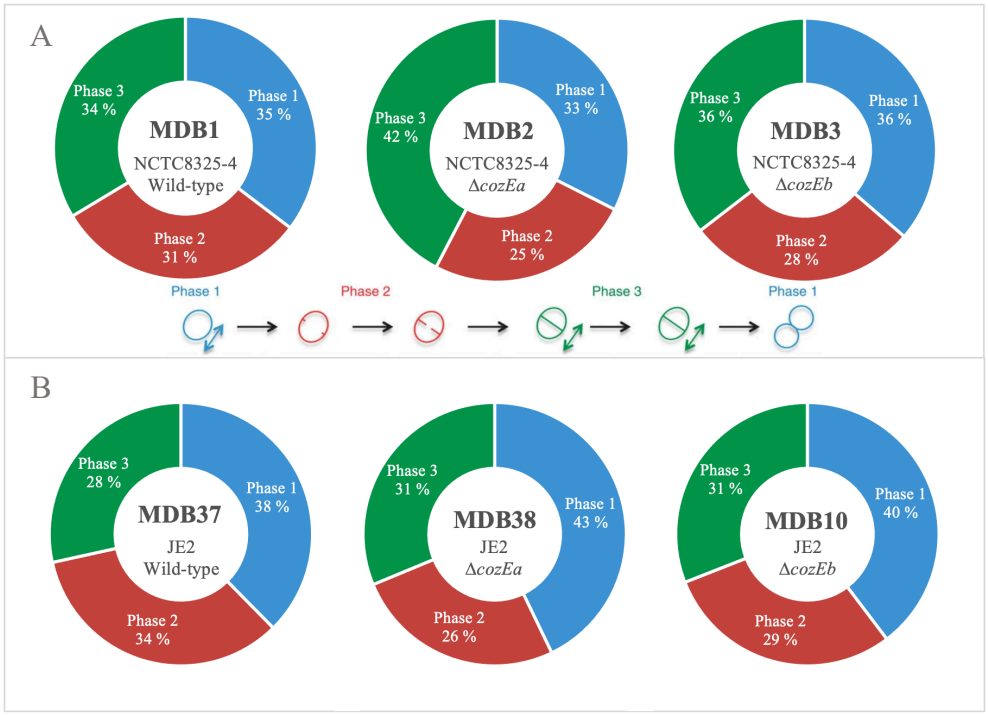

Figure 4.3 Distribution of cell cycle phases among strains with single deletions of *cozEa* and cozEb in *S. aureus* NCTC8325-4 (A) and JE2 (B) cells. Obtained by manual counting the different cell phases of 100-150 random VanFL stained cells from each strain.

4.3 A double *cozE* deletion mutant cannot be obtained in NCTC8325-4.

To investigate the effect of deleting both *cozE* genes at the same time, deletion of *cozEa* using the pMAD-Δ*cozEa*::*cam* plasmid was attempted in MDB3 (NCTC8325-4 Δ*cozEb*), as described in **Section 3.11.3**. However, this double deletion strain could not be obtained. No colonies formed on the TSA plates with X-gal and chloramphenicol grown at 42-44 ºC, most likely because cells that were able to integrate the plasmid (double crossover) were non-viable. This suggests that CozEa and CozEb have essential, complementary functions in NCTC8325-4. Furthermore, Stamsås et al. (2018) were unable to obtain a double deletion strain in *S. aureus* SH1000, despite multiple attempts, indicating that the essential function(s) of the CozE proteins are conserved among different *S. aureus* strains.

4.4 The lack of both CozEa and CozEb at the same time greatly affect growth and cell morphogenesis of different *S. aureus* strains.

Since the double deletion strain could not be obtained, the CRISPRi system, described in **section 1.5**, was employed to confirm the synthetic relationship between *cozEa* and *cozEb* in NCTC8325-4 and JE2. sgRNA plasmids targeting *cozEa* and *cozEb* were constructed, as well as a double sgRNA plasmid targeting both *cozE* genes. A strain with a non-targeting sgRNA

(described as sgRNA(*luc*), MM75) was used as a control in this work. Since no genes in *S. aureus* are targeted and thus depleted using this control construct, it is used to recognise the effect the CRISPRi system itself has on cells' growth and morphology. **Figure 4.4A** demonstrates that this effect is minimal, due to the fact that uninduced and induced MM75 cells are equivalent to each other. No growth reduction nor morphological abnormalities were observed upon knockdown of the individual *cozE* genes in wild-type cells (**Figure 4.4 and 4.5**), which is expected as single deletions did not alter vitality (**Section 4.2**). Knockdown of *cozEa* and *cozEb* in a Δ*cozEb* and Δ*cozEa* genetic background, respectively, did however cause dramatic reduction in growth (**Figure 4.4B/C and 4.5C**), further indicating that the two CozE proteins have overlapping functions in *S. aureus*. The same was observed when depleting both *cozE* genes, using the CRISPRi system, in wild-type cells, although they had a slightly less dramatic reduction in growth (compared to the deletion-depletion strain) owing to the fact that the depleted genes still have some transcription (**Figure 4.4A and 4.5B**). Thus, *cozEa* and *cozEb* constitute a synthetic lethal gene pair in *S. aureus* NCTC8325-4 and JE2, since these strains are not able to tolerate the absence of both genes at the same time despite their individual deletion having no significant effects.

The phenotypes for the deletion-depletion- and double depletion strains were further investigated by microscopy. Phase contrast micrographs of the IPTG induced mutants (**Figure 4.4D and 4.5D**) revealed severely perturbed cell morphologies when both CozE proteins were absent, as seen in **Figure 4.4D and 4.5D**. These cells displayed variable cell shapes. Cell size analysis, using MicrobeJ, demonstrated that the NCTC8325-4 and JE2 mutants lacking both CozE proteins also displayed variable cell sizes. Analysis of NCTC8325-4 demonstrated that MDB13 (WT + CRISPRi(*cozEa*+*cozEb*)) and MDB12 (Δ*cozEb* + CRISPRi(*cozEa*)) were significantly smaller than the control MM75 ($p < 0.001$, Mann–Whitney test) (**Figure 4.6**). While analysis of JE2 demonstrated that MDB19 (WT + CRISPRi(*cozEa*+*cozEb*)) and MDB21 (Δ*cozEb* + CRISPRi(*cozEa*)) have a very wide distribution of cell sizes compared to the wild-type cells (**Figure 4.7**).

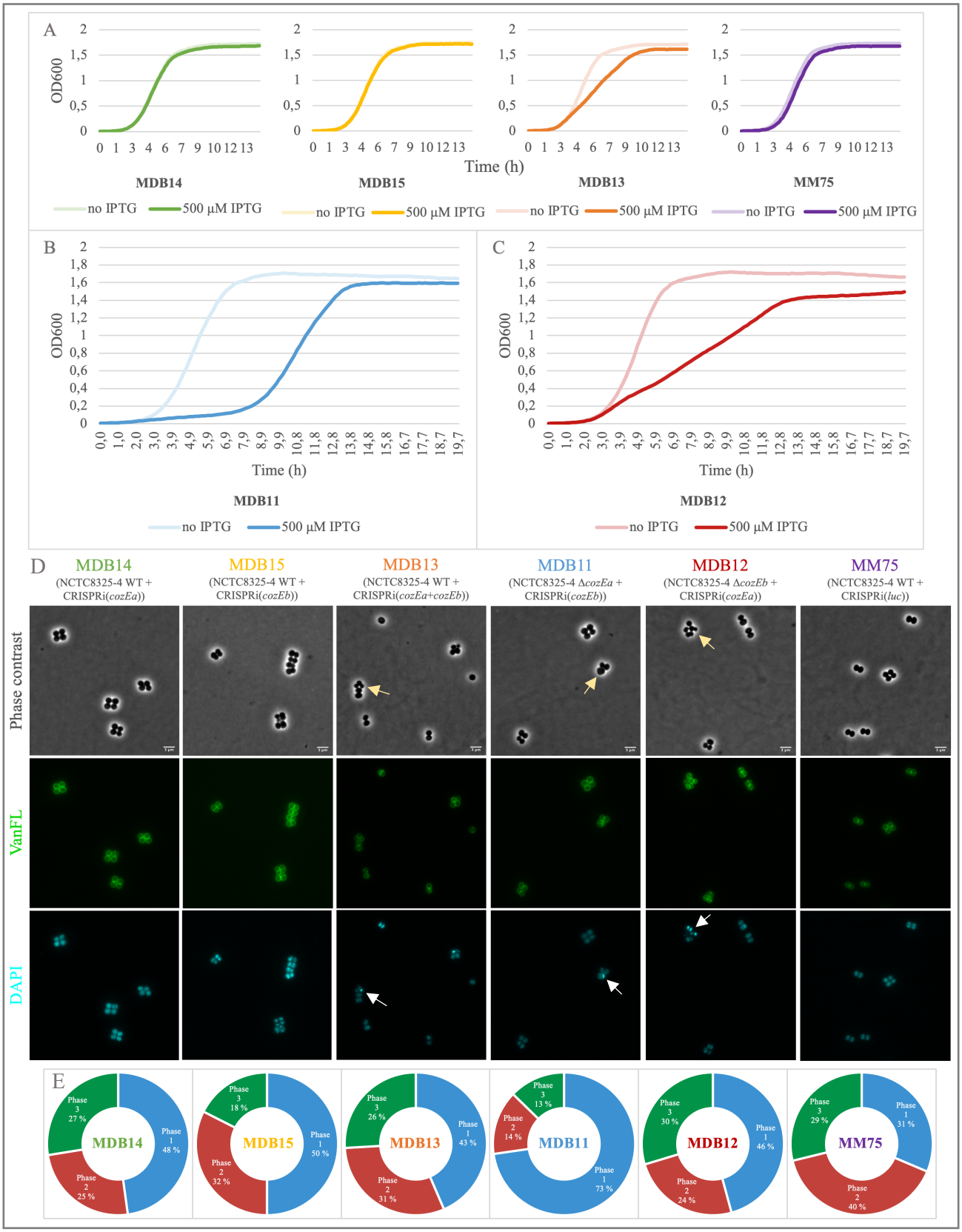

Figure 4.4 Deletion-depletion and double depletion of the *cozE* genes in *S. aureus* NCTC8325-4.
A. Growth curves of NCTC8325-4 wild-type with single- (MDB14 and MDB15) and double depletions (MDB13) of *cozE* (in addition to the control strain MM75).
B-C. Growth curves of NCTC8325-4 deletion-depletion strains. A growth curve for the NCTC8325-4 Δ*cozEa* strain with depletion of *cozEb* (MDB11) (**B**), and a growth curve for the NCTC8325-4 Δ*cozEb* strain with depletion of *cozEa* (MDB12) (**C**).
D. Phase contrast, VanFL staining and DAPI staining micrographs of NCTC8325-4 with single depletions (MDB14 and MDB15), double depletion (MDB13), and deletion-depletion (MDB11 and MDB12) of *cozE* (in addition to the control strain MM75). The cultures are induced with 500 µM IPTG. Yellow arrows point to examples of cells with perturbed cell morphologies, while the white arrows point to examples of cells with irregular DAPI signal. Scale represents 3 µm.
E. Distribution of cell cycle phases among NCTC8325-4 cells with single depletions (MDB14 and MDB15), double depletion (MDB13), and deletion-depletion (MDB11 and MDB12) of *cozE* (in addition to the control strain MM75). The data was obtained by manual counting the different cell phases of 100-150 random VanFL stained cells from each strain.

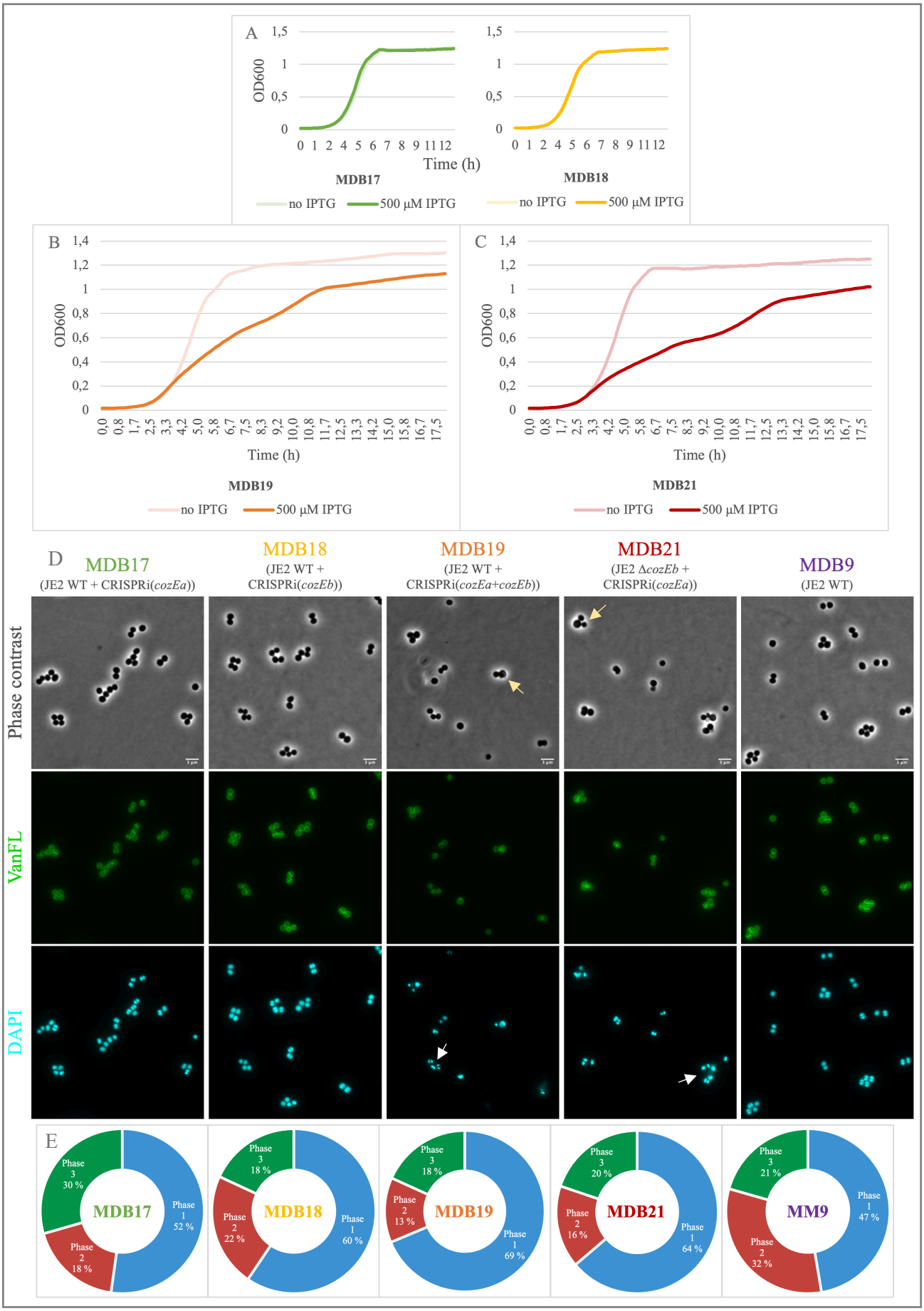

Figure 4.5 Deletion-depletion and double depletion of the *cozE* genes in *S. aureus* JE2.
A. Growth curves of JE2 with single depletions of *cozE* (MDB17) and *cozEb* (MDB18).
B-C. Growth curves of JE2 strains lacking both *cozE* genes. MDB19 have double depletion of *cozE* (**B**), while MDB21 have deletion-depletion of *cozE* (**C**).

D. Phase contrast, VanFL staining and DAPI staining micrographs of JE2 with single depletions (MDB17 and MDB18), double depletion (MDB19), and deletion-depletion (MDB21) of *cozE* (in addition to the control strain MDB9). The cultures are induced with 500 µM IPTG. Yellow arrows point to examples of cells with perturbed cell morphologies, while white arrows point to examples of cells with irregular DAPI signal. Scale represents 3 µm.
E. Distribution of cell cycle phases among JE2 cells with single depletions (MDB17 and MDB18), double depletion (MDB19), and deletion-depletion (MDB21) of *cozE* (in addition to the control strain MDB9). The data was obtained by manual counting the different cell phases of 100-150 random VanFL stained cells from each strain.

As before, cell wall staining (VanFL) of the cells lacking CozEa and CozEb displayed similar staining pattern as their respective wild-types (**Figure 4.4D and 4.5D**). However, it should be noted that the analysis of the cell cycle phases suggested that the absence of both CozE proteins have an impact on the cell cycle, as a higher percentage of cells are in the initial cell cycle phase 1 in most of the double mutant strains (MDB11, MDB19, MDB21). Nucleoid staining (DAPI) of the cells lacking both CozE proteins displayed non-homogeneous staining patters, where a fraction of the cells exhibited a highly intense DAPI signal, highlighted with white arrows in **Figure 4.4D and 4.5D**. This abnormal nucleoid staining was not observed in the wild-type- nor single deletion strains.

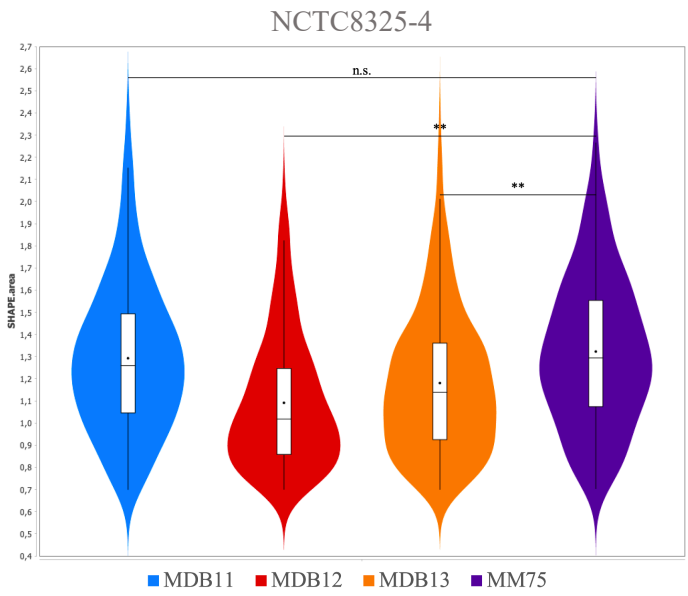

Figure 4.6 Distribution of cell sizes among NCTC8325-4 strains with depletion of one or both *cozE* gene(s). Visualised by violin plot of the cell areas of MDB11 (Δ*cozEa* + CRISPRi(*cozEb*)) (n = 453), MDB12 (Δ*cozEb* + CRISPRi(*cozEa*)) (n = 434), MDB13 (WT + CRISPRi(*cozEa+cozEb*)) (n = 748), and MM75 (WT + CRISPRi(*luc*)) (n = 532) determined using MicrobeJ. The ** indicates strains that are significantly different (p > 0.001, Mann–Whitney test), while n.s indicates strains that are not significantly different (p < 0.001, Mann–Whitney test).

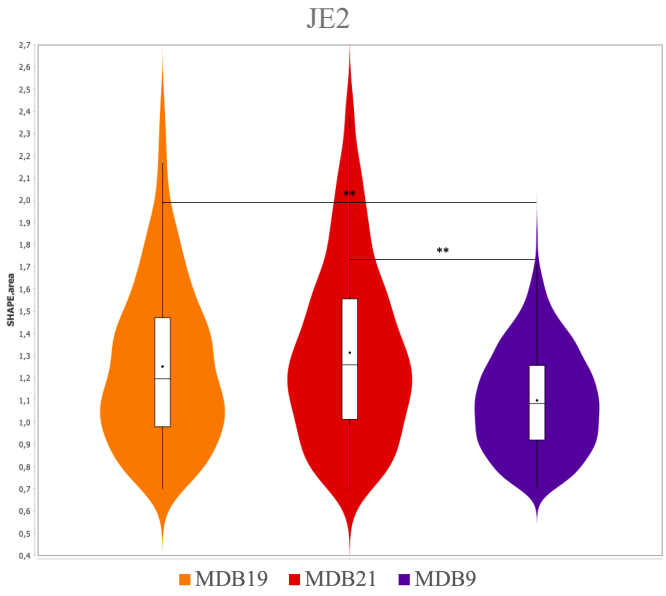

Figure 4.7 Distribution of cell sizes among JE2 strains with depletion of one or both *cozE* gene(s). Visualised by violin plot of the cell areas of MDB19 (WT + CRISPRi(*cozEa+cozEb*)) (n = 1014), MDB21 (Δ*cozEb* + CRISPRi(*cozEa*)) (n = 1206), and MDB9 (WT) (n = 2026) determined using MicrobeJ. The ** indicates strains that are significantly different (p > 0.001, Mann–Whitney test).

4.5 Cells lacking both CozE proteins have mis-localised cell wall synthesis.

Given that VanFL staining did not give any indication of septum abnormalities, localisation of peptidoglycan synthesis was further investigated by staining with the fluorescent D-amino acid HADA. The cells where incubated with HADA for 2 minutes at 37 ºC. Since HADA is

incorporated into newly synthesised peptidoglycan, during this labelling period, it is possible to distinguish sites of active growth from older cell wall. Single deletions of *cozEa* and *cozEb* did not have an impact on the localisation of nascent peptidoglycan, in NCTC8325-4, it was located properly at midcell in distinct ring structures (MDB2 and MDB3 in **Figure 4.8**). However, when both CozE proteins were absent, the synthesis of peptidoglycan was highly altered. The HADA signal of the IPTG induced MDB11 (NCTC8325-4 Δ*cozEa* + CRISPRi(*cozEb*)) cells was shown in clumps rather than at the septum, pointed to by arrows in **Figure 4.8**. Some of the induced MDB11 cells displayed a highly intense HADA signal, while other had no signal. These observations suggest that the peptidoglycan synthesis in *S. aureus* is disturbed when both CozE proteins are absent. This result prompted further analysis of the cell division placement, in *S. aureus* JE2 cells depleted of both CozE proteins, by transmission electron microscopy (TEM). MDB19 (JE2 WT + CRISPRi(cozEa+cozEb)) cells induced with 500 µM IPTG and uninduced MDB19 cells were cut into thin sections (60 nm thick), allowing for observations of their fine internal cell structures. The induced cells displayed a high degree of cells with misplaced and aberrant septa, in addition to a large number of lysed cells (**Figure 4.9B**). Several cells produced non-perpendicular septa resulting in misshaped cells. These phenotypes were not observed in the uninduced cells (**Figure 4.9A**). The TEM images thus revealed that the spatial and temporal coordination of cell division is compromised when cells are lacking both CozEa and CozEb.

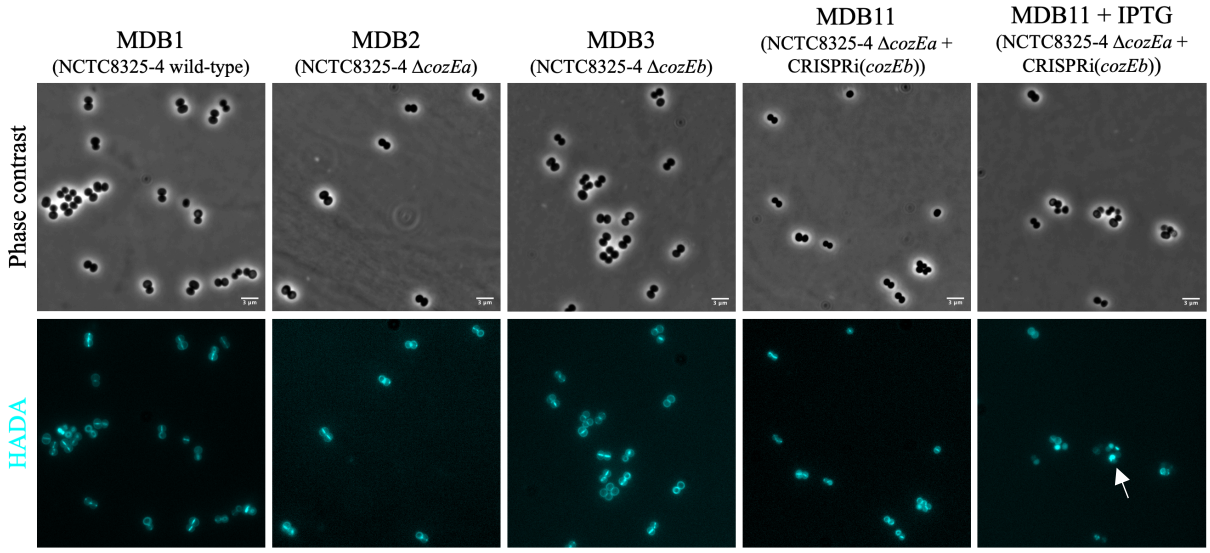

Figure 4.8 Localisation of peptidoglycan synthesis in NCTC8325-4 strains with loss of one or both CozE proteins using HADA staining. Phase contrast and HADA staining micrographs were taken of wild-type (MDB1), Δ*cozEa* (MDB2), Δ*cozEb* (MDB3), and Δ*cozEa* + CRISPRi(*cozEb*) (MDB11) (uninduced and induced with 500 µM IPTG) cells. The cells were incubated with HADA for 2 minutes. Induced MDB11 cells displayed irregular HADA staining (indicated by the white arrow). The scale bars on the phase contrast images represents 3 µm.

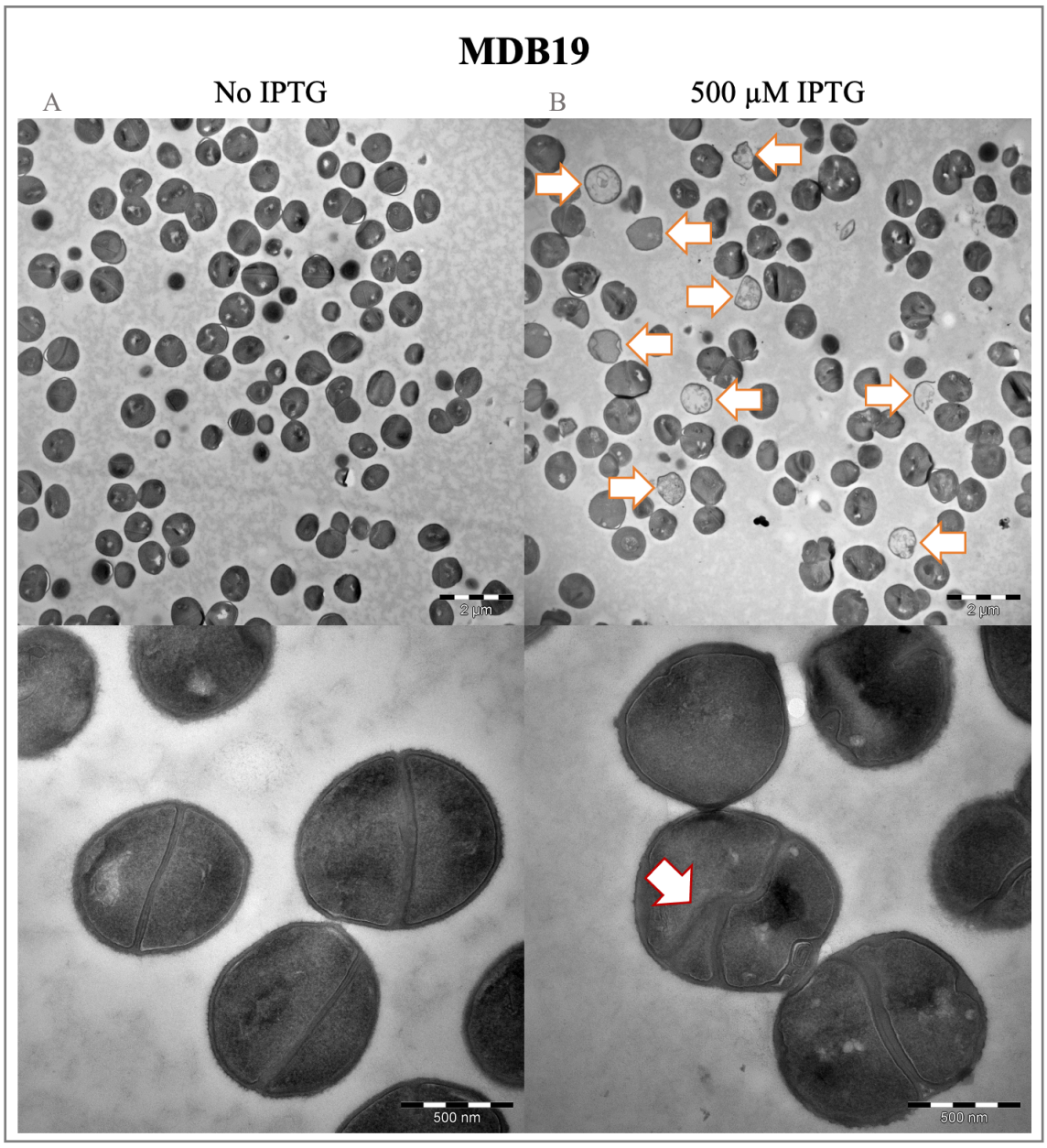

Figure 4.9 Transmission electron micrographs of double *cozE* depleted JE2 cells. (**A**) Uninduced MDB19 (JE2 WT + CRISPRi(*cozEa*+*cozEb*)) and (**B**) MDB19 induced with 500 µM IPTG. The arrows with orange borders point at lysed cells, while the arrow with red border points to a cell with a misplaced septum. Two different magnifications are shown, as indicated by the scale bars (2 µm for the top pictures and 500 nm for the bottom pictures).

4.6 CozEa and CozEb have a spotty and unique dynamic localisation in the bacterial cell membrane.

CozEa and CozEb were previously found to localise to the membrane in *S. aureus* SH1000, with no apparent enrichment in the septum (Stamsås et al., 2018). In that study, CozE-GFP fusions were expressed from a plasmid using an artificial promoter. In order to study the subcellular localisation of the proteins with normal expression levels, *gfp* fused to the 3' end of *cozEa* and *cozEb*, individually, were integrated into the chromosome of the NCTC8325-4 wild-type, generating a strain with a *cozEa-gfp* fusion (MK1582) and a strain with a *cozEb-gfp* fusion

(MK1584). Both fusions were expressed from their native loci with their native promoters. Fluorescent microscopy of these strains demonstrated that both proteins were distributed around the membrane, with a spotty localisation (**Figure 4.10B**). Immunoblotting of MK1582 and MK1584 was performed to verify the expression of the fusion proteins and to compare the relative expression levels of CozEa and CozEb in NCTC8325-4. The immunoprecipitates were resolved by SDS-PAGE and immunoblotted with an anti-GFP antibody. Both mutants expressed the CozE-GFP fusion proteins, considering that the expected sizes of the fusion proteins (67.03 kDa for CozEa-GFP and 71.93 kDa for CozEb-GFP) corresponded to the bands in **Figure 4.10A**. The immunoblot of CozEa-GFP and CozEb-GFP (**Figure 4.10A**) further indicates that there is not a big difference in the expression of the two CozE proteins, although this has to be further verified (**Section 5.3**).

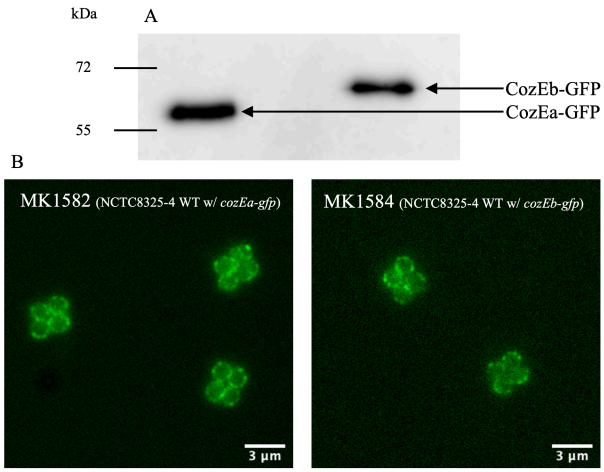

Figure 4.10 The relative expression of CozEa and CozEb (A) and their localisation in the NCTC8325-4 strain (B).
A. The relative expression of CozEa and CozEb is indicated by the band density of CozEa-GFP and CozEb-GFP (from MK1582 and MK1584) in an immunoblot assay using an anti-GFP antibody.
B. The subcellular localisation of CozEa and CozEb analysed by florescent microscopy of MK1582 and MK1584. Scale represents 3 µm.

Time-lapse fluorescent microscopy of MK1582 and MK1584 was also performed to analyse the spatiotemporal localisation of CozEa and CozEb. Interestingly, this revealed that the spotty localisation of the CozE proteins is not static (see the arrows in **Figure 4.11**). Instead, the fluorescence signals move rapidly around in the cell membrane for both, CozEa-GFP and CozEb-GFP.

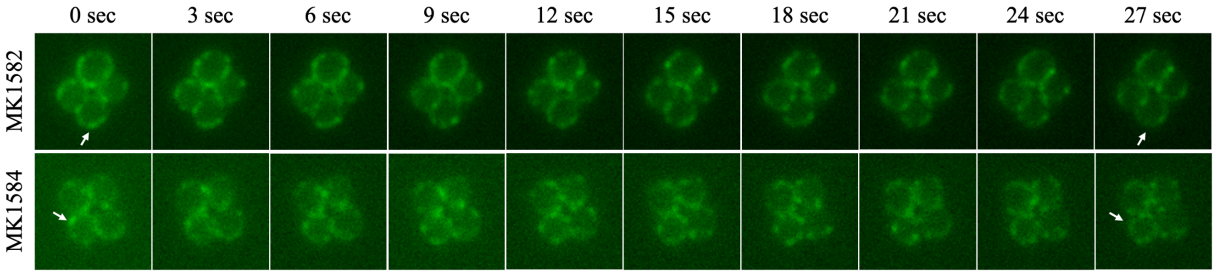

Figure 4.11 Spatiotemporal localisation of CozEa and CozEb in the NCTC8325-4 strain. The movement of the CozE proteins were analysed by time-lapse florescent microscopy of MK1582 (with *cozEa-gfp* fusion) and MK1584 (with *cozEb-gfp* fusion). A picture was taken of the cells every third second (x10). The white arrows indicate that CozEa-GFP and CozEb-GFP move in the membrane, given that the signals pointed to in the first images are not apparent at the same location in the membrane after 27 seconds.

4.7 There is a synthetic genetic link between the *cozE* gens and genes involved in lipoteichoic acid (LTA) synthesis.

The phenotypes of the double *cozE* mutants (Δ*cozEa* + CRISPRi(*cozEb*), Δ*cozEb* + CRISPRi(*cozEa*) and WT + CRISPRi(*cozEa*+*cozEb*)), in both NCTC8325-4 and JE2, are reminiscent of the phenotypes of *S. aureus* mutants affecting teichoic acid (TA) synthesis previously published in literature (Hesser et al., 2020). We therefore wanted to study the CozE proteins in relation to the synthesis of LTA. The interest in studying this relationship also stems from a study performed by Corrigan et al. (2011) that demonstrated that *S. aureus* Δ*ltaS* strains acquired suppressor mutations in *cozEb* (**Section 1.4.3**). A panel of mutant strains were constructed in order to identify potential functional relationships between CozE and LTA synthesis/modification proteins.

The relationship between the *cozE* genes and the genes involved in the synthesis of LTA was first studied in NCTC8325-4, by knocking down *cozE* gene expression together with the genes encoding for the three key LTA synthesising proteins (*ugtP*, *ltaA* and *ltaS*) and for one of the D-alanylating proteins (*dltA*) (**Section 1.3.2**). First, to investigate the effect of the LTA knockdowns, three single sgRNA plasmids each targeting a LTA synthesis/modification gene (*ugtP-ltaA*, *ltaS*, or *dltA*) were made. *ugtP* and *ltaA* are encoded within the same operon and were therefore depleted together in NCTC8325-4. The growth of the resulting strains were analysed in a Δ*cozEa* genetic background (**Figure 4.12,** left panel). The control strain, MDB31, harbouring the non-targeting sgRNA(*luc*) demonstrated that the CRISPRi system itself had no effect on the growth of the Δ*cozEa* mutant, as the growth curve for the uninduced and induced MDB31 cells are identical to each other (**Figure 4.12G**). A distinct growth reduction was not observed upon depletion of *dltA* (MDB30), the only difference was that the induced cells did not reach the same OD_{600} value as the uninduced ones (**Figure 4.12E**). Knockdown of *ugtP-ltaA* (MDB28) and *ltaS* (MDB29), on the other hand, caused a reduction in growth (**Figure 4.12A and 4.12C**), with somewhat more dramatic effects for the *ugtP-ltaA* knockdown compared to the *ltaS*.

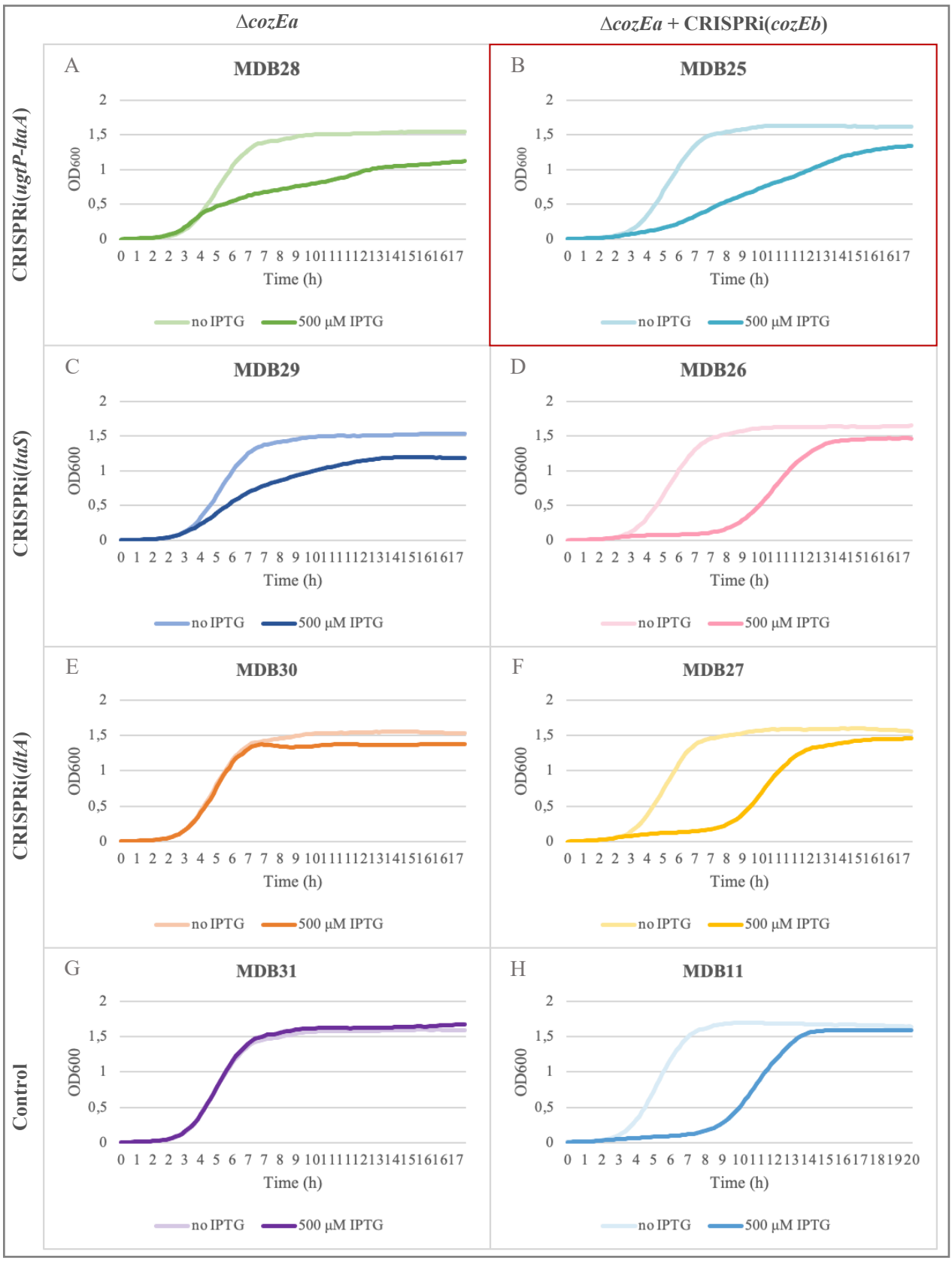

Figure 4.12 Growth of the NCTC8325-4 Δ*cozEa* mutant strains with single knockdown of LTA synthesizing/modifying proteins, and with double knockdown of LTA synthesizing/modifying proteins together with CozEb.
A-B. Growth curves for the NCTC8325-4 Δ*cozEa* mutants targeting *ugtP-ltaA* (**A**) and *ugtP-ltaA+cozEb* (marked with a red boarder) (**B**), with and without IPTG induction.
C-D. Growth curves for the NCTC8325-4 Δ*cozEa* mutants targeting *ltaS* (**C**) and *ltaS+cozEb* (**D**), with and without IPTG induction.
E-F. Growth curves for the NCTC8325-4 Δ*cozEa* mutants targeting *dltA* (**E**) and *dltA+cozEb* (**F**), with and without IPTG induction.
G-H. Growth curves for the NCTC8325-4 Δ*cozEa* mutants targeting *luc* (**G**) and *cozEb* (**H**), with and without IPTG induction (used as controls to find the relation between the LTA synthesising/modifying proteins and the CozE proteins).

We then went on to study the depletion of these LTA synthesis/modification proteins in strains where both *cozEa* and *cozEb* are deleted/depleted at the same time. Three double sgRNA plasmids targeting the LTA synthesis/modification genes together with *cozEb* were constructed (i.e., sgRNA(*ugtP-ltaA*+*cozEb*), sgRNA(*ltaS*+*cozEb*), and sgRNA(*dltA*+*cozEb*), see **Section 3.9.1**, and introduced into a Δ*cozEa* genetic background. Growth in the resulting strains were monitored (**Figure 4.12**, right panel). As before, the depletion of both *cozE* genes resulted in a severe growth defect (**Figure 4.12A**, MDB11, Δ*cozEa* + CRISPRi(*cozEb*)). The growth rate of MDB26 and MDB27, where, respectively, *ltaS* and *dltA* is depleted together with both *cozEb* in a Δ*cozEa* background, was reminiscent of the growth rate of MDB11 (**Figure 4.12D, 4.12F and 4.12H**). This was expected given that the CozE proteins have an overlapping function that is essential to *S. aureus* cells. However, the deprivation of both CozE proteins in cells where *ugtP-ltaA* is depleted (MDB25), on the other hand, did not result in a dramatic growth reduction (**Figure 4.12B**). This double-mutant phenotype was less severe than expected. The Δ*cozEa* + CRISPRi(*cozEb*+*ugtP-ltaA*) strain (MDB25) actually grew similarly to the Δ*cozEa* + CRISPRi(*ugtP-ltaA*) strain (MDB28) (**Figure 4.12B and 4.12A**), suggesting that the detrimental effect of lacking both CozEa and CozEb is lost when UgtP/LtaA is removed. A synthetic genetic relationship was not observed when *ugtP-ltaA* was knocked down in the single Δ*cozEa* or Δ*cozEb* mutant, since these two strains display a similar growth rate to wild-type cells with *ugtP-ltaA* knockdown (**Figure 4.13**). Hence, these results suggest that CozEa and CozEb together perform a function in the cells which is essential only when UgtP/LtaA is present.

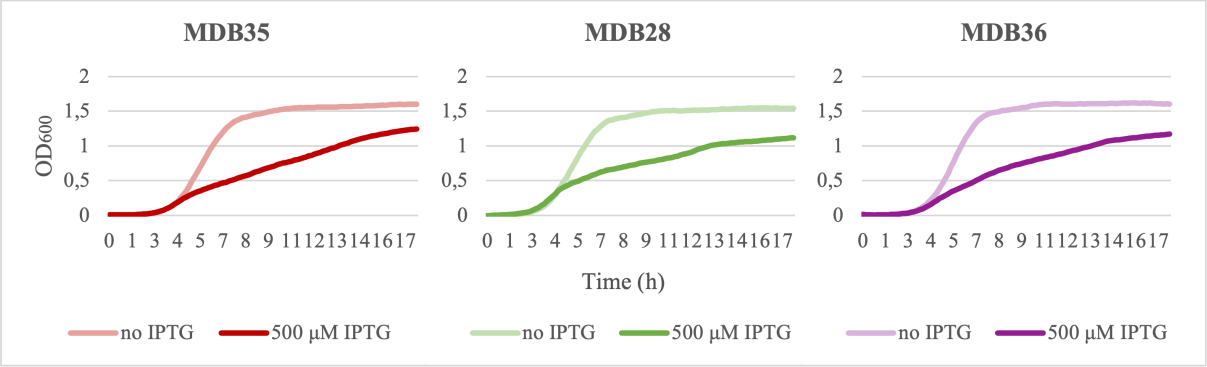

Figure 4.13 Knockdown of *ugtP-ltaA* in single Δ*cozEa* and Δ*cozEb* NCTC8325-4 mutant strains. Growth curves for knockdown of *ugtP-ltA* in wild-type (MDB35), Δ*cozEa* (MDB28), and Δ*cozEb* (MDB36), with and without IPTG induction. All strains display similar growth rates.

To follow up on this intriguing result, JE2 cells with single deletions of *ugtP* and *ltaA* were obtained (Fey et al., 2013), to see if the synthetic link observed between *ugtP*-*ltaA* and *cozE* in NCTC8325-4 was conserved in another strain. Furthermore, using these deletion strains can potentially reveal if the observed effect is due to UgtP and/or LtaA (given that they were depleted together in NCTC8325-4). Single sgRNA plasmids targeting *cozEa*, *cozEb* and *luc* (non-targeting control), as well as a double sgRNA plasmid targeting both *cozE* genes were transformed into the JE2 Δ*ugtP* and JE2 Δ*ltaA* cells. The control plasmid sgRNA(*luc*) and the double sgRNA(*cozEa*+*cozEb*) plasmid targeting both *cozE* genes were in addition transformed into JE2 wild-type cells, for determination of growth rate alterations that can be attributed to the deletion of the LTA synthesising proteins. As expected, no growth reduction was observed upon knockdown of the individual *cozE* genes in the JE2 Δ*ugtP* or Δ*ltaA* cells (MDB54 and MDB55 in **Figure A5.1A**, and MDB56 and MDB57 in **Figure A5.1B**). However, knockdown of *cozEa* and *cozEb*, simultaneously, in Δ*ugtP* or Δ*ltaA* caused dramatic, but opposite, alterations to the growth. The Δ*ugtP* mutant with of depletion both CozE proteins (MDB45) have reduced growth compared to the wild-type cells depleted of *cozEa* and *cozEb* (MDB19) (**Figure 4.14A and 4.14B**). The MDB45 cells are barely viable. On the contrary, the Δ*ltaA* mutant lacking both CozE proteins (MDB46) grew equally well as the Δ*ltaA* control strain (MDB48) (**Figure 4.14C**). Thus, the depletion of CozE proteins have no effect on growth in absence of LtaA. These results suggest: (1) that the CozE proteins have a combined activity in the LTA synthesis, given that only depletion of CozEa and CozEb together led to alterations in growth, and (2) that both *ugtP* and *ltaA* have a pairwise synthetic genetic interaction with the *cozE* genes, given that double deletion of these genes cause stronger phenotypic effects than expected, seen in the light of deleting each gene individually (with *ugtP* increasing lethality and *ltaA* increasing fitness).

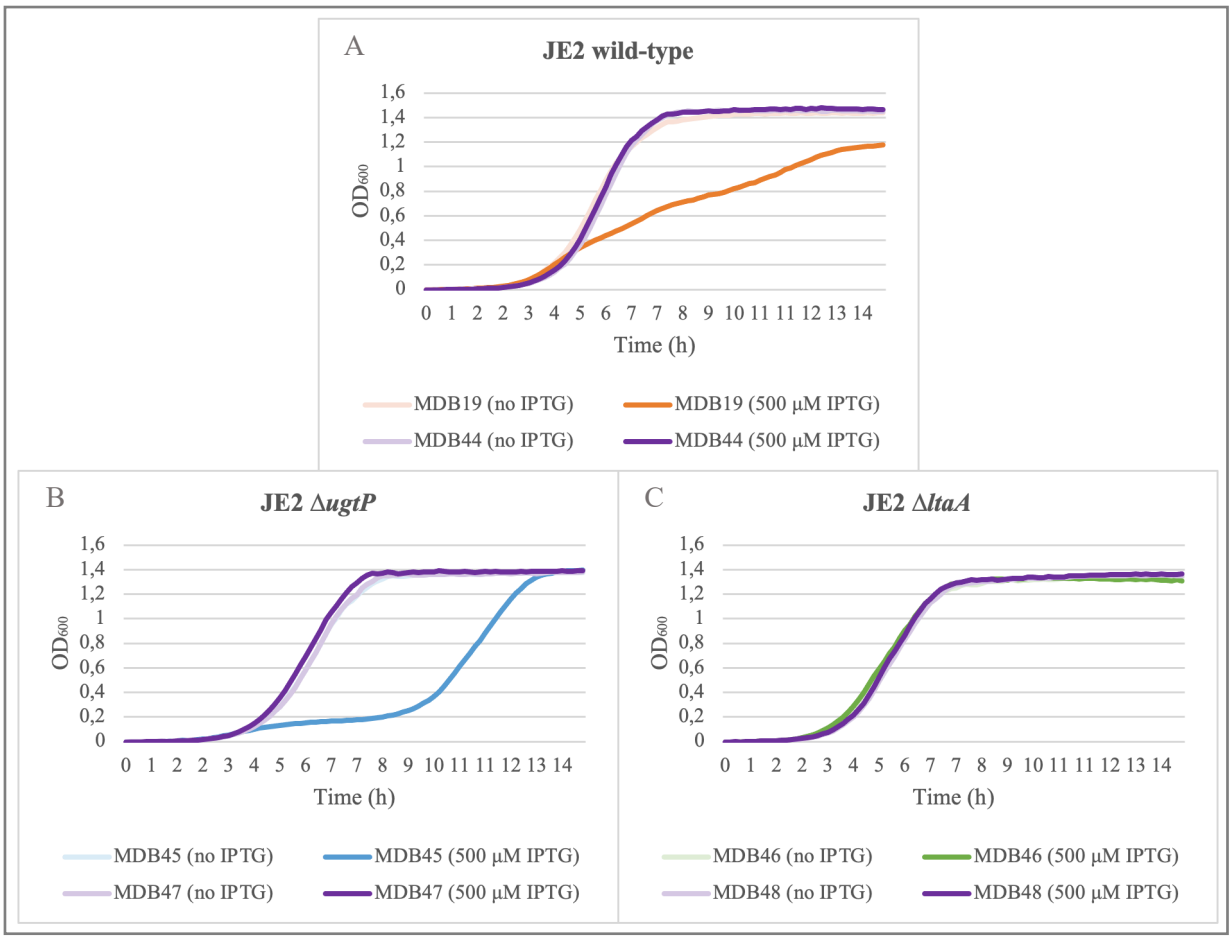

Figure 4.14 Growth of the JE2 WT, Δ*ugtP*, and Δ*ltaA* cells with double *cozE* knockdown.
A. Growth curves for the JE2 WT strains targeting *cozEa+cozEb* (MDB19) and *luc* (MDB44), with and without IPTG induction.
B. Growth curves for the JE2 Δ*ugtP* strains targeting *cozEa+cozEb* (MDB45) and *luc* (MDB47), with and without IPTG induction.
C. Growth curves for the JE2 Δ*ltaA* strains targeting *cozEa+cozEb* (MDB46) and *luc* (MDB48), with and without IPTG induction.

To further confirm if the opposite growth alterations observed when depleting both *cozE* genes in the Δ*ugtP* and Δ*ltaA* JE2 mutants can be reproduced in another *S. aureus* strains, the same analysis was conducted in *S. aureus* NCTC8325 cells. The lab had obtained a NCTC8325 wild-type strain and a NCTC8325 Δ*ltaA* strain (Zhang et al., 2020), but lacked a NCTC8325 strain with an *ugtP* deletion. The NCTC8325 Δ*ugtP* mutant strain was therefore constructed using the pMAD-Δ*ugtP*::*spc* plasmid, as described in **Section 3.11.3**. Growth assays of the different NCTC8325 strains with knockdown of both *cozE* genes (**Figure 4.15**) were done in the same manner as for JE2 (**Figure 4.14**), and indeed the same growth phenotypes were observed in NCTC8325 as in the JE2 strains. Thus, no growth reduction was observed upon knockdown of the individual *cozE* genes in Δ*ugtP* cells (MDB82 and MDB83 in **Figure A5.2**), however knockdown of *cozEa* and *cozEb*, simultaneously, in Δ*ugtP* cells resulted in severely reduced growth (MDB84 in **Figure 4.15B**) compared to the strain deprived of only CozE proteins

(**Figure 4.15A**). On the other hand, Δ*ltaA* cells with induced depletion of both *cozEa* and *cozEb* grew similarly to the uninduced cells (**Figure 4.15C**).

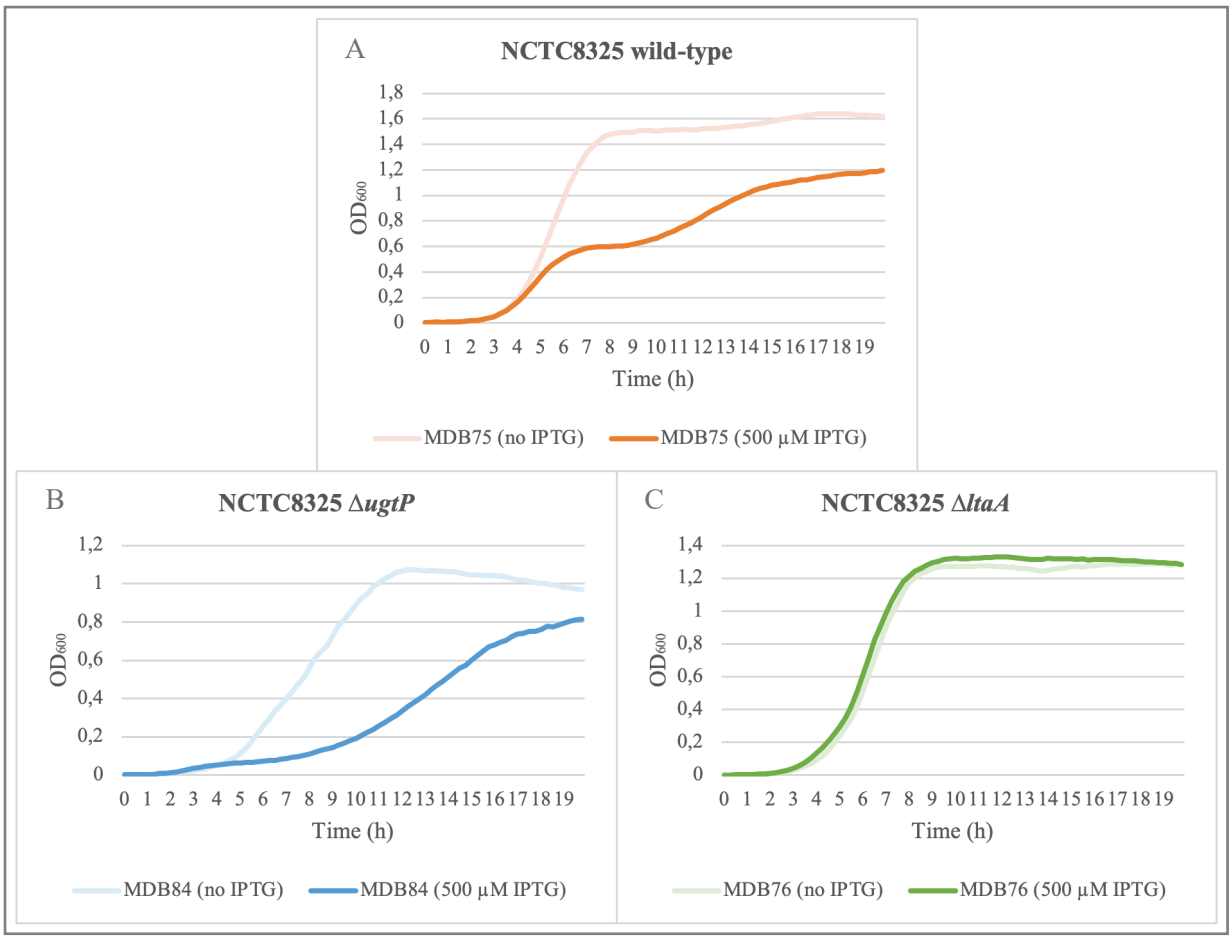

Figure 4.15 Growth of the NCTC8325 WT, Δ*ugtP*, and Δ*ltaA* cells with double *cozE* knockdown.
A. Growth curve for the NCTC8325 WT strain targeting *cozEa*+*cozEb* (MDB75), with and without IPTG induction.
B. Growth curve for the JE2 Δ*ugtP* strain targeting *cozEa*+*cozEb* (MDB84), with and without IPTG induction.
C. Growth curve for the NCTC8325 Δ*ltaA* strain targeting *cozEa*+*cozEb* (MDB76), with and without IPTG induction.

The pairwise synthetic genetic interaction between *ugtP*/*ltaA* and *cozE* were further investigated by performing TEM, of JE2 cells depleted of both *cozE* genes in Δ*ugtP* and Δ*ltaA* genetic backgrounds, to give an indication of the effect these synthetic interactions have on cell division and septum placement. As described above, it was observed that cells depleted of both CozE proteins had misplaced and aberrant septa, in addition to a large number of lysed cells (induced MDB19 cells in **Figure 4.9B**). However, in the Δ*ltaA* genetic background, double *cozE* knockdown (MDB46 in **Figure 4.16B**) displayed a similar phenotype as JE2 wild-type cells (uninduced MDB19 cells in **Figure 4.9A**), with few lysed cells and virtually no misplaced septa. This is in line with the results from the growth experiments and indicates that the spatial and temporal coordination of cell division, that is lost when both *cozE* genes are lacking in JE2

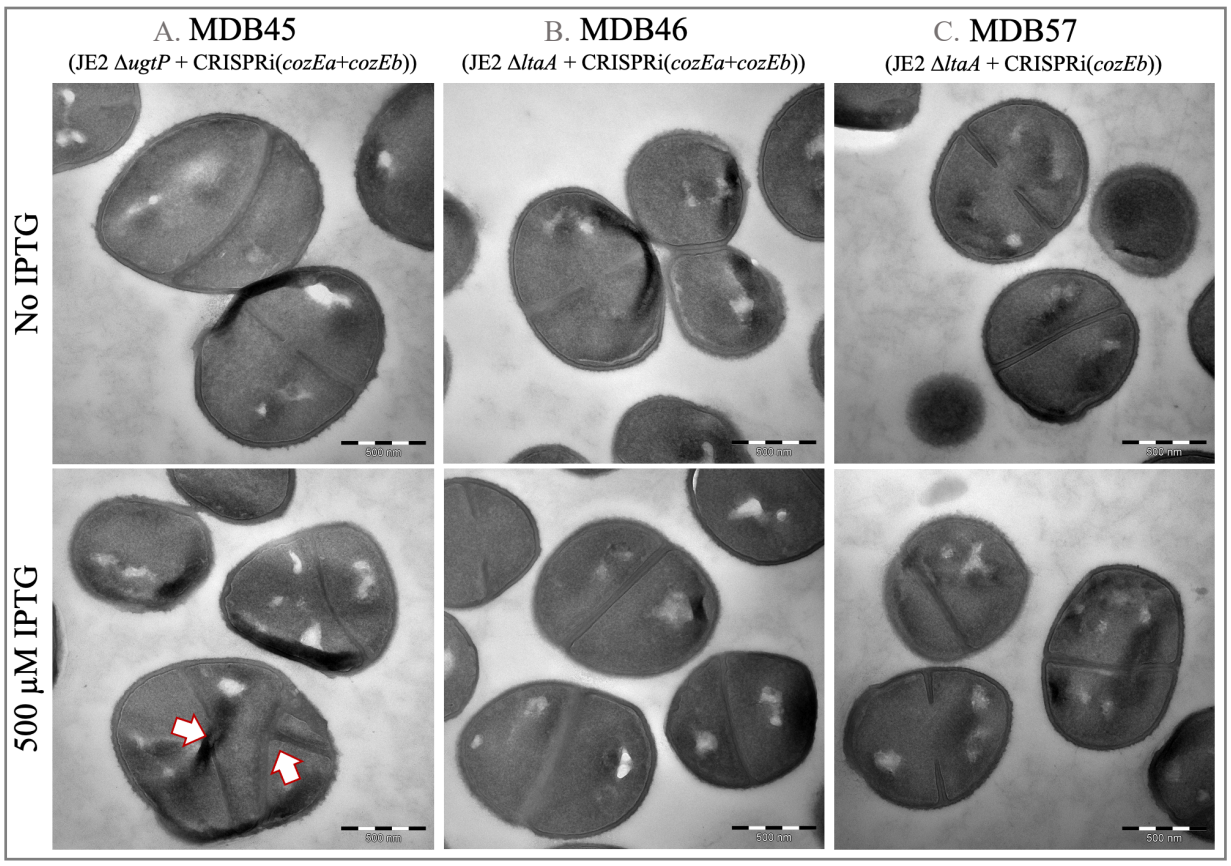

Figure 4.16 Septum placement in Δ*ugtP* and Δ*ltaA* JE2 cells with *cozE* depletions. Visualised by transmission electron micrographs of MDB45 (JE2 Δ*ugtP* + CRISPRi(*cozEa*+*cozEb*)) (**A**), MDB46 (JE2 Δ*ltaA* + CRISPRi(*cozEa*+*cozEb*)) (**B**), and MDB57 (JE2 Δ*ltaA* + CRISPRi(*cozEb*)) (**C**), with and without IPTG induction. The arrows with red border point to misplaced septa. The scale bars on the TEM images represents 500 nm.

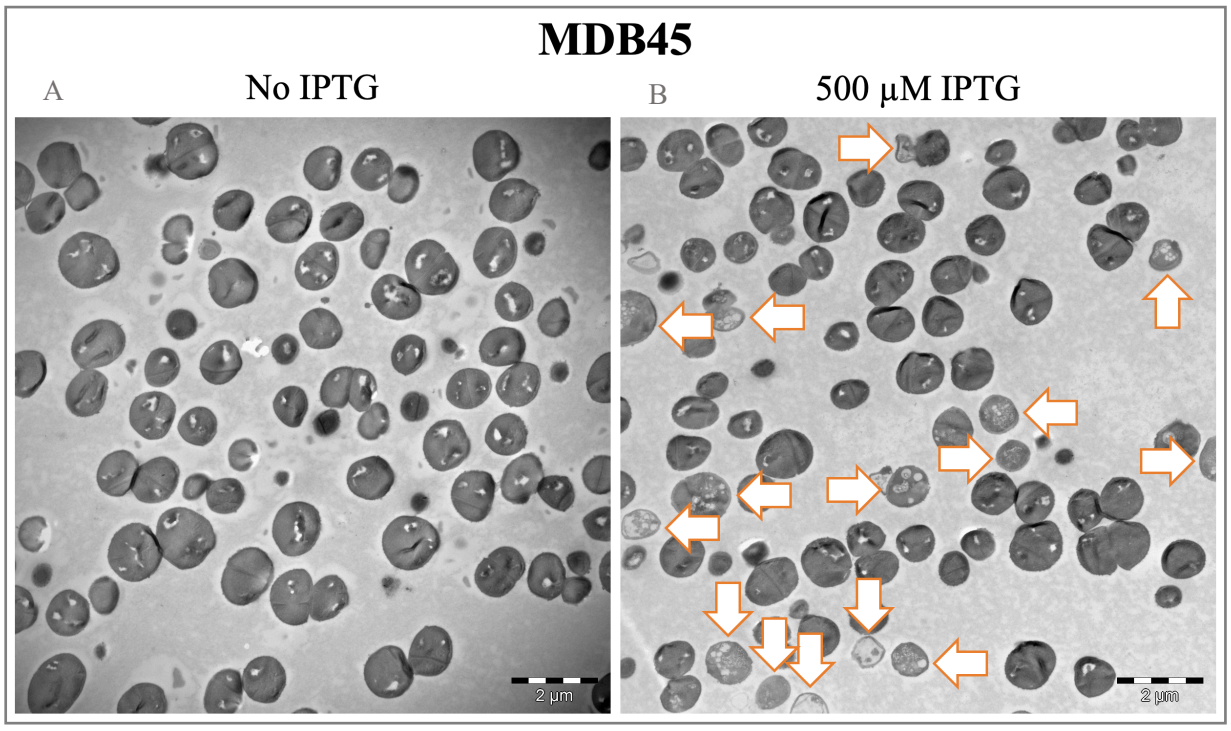

Figure 4.17 The extent of cell lysis in the JE2 ΔugtP strain with and without double *cozE* depletion. Visualised by transmission electron micrographs of MDB45 (JE2 Δ*ugtP* + CRISPRi(*cozEa*+*cozEb*)) with no induction (**A**) and induced with 500 µM IPTG (**B**). The arrows with orange borders point to lysed cells. The scale bars on the TEM images represents 2 µm.

wild-type cells (**Figure 4.9B**), is re-established in Δ*ltaA* cells (**Figure 4.16B**). The Δ*ugtP* cells with knockdown of both *cozEa* and *cozEb*, on the other hand, displayed several lysed cells and cells with septal abnormalities (**Figure 4.16A and 4.17B**). This suggests that cell division is still compromised when *ugtP* is deleted in cells depleted of both CozE proteins, although the phenotype of MDB45 does not appear to more extreme than the one for MDB19 (**Figure 4.9**), as observed for the growth assays.

4.8 LTA polymer length is altered in *S. aureus* Δ*cozEb* mutants.

Studies have demonstrated that *S. aureus ugtP* and *ltaA* deletion mutants display growth defects due to production of abnormally long LTA polymers (as a result of the loss of glycolipid anchors) (Hesser et al., 2020). To determine the relative lengths of LTA polymers, exponential phase *S. aureus* lysates were separated by SDS-PAGE and visualised by immunoblotting with an anti-LTA antibody. The increased length of LTA polymers in Δ*ltaA* and Δ*ugtP* mutants were confirmed here in both NCTC8325-4 and JE2. The LTA polymer size appears to be more affected by loss of *ugtP* and *ltaA* in NCTC8325-4 (MDB35 in **Figure 4.21**), than in JE2 (MDB39 and MDB40 in **Figure 4.22**), although it is difficult to compare the two given that *ugtP* and *ltaA* are depleted together in NCTC8325-4 while single deletions are studied in JE2. It was therefore interesting to test if LTA polymer length is also altered in the *S. aureus cozE* deletion mutants. Interestingly, the length of the LTA polymers increases in the Δ*cozEb* mutants, but not in the Δ*cozEa* mutants (**Figure 4.18 and 4.19**). The LTA size does not increase further in the Δ*cozEb* + CRISPRi(*cozEa*) double mutant (MDB12 in **Figure 4.18**), suggesting that only *cozEb* play a role in controlling LTA polymer length in *S. aureus*. The quantity of LTA polymers produced in the cells does not seem to be affected by deletion of *cozE*, indicated by relatively similar band intensities in the immunoblots in **Figure 4.18 and 4.19**.

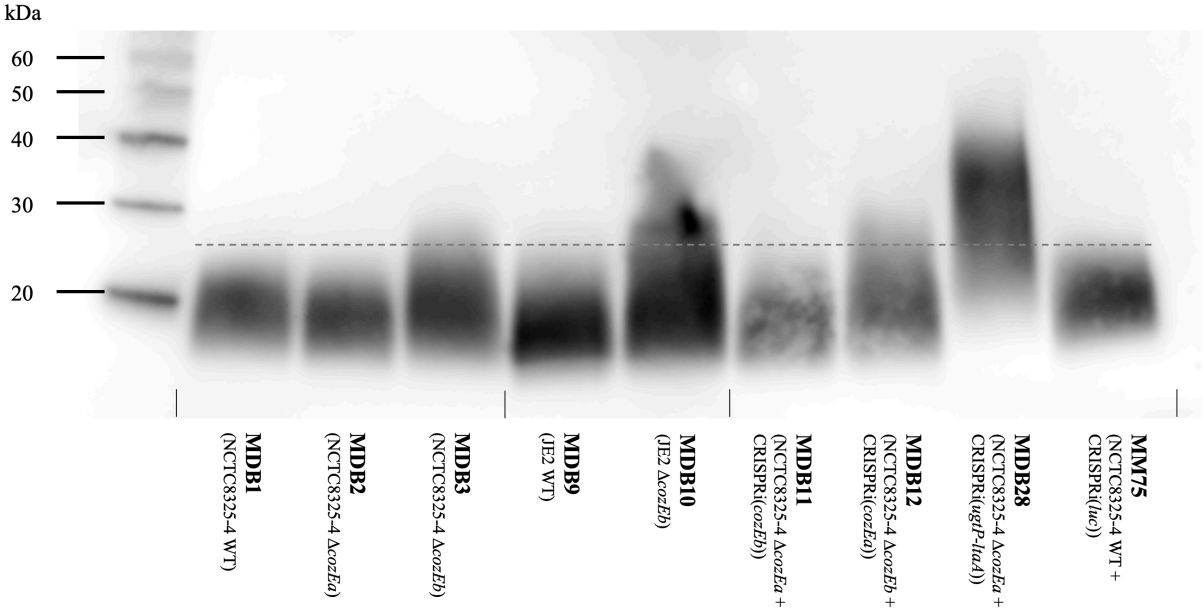

Figure 4.18 Anti-LTA immunoblot of *S. aureus* (NCTC8325-4 and JE2) lysates with deletion/depletion of *cozE*. LTA polymer size is altered in MDB3, MDB10, MDB12, and MDB28 (indicated by the dotted line).

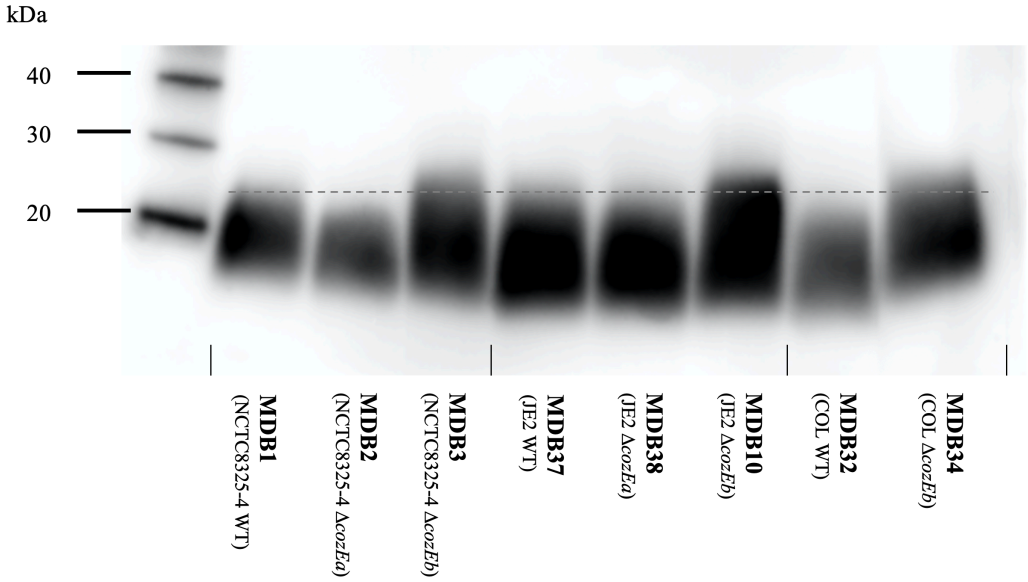

Figure 4.19 Anti-LTA immunoblot of *S. aureus* (NCTC8325-4, JE2, and COL) lysates with single *cozE* deletions. LTA polymer size is altered in MDB3, MDB10, and MDB34 (indicated by the dotted line).

4.9 The LTA size phenotype of Δ*cozEb* mutants can be complemented with ectopic expression of *cozEb*.

To see if the LTA size phenotype observed in strains lacking *cozEb* could be complemented by ectopic expression of *cozEa* and/or *cozEb*, the complementation plasmids pRAB11-*cozEa* and pRAB11-*cozEb* were transformed into NCTC8325-4 and JE2 Δ*cozEb* mutant cells. Expression of genes from the pRAB11 plasmid was induced with addition of anhydrotetracycline (aTc). First, to determine the exact concentration for induction of the *S. aureus* strains that could be

used without inhibiting growth (aTc inhibits growth at high concentrations), growth assays of MDB63 (NCTC8325-4 Δ*cozEb* + pRAB11-*lacA* (control plasmid)) and MDB61 (JE2 Δ*cozEb* + pRAB11-*lacA* (control plasmid)) were performed, with a 2-fold dilution series of aTc (**Figure 4.20**). The highest concentration of aTc that did not cause growth defects of MDB63 and MDB61 was ~0.0039 µg/mL. In this work, all strains carrying the pRAB11 plasmid were therefore induced with 0.004 µg/mL aTc.

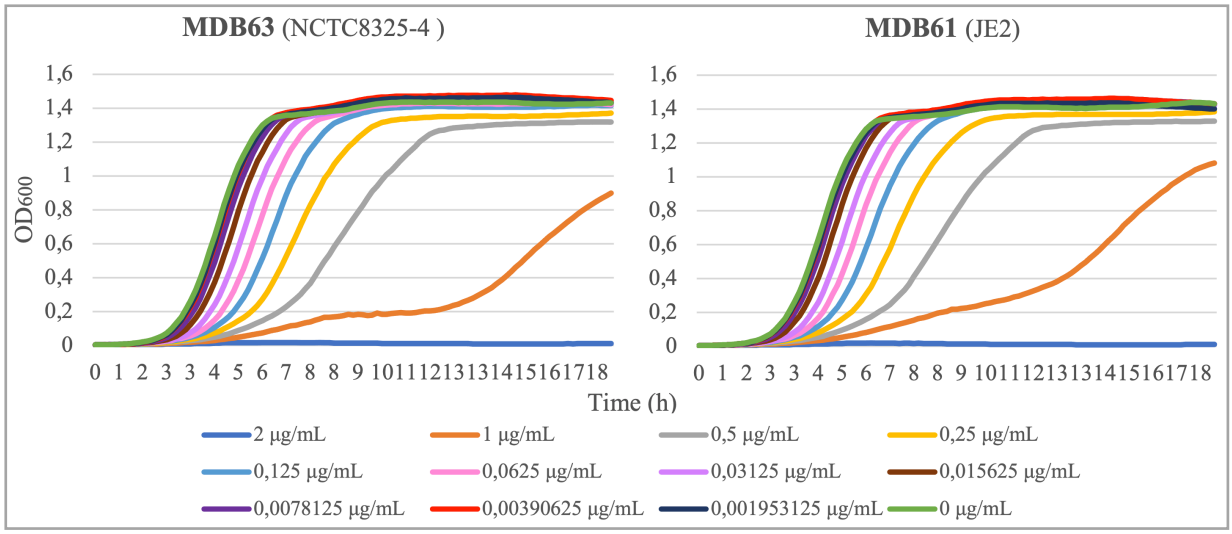

Figure 4.20 Growth curves for MDB63 and MDB61 induced with a 2-fold dilution series of aTc (starting with 2 µg/mL aTc), conducted to find the appropriate aTc concentration for induction of the *S. aureus* strains (NCTC8325-4 and JE2) carrying pRAB11 plasmids.

Using the inducible complementation plasmid for *cozEb*, the increased LTA length observed in the Δ*cozEb* mutants could indeed be restored to wild-type length, in both NCTC8325-4 and JE2 (MDB62 and MDB60 in **Figure 4.21 and 4.22**). This observation indicates that the LTA phenotype observed in the Δ*cozEb* mutants is in fact a result of the lack of CozEb and not another undetected genomic change. The LTA size of the Δ*cozEb* mutants were, however, not restored by introducing the pRAB11-*cozEa* complementation plasmid (MDB58 and MDB59 in **Figure 4.21 and 4.22**), once again suggesting that CozEb have a unique role in the LTA synthesis.

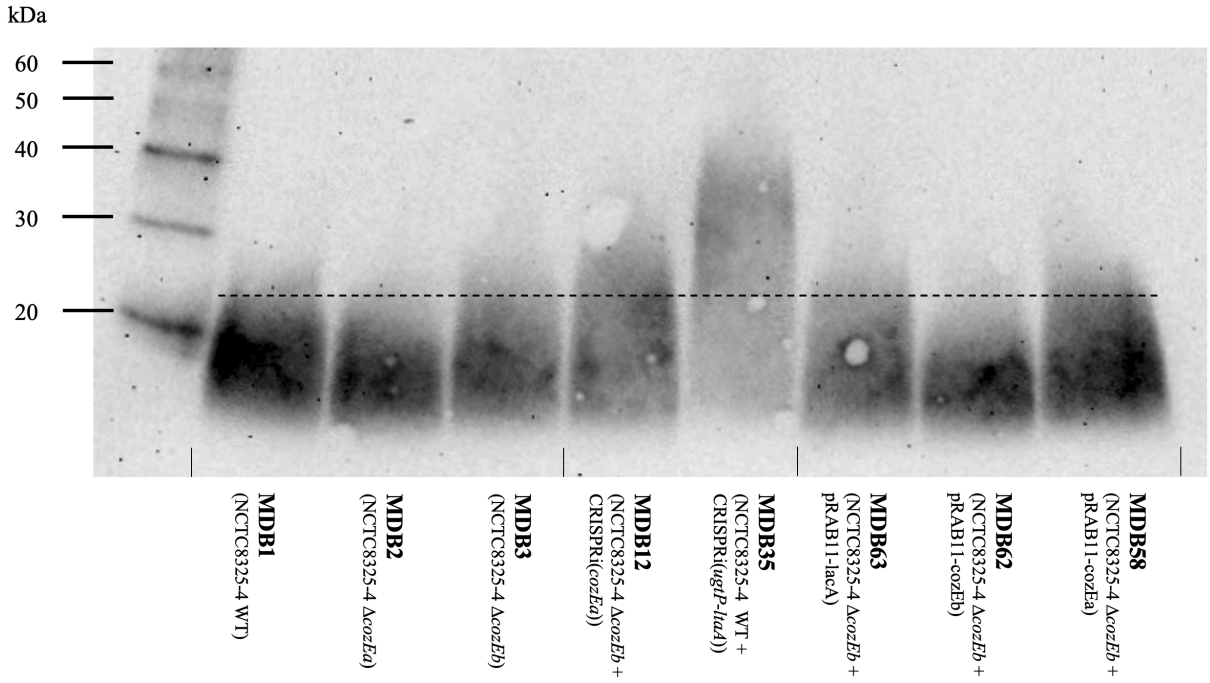

Figure 4.21 Anti-LTA immunoblot of NCTC8325-4 *S. aureus* lysates complemented with pRAB11-*cozEa*/*cozEb*. LTA polymer size is restored in MDB62 (indicated by the dotted line).

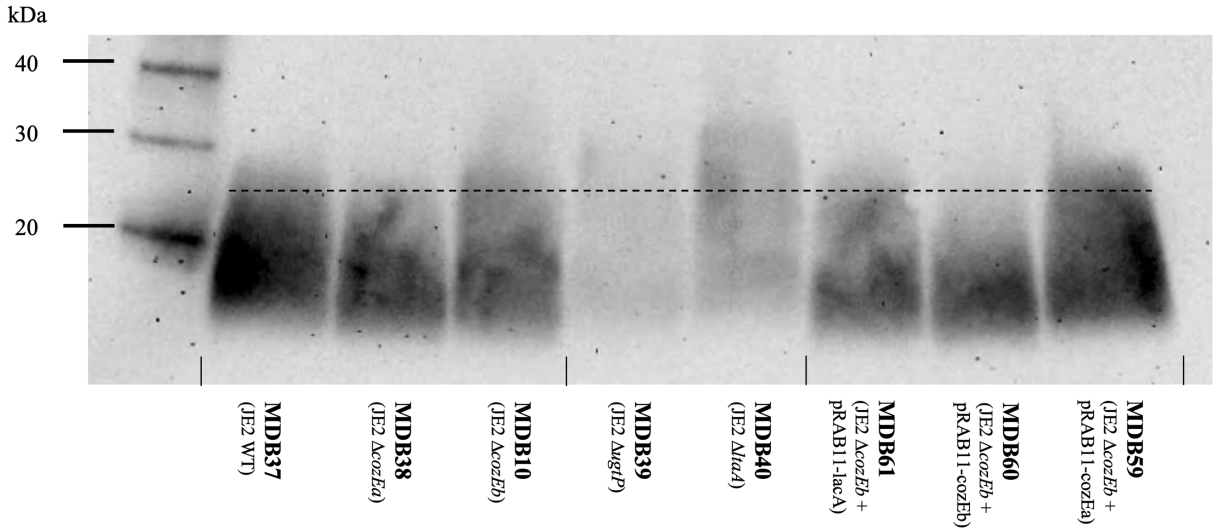

Figure 4.22 Anti-LTA immunoblot of JE2 *S. aureus* lysates complemented with pRAB11-*cozEa*/*cozEb*. LTA polymer size is restored in MDB60 (indicated by the dotted line).

4.10 LTA length is further increased in strains with combined mutations of *ltaA*, *ugtP* and *cozE*.

Above, it was shown that deletion of *cozEb* increased LTA length, similar to what was observed for *ltaA* and *ugtP* deletion strains. To study the combined effect of these genes on the LTA-length, *cozE* was depleted in JE2 strains where *ugtP* and *ltaA* were deleted individually (**Figure 4.23**). When *cozEb* or *cozEa*+*cozEb* were depleted in the Δ*ltaA* background, the polymer length seemed to be somewhat further increased (MDB46 and MDB57 compared to MD19 and

MDB48 in **Figure 4.23**). The same was not observed upon depletion of *cozEa* in Δ*ltaA* (MDB56 compared to MDB19 and MDB48 in **Figure 4.23**), again showing that CozEa has no role in LTA length control.

Regarding the Δ*ugtP* mutants, it is more difficult to conclude any effect on LTA polymer length upon depletion of the *cozE* genes. The reason for this is that Δ*ugtP* mutants appear to produce less total LTA, and thus produce weak bonds during immunoblotting. Also worth noting, the LTA polymers produced by Δ*ltaA* (MDB48) are expected to be shorter than those of Δ*ugtP* (MDB47), due to their small production of LTAs linked to Glc_2-DAGs (Hesser et al., 2020) (**Section 1.3.2**). This was, however, not observed in *S. aureus* JE2 in the present study (**Figure 4.23**).

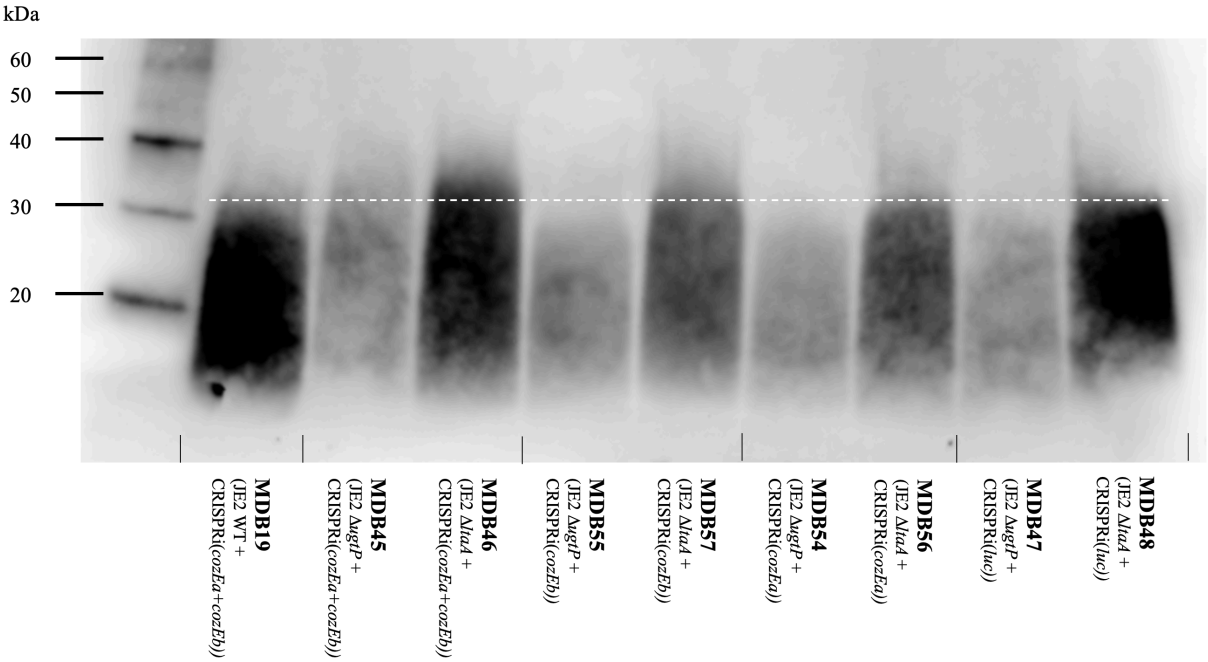

Figure 4.23 Anti-LTA immunoblot of *S. aureus* JE2 Δ*ugtP* and Δ*ltaA* lysates with *cozE* depletion. LTA polymer size appears to be further increased in MDB45, MDB46, and MDB57 (indicated by the dotted line), and the total quantity of LTAs seems to be reduced in the Δ*ugtP* mutants.

4.11 UgtP have a spotty and dynamic localisation in the bacterial cell membrane.

Above we have established that there is a synthetic genetic relationship between CozE proteins and LTA synthesis (UgtP and LtaA), and that CozEb affect LTA polymer length. We have also observed that CozE proteins have a spotty, dynamic localisation in the cell membrane. Next, trying to understand how CozE proteins may affect LTA synthesis, the subcellular localisation of UgtP was analysed. Fluorescence microscopy was used to observe the localisation of GFP-

UgtP expressed both from its native locus (constructed using pMAD-*gfp_ugtP::*spc) and ectopically from a plasmid (pLOW-*gfp_ugtP*).

The strains carrying the plasmid pLOW-*gfp_ugtP*, have the fusion genes located downstream of an IPTG-inducible promoter. The expression was initially induced with 500 µM IPTG. However, this concentration was too high for induction of these strains, resulting in oversaturated signals. MDB64 (NCTC8325-4 WT carrying pLOW-*gfp_ugtP*) was therefore induced with five different IPTG concentrations (10 µM, 50 µM, 100 µM, 250 µM and 500 µM) to find the appropriate concentration for induction of *gfp-ugtP* expression (**Figure 4.24**). The highest concentration of IPTG that gave a distinct localisation to the cell membrane was 50 µM IPTG, and this concentration was used for further induction of the strains carrying pLOW-*gfp_ugtP*.

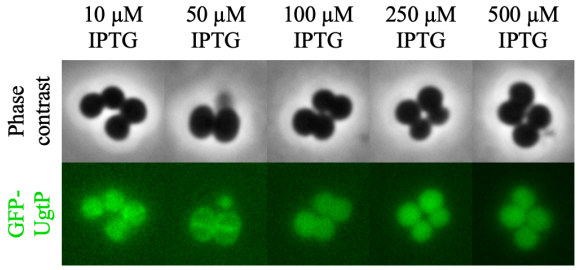

Figure 4.24 Florescent microscopy of MDB64 (NCTC8325-4 WT + pLOW-*gfp_ugtP*) induced with five different IPTG concentrations (10 µM, 50 µM, 100 µM, 250 µM, and 500 µM). Conducted to find a suitable concentration of IPTG for induction of the strains carrying pLOW-*gfp_ugtP*.

Fluorescence microscopy of MDB64 (pLOW-gfp_ugtP) and MDB77 (chromosomal *gfp-ugtP*) revealed that UgtP have a spotty localisation to the bacterial membrane in NCTC8325-4 (**Figure 4.26** (plasmid) **and 4.28** (chromosomally)). Time-lapse fluorescent microscopy of MDB64 was performed to detect the spatiotemporal localisation of UgtP. UgtP did not have any evident mobility as pointed out by the arrows in **Figure 4.25**. However, time-lapse fluorescent microscopy of MDB77 (chromosomal *gfp-ugtP*) suggest that *ugtP* actually have mobility in the membrane (**Figure 4.29**). The discrepancy observed between MDB64 and MDB77 are most likely due to their difference in GFP-UgtP expression. The observation of MDB77 is most credible as it express GFP-UgtP chromosomally.

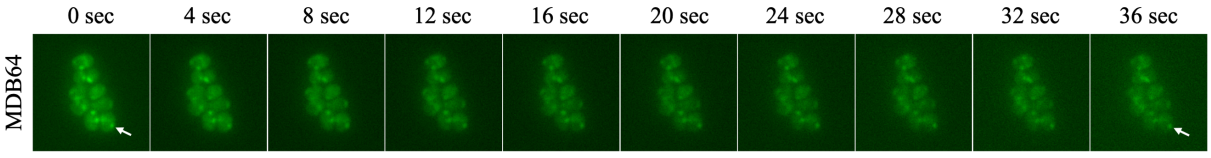

Figure 4.25 Spatiotemporal localisation of UgtP in the NCTC8325-4 wild-type strain expressing GFP-UgtP ectopically from pLOW-*gfp_ugtP*. The movement of UgtP was analysed by time-lapse florescent microscopy of MDB64 (NCTC8325-4 WT + pLOW-*gfp_ugtP*). A picture was taken of the cells every forth second (x10). The white arrows show that the fluorescence signal in the membrane does not move during the 36 seconds the cells are observed.

4.12 UgtP's localisation is not lost in the absence of CozE.

UgtP is a cytoplasmic protein with no predicted transmembrane segments. Previous work has demonstrated that UgtP's localisation to the membrane in *S. aureus* (more specifically the RN4220 strain) is independent of the UDP-Glc substrate. Though, the protein(s) or molecule(s) responsible for the recruitment of UgtP to the membrane is still unknown (Reichmann et al., 2014). The spotty and dynamic membrane localisation of UgtP, observed in NCTC8325-4, is reminiscent of the localisation observed for the two CozE proteins (**Figure 4.11**). CozEa and CozEb are multimembrane spanning proteins, and one of them/both could possibly be involved in the recruitment of UgtP to the membrane. To test this, the pLOW-*gfp_ugtP* plasmid was initially transformed into NCTC8325-4 cells where *cozEa* and *cozEb* had individually been deleted (MDB65 and MDB66, respectively). Fluorescence microscopy of MDB65 and MDB66 demonstrated that single deletions of *cozE* did not alter UgtP's localisation. UgtP had a spotty localisation in the membrane in all three strain (**Figure 4.26**). The movement of the UgtP protein was also not affected, as demonstrated by time-lapse fluorescent microscopy of MDB65 and MDB66 (**Figure 4.27**). Similar to the MDB64 cells the GFP-UgtP signals in these cells does not seem to move in the membrane.

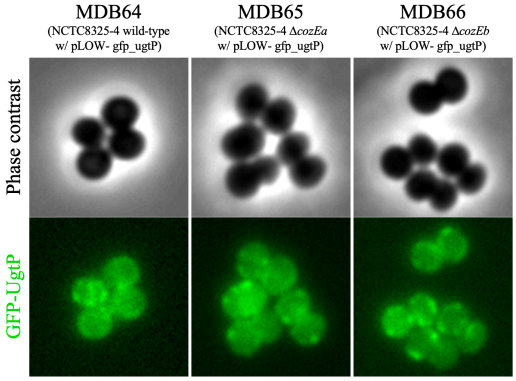

Figure 4.26 UgtP's localisation in the NCTC8325-4 strains with single *cozE* deletions expressing GFP-UgtP ectopically from pLOW-*gfp_ugtP*. The subcellular localisation of UgtP was analysed by florescent microscopy of MDB64 (wild-type), MDB65 (Δ*cozEa*), and MDB66 (Δ*cozEb*).

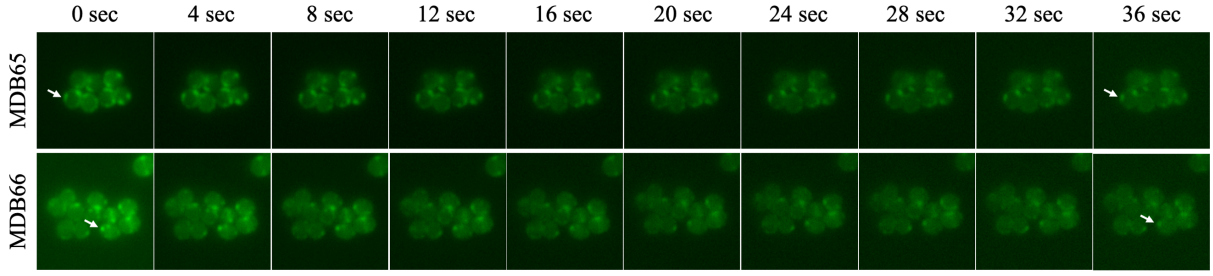

Figure 4.27 Spatiotemporal localisation of UgtP in the NCTC8325-4 strains with single *cozE* deletions expressing GFP-UgtP ectopically from pLOW-*gfp_ugtP*. The movement of UgtP was analysed by time-lapse florescent microscopy of MDB65 (Δ*cozEa*) and MDB66 (Δ*cozEb*). A picture was taken of the cells every forth second (x10). The white arrows show that the fluorescence signal in the membrane does not move during the 36 seconds the cells are observed.

Furthermore, knockdown of both *cozE* genes, in the NCTC8325-4 strain with *gfp* fused to *ugtP*, demonstrated that loss of both CozEa and CozEb did not alter UgtP's localisation either (**Figure 4.28**). UgtP still have a spotty and dynamic localisation to the cytoplasmic membrane, as demonstrated with time-lapse fluorescent microscopy of MDB79 (**Figure 4.29**). Our hypothesis that CozEa and CozEb are involved in the recruitment of UgtP to the membrane was thus falsified.

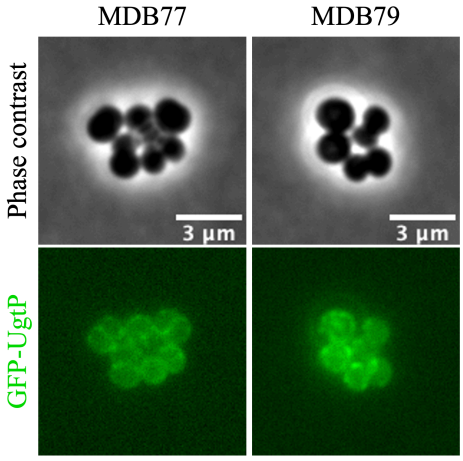

Figure 4.28 UgtP's localisation in the NCTC8325-4 strains expressing GFP-UgtP chromosomally. The subcellular localisation of UgtP was analysed by florescent microscopy of MDB77 (WT) and MDB79 (WT + CRISPRi(*cozEa+cozEb*)).

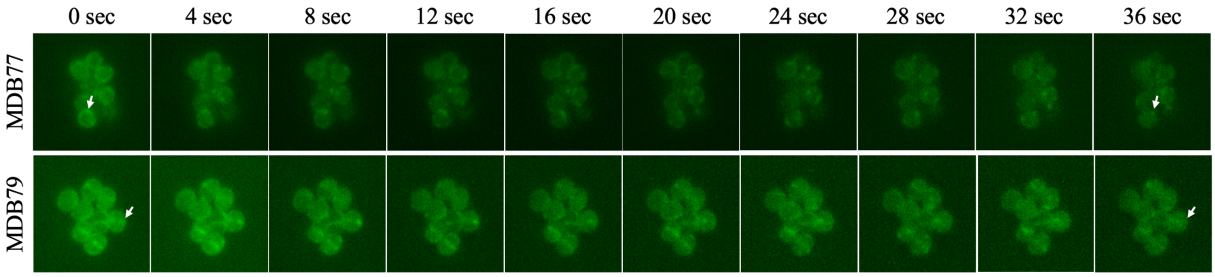

Figure 4.29 Spatiotemporal localisation of UgtP in the NCTC8325-4 strains expressing GFP-UgtP chromosomally (both wild-type and double *cozE* depleted cells). The movement of UgtP was analysed by time-lapse florescent microscopy of MDB77 (WT) and MDB79 (WT + CRISPRi(*cozEa+cozEb*)). A picture was taken of the cells every forth second (x10). The white arrows indicate that GFP-UgtP move in the membrane, given that the signals pointed to in the first images are not apparent at the same location in the membrane after 36 seconds.

4.13 Susceptibility to antibiotics targeting the cell wall and envelope is not severely altered in the NCTC8325-4 *cozE* mutants.

CozEa and CozEb are important for proper cell division and cell wall formation in *S. aureus*, and lack of them could therefore possibly alter *S. aureus'* susceptibility to cell wall and cell envelope active antibiotics. Furthermore, mutants with LTA synthesis defects have been shown to have increased sensitivity to β-lactams and other antimicrobials targeting the cell wall (Hesser et al., 2020). Therefore, NCTC8325-4 wild-type (MDB1), Δ*cozEa* (MDB2), Δ*cozEb* (MDB3) and CRISPRi(*cozEa+cozEb*) (MDB11, induced with different IPTG concentrations) were incubated in MH medium, serially diluted with daptomycin, oxacillin and vancomycin, to determine if the *cozE* mutants exhibited changed sensitivity to these antibiotics. The strains' minimum inhibitory concentration (MIC) values for the various antibiotics were set as the lowest concentration that resulted in an OD_{600} value below 0.1 after ~18 hours incubation at 37 ^{o}C.

The susceptibility of MDB2 and MDB3 to daptomycin and vancomycin were not altered compared to the MDB1 control, as they have the same MIC values (**Table 4.1**). However, the cells incubated in MH medium with oxacillin displayed slightly different susceptibility, see MIC values in **Table 4.1**. MDB1 cells have a burst of growth after ~12 hours incubation (in both parallels) (**Figure 4.30A**), indicating that susceptibility to oxacillin is altered with single *cozE* deletions in NCTC8325-4 cells, even if this alteration is only minor. The MIC values among the MDB11 cells (induced with different IPTG concentrations) are identical, with the exception of cells induced with 100 μM IPTG in daptomycin and oxacillin (**Table 4.1**), indicating that depletion of both CozE proteins only have minor effects on NCTC8325-4 cells' susceptibility to daptomycin, oxacillin or vancomycin (**Figure 4.30**).

Table 4.1 Susceptibility of NCTC8325-4 cells deprived of one or both CozE proteins (MDB1 (wild-type), MDB2 (Δ*cozEa*), MDB3 (Δ*cozEb*) and MDB11 (wild-type + CRISPRi(*cozEa*+*cozEb*), induced with four different IPTG concentrations)) to daptomycin, oxacillin and vancomycin.

Mutant	**MIC (μg/mL)**		
	Daptomycin	**Oxacillin**	**Vancomycin**
MDB1	0.3125	0.25	1.25
MDB2	0.3125	0.125	1.25
MDB3	0.3125	0.125	1.25
MDB11	0.625	0.125	1.25
MDB11 + 10 μM IPTG	0.625	0.125	1.25
MDB11 + 50 μM IPTG	0.625	0.125	1.25
MDB11 + 100 μM IPTG	0.3125	0.0625	1.25

a. The MIC values for MDB1, MDB2 and MDB3 are determined using the mean value of two parallels.

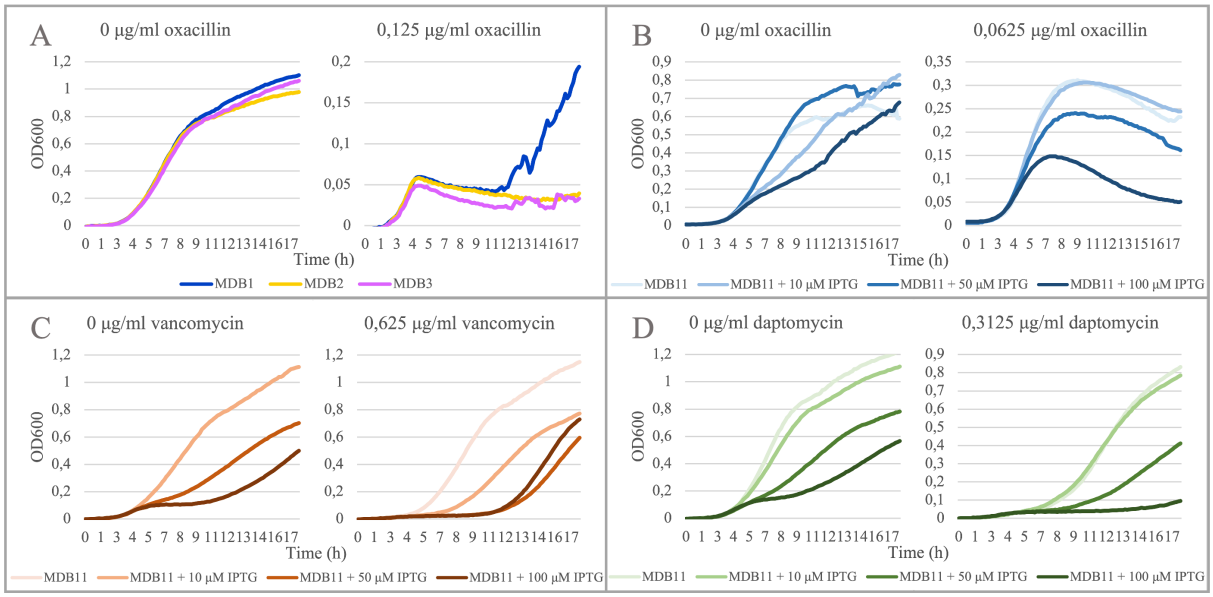

Figure 4.30 Susceptibility of NCTC8325-4 cells with depletion of one or both CozE proteins to daptomycin, oxacillin and vancomycin.
A. Growth curves for MDB1 (WT), MDB2 (Δ*cozEa*), and MDB3 (Δ*cozEb*) cells treated with 0.125 µg/mL oxacillin and no antibiotic. The curves were constructed using the mean value of two parallels.
B-D. Growth curves for MDB11 (WT + CRISPRi(*cozEa*+*cozEb*)) cells (induced with four different IPTG concentrations: 0 µM, 10 µM, 50 µM, and 100 µM) treated with 0.0625 µg/mL oxacillin (**B**), 0.625 µg/mL vancomycin (**C**), 0.3125 µg/mL daptomycin (**D**), and no antibiotics (**B-D**).

5 Discussion

In this thesis, the cellular functions of the CozE proteins were studied in *S. aureus* using a range of genetic and molecular biology approaches. The work resulted in new knowledge about the functions of CozE proteins and uncovered a link between these proteins and LTA biosynthesis.

5.1 *cozEa* and *cozEb* constitute a synthetic lethal gene pair important for cell growth and cell division in *S. aureus*.

The two CozE proteins found in *S. aureus*, CozEa and CozEb, play overlapping roles that are essential for normal cell growth and cell division. No apparent alterations in growth or morphology were observed upon single deletions of the *cozE* genes in wild-type background (SH1000, NCTC8325-4, JE2, and COL) (**Section 4.2 and A4**). A mutant with deletion of both genes simultaneously could not be obtained (SH1000 and NCTC8325-4) (**Section 4.3**), strongly suggesting a synthetic relationship between CozEa and CozEb in *S. aureus*. Both NCTC8325-4 and SH1000 are derivatives of the MSSA strain NCTC8325, and it would therefore be interesting to see if the same phenotype is conserved in a MRSA strain. Different analysis of strains with deletion-depletion and double depletion of the two *cozE* genes in JE2 indicates that it is indeed conserved (**Section 4.4)**. The individual functions of CozEa and CozEb are thus not essential, but their overlapping functionality is. Knockdown of *cozEa* or *cozEb* in their respective deletion backgrounds (Δ*cozEb* and Δ*cozEa*), or knockdown of both *cozE* genes in wild-type background using the two-plasmid CRISPRi system, caused dramatic reduction in growth, variable cell shapes, non-homogeneous DAPI and HADA staining patterns, frequent cell lysis, enrichment of cells without septa and cells with misplaced and aberrant septa (**Section 4.4 and 4.5**). Together, these observations confirm that CozE play an important role in both cell growth and spatiotemporal coordination of cell division in *S. aureus*, including MRSA.

To investigate the expression of CozE proteins in *S. aureus* we determined their relative expression levels and analysed their subcellular localisation. We speculated that CozEa and CozEb may have variable expression levels, however, immunoblot assay of chromosome integrated CozEa-GFP and CozEb-GFP with anti-GFP antibody indicated that they had approximately the same expression level (**Figure 4.10A**), although this has to be further verified. For this experiment, the OD_{600} value of each bacterial culture were normalised to 0.4, however this does not mean that the protein content of the two samples are equal when

visualised in the Azure Imager c400 (Azure Biosystems). Differences between the two samples can occur during every step of the immunoblotting procedure, see **Section 3.8.1**, and given that no quantifiable loading control was used to normalise these technical artifacts, the fold differences in protein expression between CozEa and CozEb cannot be confidently determined. An immunoblot assay with a quantifiable loading control must be included to ensure that the expression levels of CozEa and CozEb established in this work are accurate. Microscopic observations of the NCTC8325-4 strains with chromosomal *cozE-gfp* fusions revealed that both CozEa and CozEb have a spotty and dynamic localisation in the cytoplasmic membrane (**Section 4.6**). To further understand the overlapping functions of CozEa and CozEb in *S. aureus* it would be interesting to see whether they are co-localised or not. This can be investigated by tagging the two CozE proteins with different fluorochromes in the same mutant strain.

5.2 The functions of CozE proteins in *S. aureus* are linked to LTA synthesis.

The work in this thesis started out from the hypothesis that there may be a link between the functions of CozE proteins and teichoic acid biosynthesis in *S. aureus*. Using different experimental approaches, the work in this thesis clearly demonstrated the presence of such a functional link: We demonstrate a phenotypic similarity of mutants, a genetic interaction between CozE proteins and UgtP/LtaA, and show that CozEb have an effect on LTA polymer length.

Previous research has demonstrated that *S. aureus* mutants with defects in the synthesis of LTA glycolipid anchors (Glc_2-DAGs) display cell morphology defects (including multiple and misplaced septa) and increased autolysis rate (Hesser et al., 2020). These findings are consistent with the phenotypic alterations observed in *S. aureus* mutants lacking both CozE proteins in this work (**Section 4.4**). Like the Δ*ugtP* and Δ*ltaA* mutants, the double *cozE* depletion/deletion-depletion mutants also appear to have a higher percentage of cells without partial or complete septa (Hesser et al., 2020), at least for the JE2 strain (**Figure 4.4G and 4.5G**). Although it is hard to conclude, given that this analysis is based on manually deciding the cell cycle phases of wall stained (VanFL) cells on micrographs. In addition, the analysis is based on a relatively small number of cells (100-150) from each strain. The enrichment of cells without septa for the mutants lacking both CozE proteins, however, implies that these cells spend longer time growing prior to initiating septal synthesis. This cell division delay may be a result of the alterations lack of CozE have on the LTA synthesis. For instance, production of abnormally

long LTA polymers, as shown here (see discussion below), is likely more time-consuming than LTA production in wild-type cells. Cells with delayed cell division are expected to be enlarged. Both Δ*ugtP* and Δ*ltaA S. aureus* mutants are demonstrated to be larger than wild-type cells (Hesser et al., 2020). Cell size analysis of NCTC8325-4 and JE2 mutants lacking both CozE proteins, using MicrobeJ, showed that the JE2 mutants indeed were significantly larger that their wild-type (**Figure 4.7**). However, the NCTC8325-4 mutants were on the contrary significantly smaller (**Figure 4.6**). The conflicting results may be a result of different sample sizes (n) between the two strains. The mean number of cells analysed per mutant was 2.6 times greater for JE2 compared to NCTC8325-4 (JE2 = 1415 mean cells and NCTC8325-4 = 542 mean cells). It could also be a result of inherent differences between MSSA and MRSA strains, but Stamsås et al. have demonstrated that *cozE* deletion-depletion mutants of the MSSA strain SH1000 have increased cell sizes compared to their wild-type (Stamsås et al., 2018). The reason for this strain difference, with respect to cell sizes, is therefore unknown. Nevertheless, comparisons of the phenotypes for *S. aureus* cells lacking both CozE proteins and *S. aureus* mutants affecting LTA glycolipid anchor synthesis indicate that there is a potential link between them.

Some of the most interesting findings in this work was obtained when studying the CozE proteins in relation to the synthesis of LTA by constructing a panel of mutant strains lacking *cozE* and genes for LTA synthesis/modification proteins (*ugtP*, *ltaA*, *ltaS*, and *dltA*) (**Section 4.7**). Results acquired from growth assays with these mutant strains are simplified in **Figure 5.1**. The Δ*ugtP* and Δ*ltaA* mutants (NCTC8325 and JE2) lacking either CozEa or CozEb, displayed normal growth rate, which concurs with our finding of the overlapping functionality of the CozE proteins in *S. aureus*. However, interestingly, the Δ*ugtP* and Δ*ltaA* mutants (NCTC8325 and JE2) lacking both CozE proteins displayed dramatic, but opposite alterations to their growth. The Δ*ugtP* mutants had reduced growth compared to knockdown of *cozEa* and *cozEb* in wild-type background, thus showing a so-called synthetic lethal effect. On the other hand, the Δ*ltaA* mutants re-established normal growth in cells lacking both CozEa and CozEb, thus showing a synthetic viable combination (**Figure 5.1**).

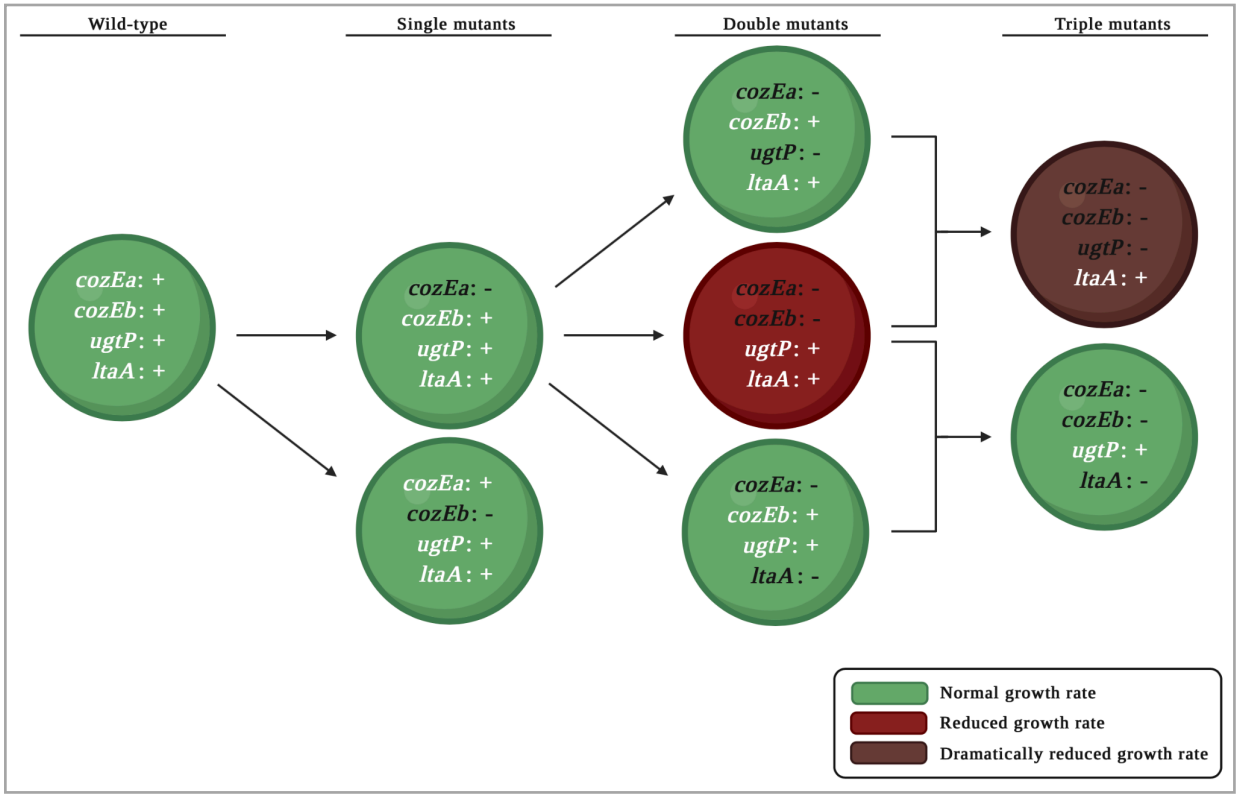

Figure 5.1 Simplistic representation of growth alteration observed in *S. aureus* (NCTC8325 and JE2) cells with single, double, and triple deletion/depletion of *cozE* (*cozEa* and *cozEb*) and LTA synthesis genes (*ugtP* and *ltaA*). The colour of the cells represents the growth rate of the mutant strain: green = normal growth, red = reduced growth, and brownish red = dramatically reduced growth. Created with BioRender.com.

The JE2 Δ*ltaA* mutant with double *cozE* depletion also re-establish normal cell division, as demonstrated by the TEM analysis (**Figure 4.16**). While knockdown of both *cozE* genes in wild-type background resulted in cells with misplaced and aberrant septa and high degree of cell lysis (**Figure 4.9**), it did not appear to result in any morphological alteration in the Δ*ltaA* background (few lysed cells and virtually no misplaced septa). Δ*ugtP* cells with knockdown of *cozEa* and *cozEb* (**Figure 4.16 and 4.17**) displayed the lysis phenotype as expected, in light of the growth assays (**Figure 4.14A and 4.14B**). However, it is not possible to conclude from the TEM images whether the triple mutant *cozEa*/*cozEb*/*ugtP* has a more prominent phenotype than the *cozEa*/*cozEb* double mutant, given that no analyses were performed on these micrographs besides manual observations. The growth assays and TEM images of the Δ*ugtP* and Δ*ltaA* mutants lacking *cozE* (NCTC8325 and JE2) nonetheless indicate that both *ugtP* and *ltaA* have a pairwise synthetic genetic interaction with the *cozE* genes, which affect cell growth and cell division in *S. aureus*.

5.3 The functions of CozEa and CozEb are conserved among *Staphylococcus* and *Macrococcus*, and CozEb appear to have a unique feature related to LTA synthesis in these genera.

The CozE proteins are widely conserved among bacteria, considering CozE homologues are demonstrated to be present in the genome of bacteria belonging to different phyla with diverse morphologies (Fenton et al., 2016). However, the degree of conservation for the functions of the CozE proteins are still unknown. The functions of CozEa and CozEb are demonstrated to be conserved among various *S. aureus* strains in this work, but previous research has demonstrated that CozE proteins from strains belonging to *Lactobacillales* possess roles that differs greatly from those found in *S. aureus* as depletion of these genes in *Lactobacillus plantarum* did not result in any phenotypic change (Myrbråten et al., 2019). Furthermore, CozE was first found in *S. pneumoniae* as a coordinator of zonal elongation (Fenton et al., 2016).

A phylogenetic analysis of CozE proteins, derived from 28 representative *Staphylococcaeceae* strains, was performed to determine the conservation of CozE proteins within the *Staphylococcaeceae* family (**Section 4.1**). The phylogenetic analysis revealed that all strains encode two homologues to the CozEa protein found in *S. aureus*. However, the CozE homologues interestingly generated three separate subgroups in the phylogenetic tree (**Figure 4.1**). The CozEa proteins from *Staphylococcus* and *Macrococcus*, and the CozEb proteins from the same genera, belong to two separate subgroups. While the CozE homologues found in the other genera of *Staphylococcaeceae* (*Jeotgalicoccus*, *Salinicoccus*, and *Nosocomiicoccus*) make up the third subgroup. The clustering of the CozE homologues indicates that the function of CozEa and CozEb are conserved among *Staphylococcus* and *Macrococcus*, but not among the more distantly related genera of *Staphylococcaeceae*. In addition to their overlapping function, it indicates that the two CozE proteins found in *Staphylococcus* and *Macrococcus*, have features that separate them from each other as they form clearly separate subgroups. The subgroup consisting of CozEa and CozEb from *Jeotgalicoccus*, *Salinicoccus*, and *Nosocomiicoccus* (coloured green in **Figure 4.1**) is more closely related to the CozEa subgroup than the CozEb subgroup of *Staphylococcus* and *Macrococcus* (coloured, respectively, blue and red in **Figure 4.1**), suggesting that CozEb have a unique function in *Staphylococcus* and *Macrococcus*.

In this work, such a unique, conserved feature of CozEb, indicated in the phylogenetic analysis, is observed when analysing the CozE proteins' role on LTA length. Previous research has demonstrated that *S. aureus* mutants with defects in the synthesis of the LTA glycolipid anchors (Δ*ugtP* and Δ*ltaA* mutant strains) produce abnormally long LTA polymers compared to wild-type (Hesser et al., 2020), and this was confirmed in this thesis (**Section 4.8**). Interestingly, of the two *cozE* mutants in *S. aureus*, only Δ*cozEb* (in NCTC8325-4, JE2, and COL) produced abnormally long LTA polymers, and the size was not further increased in the Δ*cozEb* + CRISPRi(*cozEa*) double mutants (**Section 4.8**). In addition, the LTA size phenotype observed in the Δ*cozEb* mutants (NCTC8325-4 and JE2) could be complemented with ectopic expression of *cozEb*, but not with ectopic expression of *cozEa* (**Section 4.9**). This indicates that CozEb play a unique role in LTA length maintenance, that CozEa cannot perform. Actually, the LTA size in the cells carrying the pRAB11-*cozEb* complementation plasmid appeared to be shorter than wild-type LTA (**Figure 4.21 and 4.22**). The differences in band size observed between the Δ*cozEb* + pRAB11-*cozEb* mutants and their respective wild-types are likely not a result of altered LTA length, but rather a limitation of the method that gives an indication of the margin of error to be expected in an immunoblot assay. The results obtained from the immunoblot assays of the different *cozE* mutants suggest that CozEb have a unique role in the LTA synthesis. On one hand, this is surprising considering that the other assays in this work suggest that the functions of CozEa and CozEb are, at least to some extent, overlapping. On the other hand, it is consistent with the phylogenetic analysis.

Knockdown of *cozEb* (and *cozEa*+*cozEb*) in the JE2 Δ*ltaA* background appeared to further increase the LTA polymer length (**Section 4.10**). The perpetuated LTA size phenotype observed in JE2, confirms the unique feature CozEb have on LTA size and further indicates a functional relationship between LtaA and CozEb in *S. aureus*. It should be noted that only double knockdown of *cozEa* and *cozEb* seemed to alter LTA polymer length in the JE2 Δ*ugtP* background (**Figure 4.23**), but this is difficult to conclude since the Δ*ugtP* mutants produce weak signals during immunoblotting. The weak signals are likely the result of lower total LTA production in the Δ*ugtP* mutants compared to the Δ*ltaA* mutants. The Δ*ltaA* mutants appear to produce approximately the same total LTA quantity as wild-type mutants, as demonstrated by comparing the signal-intensity for MDB19 (WT + CRISPRi(*cozEa*+*cozEb*)) and MDB46 (Δ*ltaA* + CRISPRi(*cozEa*+*cozEb*)) in **Figure 4.23**. Δ*ugtP* mutant cells produce LTA polymers linked to simpler lipid anchors (usually DAGs) than wild-type cells, since they cannot produce the Glc_2-DAG glycolipid anchors (Reichmann & Gründling, 2011). Δ*ltaA* mutant cells still

express UgtP, and therefore synthesise Glc_2DAG. Yet they are unable to translocate these glycolipid anchors to the outer leaflet of the membrane efficiently, since they lack the LtaA flippase that export Glc_2DAG. However, Δ*ltaA* mutant cells have been demonstrated to produce a mixture of LTAs linked to both DAGs and Glc_2-DAGs. This is described to an unknown mechanism that can translocate Glc_2-DAG produced by UgtP to the outer leaflet of the membrane, in the absence of LtaA (Gründling & Schneewind, 2007). This alternative, unknown mechanism may be the reason Δ*ltaA* mutants appear to have normal LTA quantity production as opposed to the lowered total LTA production observed in Δ*ugtP* mutants. For future experiments, at least twice as much lysate from Δ*ugtP* mutant strains should be used when immunoblotting LTA from JE2 Δ*ugtP* mutants, together with LTA from wild-type and/or Δ*ltaA* mutants, due to their reduced LTA production.

5.4 A model for the functions of CozE proteins in *S. aureus*.

Although the results in this thesis clearly demonstrates a functional link between CozE proteins and LTA, the exact functions of the CozE proteins are unknown. They appear to perform a function which acts upstream of either UgtP or LtaA in the LTA synthesizing pathway, considering that their deletion-depletion phenotype is reminiscent of mutants affecting LTA glycolipid anchor synthesis, and that they affect LTA length. In addition, the CozE proteins are distributed throughout the membrane similarly to UgtP and LtaA, but unlike LtaS that predominantly accumulates at the cell division site (Reichmann et al., 2014). This may indicate that CozEa and CozEb play a role in the synthesis, localisation, or turnover of the glycolipid anchor, rather than the polymerisation of the poly-Gro-P backbone chain. **Figure 5.2** show a schematic model of the functional interactions the CozE proteins from *S. aureus* are found to have in this work.

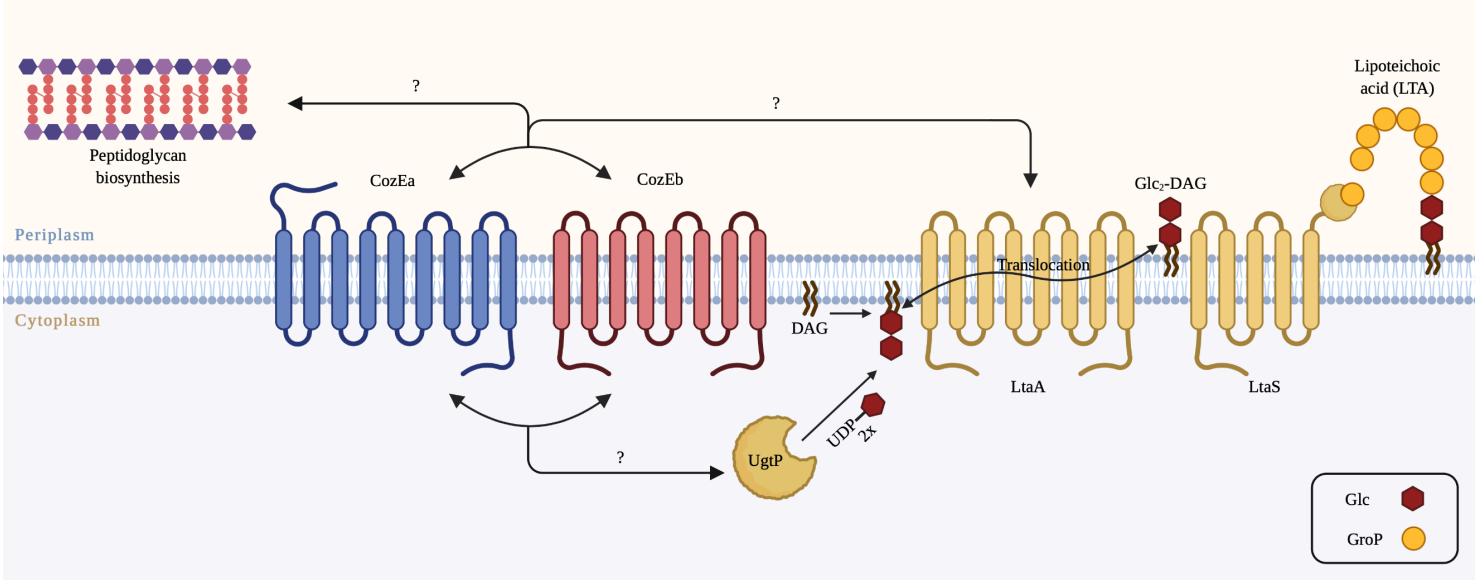

Figure 5.2 Schematic representation of the functional relationship between the CozE proteins and the synthesis of LTA (and peptidoglycan) in *S. aureus*. The arrows marked with a question mark indicate the functional interactions the CozE proteins have been found to have in this work, which includes LtaA and UgtP from the synthesis of LTA, as well as the synthesis of peptidoglycan. Created with BioRender.com.

We hypothesised that CozEa and CozEb might play a role in recruiting UgtP to the cytoplasmic membrane. If the CozE proteins are important for correct UgtP localisation, one would expect reduced growth when these two genes are deleted together. Indeed, following growth demonstrated that deletion/depletion of *cozE* and *ugtP* together caused a stronger phenotypic effect than expected in light of deleting each gene individually (NCTC8325-4 and JE2) (**Figure 4.14B and 4.15B**). The *B. subtilis* homologue of UgtP have been shown to accumulate specifically to the division site in this organism, though the localisation of UgtP is disrupted in the absence of its cytoplasmic substrate UDP-Glc. The signal of fluorescently tagged UgtP in *B. subtilis* mutants lacking UDP-Glc is delocalised from the septum to randomly distributed spots in the cell (Nishibori, Kusaka, Hara, Umeda, & Matsumoto, 2005; Weart et al., 2007). Reichmann et al. (2014) have demonstrated that UgtP also localised to the membrane in *S. aureus* (more specifically in the RN4220 and LAC* strains), though not specifically to the division site. UgtP have a spotty membrane localisation in these *S. aureus* strain that is not lost in the absent of UDP-Glc, thereby confirming that UgtP's localisation in *S. aureus* is independent of UDP-Glc production (Reichmann et al., 2014). Microscopic analysis of *S. aureus* NCTC8325-4 cells expressing GFP-UgtP from its native locus, and from the pLOW-*gfp_ugtP* plasmid, confirms that the spotty membrane localisation discovered in RN4220 and LAC* is conserved among other *S. aureus* strains (MDB64 in **Figure 4.26** and MDB77 in **Figure 4.28**). In addition, it revealed that UgtP have a dynamic localisation reminiscent of what was observed for the two CozE proteins (**Figure 4.29 and 4.11**), which reinforced the

hypothesis that the CozE proteins are involved in correct localisation of UgtP. However, microscopic analysis of cells expressing GFP-UgtP revealed that lack of CozE did not alter UgtP localisation or mobility (**Figure 4.27 and 4.29**), and this hypothesis was therefore rejected. Thus, another protein(s) or molecule(s) is responsible for the recruitment of UgtP to the membrane. UgtP is distributed all around the membrane, so the protein responsible for its localisation is likely not a cell division or peptidoglycan synthesis protein expected to localise to the division site. DAG, the receptor molecule UgtP transfer UDP-Glc to in Glc_2-DAG production, has been proposed to be involved in UgtP localisation, and further investigation of this link would therefore be interesting.

After discovering that CozEa and CozEb do not have a role in UgtP's localisation to the cytoplasmic membrane, a new hypothesis regarding their function can be proposed. Considering CozEa and CozEb have a function that is only essential when LtaA is present (knockdown of the *cozE* genes have no effect on growth nor cell division in the absence of LtaA), and considering the highly dynamic localisation of CozEa and CozEb we now speculate that the CozE proteins may act as a flippase whose function is to catalyse the flipping of phospholipids or glycolipids between the bilayers of the membrane. This speculation is based on the fact that LTA-length is depended on the synthesis of Glc_2-DAG, which again depends on the availability of phospholipid precursor DAG on the inner membrane leaflet in close proximity to UgtP. Alterations in lipid flipping (e.g., in *cozE* mutants) would then change the distribution and homeostasis of lipids in the membrane and influence synthesis of Glc_2-DAG in various ways. Such a mechanism could also explain why CozE proteins are so widely distributed in bacteria (since the same lipids are found across bacterial phyla), but at the same time result in variable phenotypes between species (since lipid composition and function may vary between species). Furthermore, changes in lipid distribution could have pleiotropic effects on the cells, resulting in abnormally localised peptidoglycan synthesis and mis-localised cell division (see below). However, this is only assumptions based on the results obtained in this work and they have to be further investigated experimentally, for instance by analysing the differences in lipids between bilayers (the phospholipid/glycolipid composition in double *cozE* mutants compared to wild-type).

The CozE proteins appear to have a link to the synthesis of cell wall, in addition to LTA synthesis in *S. aureus* (**Figure 5.2**), considering NCTC8325-4 cells lacking both CozEa and CozEb simultaneously displayed a highly altered HADA signal (**Figure 4.8**). HADA visualise

sites of nascent peptidoglycan in bacterial cells, so alteration to its signal indicate disruption of the cell wall synthesis. While the HADA incorporation in single *cozEa* and *cozEb* deletion mutants were similar to wild-type (MDB1, MDB2, and MDB3 in **Figure 4.8**), the cell wall synthesis was highly disturbed in the double depletion mutant (MDB11 in **Figure 4.8**). The NCTC8325-4 mutant strain with knockdown of both *cozE* genes displayed some cells with no HADA signal and others with a highly intense signal, shown in clumps rather than at the septum. These observations suggest that the CozE proteins are involved in coordinating peptidoglycan synthesis to the correct location in *S. aureus* cells. It has previously been shown in *S. pneumoniae* that CozE proteins are involved in spatiotemporal localisation of peptidoglycan synthesis through their interaction and control of the bifunctional class A PBPs (Fenton et al., 2016; Stamsås et al., 2020). However, no interactions have been found between CozEa/CozEb and any of the PBPs found in *S. aureus* (PBP1, PBP2, PBP3, or PBP4). The early cell division protein EzrA, which is important for linking Z-ring formation and the cell wall synthesis machinery, is the only protein found to have a direct interaction to both CozEa and CozEb. The CozE proteins in *S. aureus* therefore may mediate peptidoglycan synthesis via this interaction (Stamsås et al., 2018; Steele, Bottomley, Garcia-Lara, Kasturiarachchi, & Foster, 2011), however, this also needs to be further confirmed. Alternatively, the disruption of cell wall synthesis observed in the double *cozE* knockdown mutants could be indirect as a result of altered lipid composition (see hypothesis above) or as a result of alteration in the LTA synthesis. In order to test the latter idea, one should analyse HADA incorporation in the NCTC8325 and JE2 *ugtP* and *ltaA* deletion mutants. If the Δ*ugtP* or Δ*ltaA* mutant strains display the same abnormal HADA staining as cells lacking both CozE proteins, it is unlikely that CozEa and CozEb directly affect peptidoglycan synthesis.

5.5 Lack of CozE proteins do not significantly alter susceptibility to cell envelope targeting antibiotics in *S. aureus*.

Considering that absence of CozEa and CozEb have severe effects on cell division and cell wall formation in *S. aureus*, we tested if *S. aureus'* susceptibility to cell wall- and cell envelope active antibiotics (daptomycin, oxacillin, and vancomycin) is altered in cells lacking one or both CozE proteins (**Section 4.12**). All three antibiotics tested attack the bacterial cell wall/envelope, but they have different modes of action. The mode of action of daptomycin (which is a cyclic lipopeptide antibiotic) is associated with depolarisation/disruption of the bacterial membrane of *S. aureus*, and it is in addition predicted to inhibit peptidoglycan

synthesis, which both oxacillin (a β-lactam antibiotic) and vancomycin (a glycopeptide) are proven to do. Oxacillin inhibits PBPs and peptidoglycan crosslinking, while vancomycin binds to the D-ala-D-ala of lipid II and prevents transglycosylation and transpeptidation of peptidoglycan (Dengler, Meier, Heusser, Berger-Bächi, & McCallum, 2011).

Uninduced MDB11 cells (WT + CRISPRi(*cozEa*+*cozEb*)) exhibit higher MIC values for daptomycin and vancomycin than MDB1 (WT) (**Table 4.1**), even though they in theory should exhibit the same phenotype. This is most likely due to the fact that the experiments were performed on two different days, which slightly alters the steps of the procedure. This has to be taken into consideration when comparing MDB1/MDB2/MDB3 with MDB11. In addition, all the growth curves of uninduced MDB11 should be similar (**Figure 4.30B-D**). However, the growth curves for uninduced MDB11 with oxacillin are slightly different than the others, probably because they were incubated in a separate microtiter plate in the Synergy™ H1 Hybrid Multi-Mode Reader (BioTek Instruments) rather than in the Hidex Sense (Hidex Oy).

Absence of the CozE proteins appears to have minor effect on NCTC8325-4 cells' susceptibility to oxacillin and vancomycin (**Table 4.1** and **figure 4.30A-C**). A previous study has shown that Δ*ugtP* and Δ*ltaA* MRSA mutants were sensitised to β-lactam antibiotics. The MIC value for oxacillin decreased 8-fold and 64-fold for Δ*ugtP* and Δ*ltaA* MRSA mutants, respectively, although the MIC value for oxacillin only modestly decreased when *ugtP* or *ltaA* was deleted in a MSSA background (Hesser et al., 2020). The susceptibility assays conducted in this study were done with the MSSA strain NCTC8325-4. It would therefore be interesting to do the same assays for the MRSA strains JE2 and/or COL. NCTC8325-4 cells with knockdown of both CozE proteins appeared to be slightly more susceptible to daptomycin (**Table 4.1** and **Figure 4.30D**). Other antibiotics may cause stronger susceptibility alteration upon depletion of both *cozE* genes in *S. aureus*, for instance antibiotics linked to the LTA synthesis (e.g., amsacrine or *o*-AMSA) (L. Pasquina et al., 2016). Such antibiotics are relevant for further analysis of CozE proteins effect on *S. aureus*' susceptibility to antibiotics and may substantiate the established genetic link between CozE and LTA synthesising proteins.

6 Concluding remarks and future research

This work has demonstrated that the CozE proteins found in *S. aureus*, CozEa and CozEb, have a functional link to LTA biosynthesis (and possible peptidoglycan biosynthesis). They appear to perform a function which acts upstream of either UgtP or LtaA, possible related to translocation of phospholipids or glycolipids between the bilayers of the bacterial membrane. The presence of a functional link between CozE and LTA biosynthesis in *S. aureus* is demonstrated with several different experiments in this work: (1) mutants deprived of both CozE proteins are demonstrated to have phenotypic similarities to mutants affecting LTA glycolipid anchor synthesis (growth assays and microscopy), (2) CozEa and CozEb are shown to have a highly dynamic localisation in the cytoplasmic membrane similar to UgtP (and LtaA) (microscopy of GFP-tagged proteins), (3) CozEb is demonstrated to play a unique role in LTA length maintenance (immunoblot assays), and (4) *ugtP* and *ltaA* are found to have a pairwise synthetic genetic interactions with the *cozE* genes (growth assays and TEM). The synthetic interactions found between the *cozE* genes and *ugtP* and between the *cozE* genes and *ltaA* are opposite. Double knockdown of the *cozE* genes in Δ*ugtP* background resulted in barely viable cells (synthetic lethal effect), while normal cell growth/division was re-established in Δ*ltaA* cells with double *cozE* knockdown (synthetic viable effect). Understanding the effects CozEa and CozEb have on glycolipid anchor production *in S. aureus* will be of great importance to get even further insight in the function of this highly conserved family of proteins.

The synthetic relationship between CozEa and CozEb in *S. aureus* was confirmed in this work, in addition to their functional relationship to LTA synthesis. Lack of both CozE proteins caused major phenotypic alterations to both MSSA (NCTC8325-4) and MRSA (JE2) strains, while individual deletions had minimal effects. CozEa and CozEb have been found to interact with each other (Stamsås et al., 2018). To identify if UgtP and/or LtaA have direct protein–protein interactions with one or both CozE proteins one should perform a bacterial two-hybrid analysis/co-immunoprecipitation assay with these proteins. Although research on UgtP's membrane localisation, in this work, indicates that the CozE proteins do not directly interact with UgtP, at least they do not recruit UgtP to the membrane.

The results obtained in this work not only reveal novel knowledge regarding the functional interactions of the CozE proteins in *S. aureus*, but they also reveal potential targets for therapeutic development in the future. LTAs play fundamental roles in physiology and

pathogenesis of Gram-positive bacteria, and they are essential for survival *in vitro* under most environmental conditions. Inhibition of the different steps of LTA synthesis are therefore promising strategies for antibiotic attack (L. W. Pasquina et al., 2013). However, the mechanisms underpinning CozE's relationship to LTA synthesis have to be fully understood for this for this development to be possible. Future studies on CozEa and CozEb's functional relationships have to be carried out to reveal the complex molecular mechanisms of CozEa and CozEb and to realise their potential as antibiotic targets.

References

Agarwal, A., Singh, K. P., & Jain, A. (2010). Medical significance and management of staphylococcal biofilm. *FEMS Immunology & Medical Microbiology, 58*(2), 147-160. doi:10.1111/j.1574-695X.2009.00601.x

Alberts, B., Johnson, A., Lewis, J., Raff, M., Roberts, K., & Walter, P. (2002). Chapter 8 - Manipulating Proteins, DNA, and RNA. In *Molecular Biology of the Cell (Fourth Edition)*. New York: Garland Science.

Aly, R., Shinefield, H. R., Litz, C., & Maibach, H. I. (1980). Role of Teichoic Acid in the Binding of *Staphylococcus aureus* to Nasal Epithelial Cells. *The Journal of Infectious Diseases, 141*(4), 463-465. doi:10.1093/infdis/141.4.463

Analytical Methods Committee, AMCTB No. 59. (2014). PCR – the polymerase chain reaction. *Analytical Methods, 6*(2), 333-336. doi:10.1039/C3AY90101G

Archer, G. L. (1998). *Staphylococcus aureus*: A Well-Armed Pathogen. *Clinical Infectious Diseases, 26*(5), 1179-1181. doi:10.1086/520289

Argudín, M. Á., Mendoza, M. C., & Rodicio, M. R. (2010). Food Poisoning and *Staphylococcus aureus* Enterotoxins. *Toxins, 2*(7), 1751-1773. doi:10.3390/toxins2071751

Arnaud, M., Chastanet, A., & Débarbouillé, M. (2004). New vector for efficient allelic replacement in naturally nontransformable, low-GC-content, gram-positive bacteria. *Applied and environmental microbiology, 70*(11), 6887-6891. doi:10.1128/AEM.70.11.6887-6891.2004

Balasubramanian, D., Harper, L., Shopsin, B., & Torres, V. J. (2017). *Staphylococcus aureus* pathogenesis in diverse host environments. *Pathogens and Disease, 75*(1). doi:10.1093/femspd/ftx005

Belete, T. M. (2019). Novel targets to develop new antibacterial agents and novel alternatives to antibacterial agents. *Human Microbiome Journal, 11*, 100052. doi:10.1016/j.humic.2019.01.001

Bera, A., Biswas, R., Herbert, S., Kulauzovic, E., Weidenmaier, C., Peschel, A., & Götz, F. (2007). Influence of wall teichoic acid on lysozyme resistance in *Staphylococcus aureus*. *Journal of bacteriology, 189*(1), 280-283. doi:10.1128/JB.01221-06

Bhunia, A. K. (2018). Chapter 10 - *Staphylococcus aureus*. In *Foodborne microbial pathogens: mechanisms and pathogenesis (Second Edition)* (pp. 181-192). New York: Springer.

Bikard, D., Jiang, W., Samai, P., Hochschild, A., Zhang, F., & Marraffini, L. A. (2013). Programmable repression and activation of bacterial gene expression using an engineered CRISPR-Cas system. *Nucleic Acids Research, 41*(15), 7429-7437. doi:10.1093/nar/gkt520

Booth, S., & Lewis, R. J. (2019). Structural basis for the coordination of cell division with the synthesis of the bacterial cell envelope. *Protein science, 28*(12), 2042-2054. doi:10.1002/pro.3722

Cao, M., Fu, Y., Guo, Y., & Pan, J. (2009). *Chlamydomonas* (Chlorophyceae) colony PCR. *Protoplasma, 235*(1), 107-110. doi:10.1007/s00709-009-0036-9

Chalfie, M., Tu, Y., Euskirchen, G., Ward, W., & Prasher, D. (1994). Green fluorescent protein as a marker for gene expression. *Science, 263*(5148), 802-805. doi:10.1126/science.8303295

Chambers, H. F. (2001). The changing epidemiology of *Staphylococcus aureus*? *Emerging infectious diseases, 7*(2), 178-182. doi:10.3201/eid0702.010204

Chambers, H. F., & DeLeo, F. R. (2009). Waves of resistance: *Staphylococcus aureus* in the antibiotic era. *Nature Reviews Microbiology, 7*(9), 629-641. doi:10.1038/nrmicro2200

Chan, H., Söderström, B., & Skoglund, U. (2020). Spo0J and SMC are required for normal chromosome segregation in *Staphylococcus aureus*. *MicrobiologyOpen, 9*(4), e999. doi:10.1002/mbo3.999

Chan, Y. G.-Y., Kim, H. K., Schneewind, O., & Missiakas, D. (2014). The Capsular Polysaccharide of *Staphylococcus aureus* Is Attached to Peptidoglycan by the LytR-CpsA-Psr (LCP) Family of Enzymes. *Journal of Biological Chemistry, 289*(22), 15680-15690. doi:10.1074/jbc.M114.567669

Chan, Y. G. Y., Frankel, M. B., Missiakas, D., & Schneewind, O. (2016). SagB Glucosaminidase Is a Determinant of *Staphylococcus aureus* Glycan Chain Length, Antibiotic Susceptibility, and Protein Secretion. *Journal of bacteriology, 198*(7), 1123-1136. doi:10.1128/JB.00983-15

Charpentier, E., Anton, A. I., Barry, P., Alfonso, B., Fang, Y., & Novick, R. P. (2004). Novel cassette-based shuttle vector system for gram-positive bacteria. *Applied and environmental microbiology, 70*(10), 6076-6085. doi:10.1128/AEM.70.10.6076-6085.2004

Chaudhuri, R. R., Allen, A. G., Owen, P. J., Shalom, G., Stone, K., Harrison, M., . . . Charles, I. G. (2009). Comprehensive identification of essential *Staphylococcus aureus* genes using Transposon-Mediated Differential Hybridisation (TMDH). *BMC genomics, 10*, 291-291. doi:10.1186/1471-2164-10-291

Chen, J., Li, Y., Zhang, K., & Wang, H. (2018). Whole-Genome Sequence of Phage-Resistant Strain *Escherichia coli* DH5α. *Genome announcements, 6*(10), e00097-00018. doi:10.1128/genomeA.00097-18

Chung, K.-M., Hsu, H.-H., Yeh, H.-Y., & Chang, B.-Y. (2007). Mechanism of Regulation of Prokaryotic Tubulin-like GTPase FtsZ by Membrane Protein EzrA. *Journal of Biological Chemistry, 282*(20), 14891-14897. doi:10.1074/jbc.M605177200

Cong, Y., Yang, S., & Rao, X. (2020). Vancomycin resistant *Staphylococcus aureus* infections: A review of case updating and clinical features. *Journal of Advanced Research, 21*, 169-176. doi:10.1016/j.jare.2019.10.005

Corrigan, R. M., Abbott, J. C., Burhenne, H., Kaever, V., & Gründling, A. (2011). c-di-AMP Is a New Second Messenger in *Staphylococcus aureus* with a Role in Controlling Cell Size and Envelope Stress. *PLOS Pathogens, 7*(9), e1002217. doi:10.1371/journal.ppat.1002217

Davey, R. X., & Tong, S. Y. C. (2019). The epidemiology of *Staphylococcus aureus* skin and soft tissue infection in the southern Barkly region of Australia's Northern Territory in 2017. *Pathology, 51*(3), 308-312. doi:10.1016/j.pathol.2018.11.010

DeLeo, F. R., Otto, M., Kreiswirth, B. N., & Chambers, H. F. (2010). Community-associated meticillin-resistant *Staphylococcus aureus*. *The Lancet, 375*(9725), 1557-1568. doi:10.1016/S0140-6736(09)61999-1

Dengler, V., Meier, P. S., Heusser, R., Berger-Bächi, B., & McCallum, N. (2011). Induction kinetics of the *Staphylococcus aureus* cell wall stress stimulon in response to different cell wall active antibiotics. *BMC Microbiology, 11*(1), 16. doi:10.1186/1471-2180-11-16

Dolgova, A. S., & Stukolova, O. A. (2017). High-fidelity PCR enzyme with DNA-binding domain facilitates *de novo* gene synthesis. *3 Biotech, 7*(2), 128. doi:10.1007/s13205-017-0745-2

Ducret, A., & Grangeasse, C. (2017). Bacterial physiology: Wrapping the cell in a CozE shell. *Nature Microbiology, 2*(3), 16262. doi:10.1038/nmicrobiol.2016.262

Emami, K., Guyet, A., Kawai, Y., Devi, J., Wu, L. J., Allenby, N., . . . Errington, J. (2017). RodA as the missing glycosyltransferase in *Bacillus subtilis* and antibiotic discovery for the peptidoglycan polymerase pathway. *Nature Microbiology, 2*(3), 16253. doi:10.1038/nmicrobiol.2016.253

EMD Biosciences. (2003). TB146 Pellet Paint® Co-Precipitant. Retrieved from https://www.merckmillipore.com/NO/en/product/Pellet-Paint-Co-Precipitant,EMD_BIO-69049?ReferrerURL=https%3A%2F%2Fwww.google.com%2F#anchor_USP

Erickson, H. P. (2017). How bacterial cell division might cheat turgor pressure – a unified mechanism of septal division in Gram-positive and Gram-negative bacteria. *BioEssays, 39*(8), 1700045. doi:10.1002/bies.201700045

Euzéby, J. P. (2021). List of Prokaryotic names with standing in Nomenclature - Genus *Staphylococcus*. Retrieved from https://lpsn.dsmz.de/genus/staphylococcus

Fenton, A. K., El Mortaji, L., Lau, D. T. C., Rudner, D. Z., & Bernhardt, T. G. (2016). CozE is a member of the MreCD complex that directs cell elongation in *Streptococcus pneumoniae*. *Nature Microbiology, 2*(3), 16237. doi:10.1038/nmicrobiol.2016.237

Fey, P. D., Endres, J. L., Yajjala, V. K., Widhelm, T. J., Boissy, R. J., Bose, J. L., & Bayles, K. W. (2013). A genetic resource for rapid and comprehensive phenotype screening of nonessential *Staphylococcus aureus* genes. *mBio, 4*(1), e00537. doi:10.1128/mBio.00537-12

Foster, T. (1996). Chapter 12 - *Staphylococcus*. In S. Baron (Ed.), *Medical Microbiology (Fourth Edition)*. Galveston, Texas: The University of Texas Medical Branch at Galveston.

Gardete, S., & Tomasz, A. (2014). Mechanisms of vancomycin resistance in *Staphylococcus aureus*. *The Journal of clinical investigation, 124*(7), 2836-2840. doi:10.1172/JCI68834

Gill, S. R., Fouts, D. E., Archer, G. L., Mongodin, E. F., Deboy, R. T., Ravel, J., . . . Fraser, C. M. (2005). Insights on evolution of virulence and resistance from the complete genome analysis of an early methicillin-resistant *Staphylococcus aureus* strain and a biofilm-producing methicillin-resistant *Staphylococcus epidermidis* strain. *Journal of bacteriology, 187*(7), 2426-2438. doi:10.1128/JB.187.7.2426-2438.2005

Gnanamani, A., Periasamy, H., & Paul Satyaseela, M. (2017). Chapter 1 - Staphylococcus aureus: Overview of Bacteriology, Clinical Diseases, Epidemiology, Antibiotic Resistance and Therapeutic Approach. In *Frontiers in Staphylococcus aureus*: IntechOpen.

Gorwitz, R. J., Kruszon-Moran, D., McAllister, S. K., McQuillan, G., McDougal, L. K., Fosheim, G. E., . . . Kuehnert, M. J. (2008). Changes in the Prevalence of Nasal Colonization with *Staphylococcus aureus* in the United States, 2001–2004. *The Journal of Infectious Diseases, 197*(9), 1226-1234. doi:10.1086/533494

Gross, M., Cramton, S. E., Götz, F., & Peschel, A. (2001). Key Role of Teichoic Acid Net Charge in *Staphylococcus aureus* Colonization of Artificial Surfaces. *Infection and immunity, 69*(5), 3423-3426. doi:10.1128/iai.69.5.3423-3426.2001

Gründling, A., & Schneewind, O. (2007). Genes Required for Glycolipid Synthesis and Lipoteichoic Acid Anchoring in *Staphylococcus aureus*. *Journal of bacteriology, 189*(6), 2521-2530. doi:10.1128/jb.01683-06

Guimaraes, A. O., Cao, Y., Hong, K., Mayba, O., Peck, M. C., Gutierrez, J., . . . Rosenberger, C. M. (2018). A Prognostic Model of Persistent Bacteremia and Mortality in Complicated *Staphylococcus aureus* Bloodstream Infection. *Clinical Infectious Diseases, 68*(9), 1502-1511. doi:10.1093/cid/ciy739

Guzzo, M., Castro, L. K., Reisch, C. R., Guo, M. S., & Laub, M. T. (2020). A CRISPR Interference System for Efficient and Rapid Gene Knockdown in *Caulobacter crescentus*. *mBio, 11*(1), e02415-02419. doi:10.1128/mBio.02415-19

Hamoen, L. W., Meile, J.-C., De Jong, W., Noirot, P., & Errington, J. (2006). SepF, a novel FtsZ-interacting protein required for a late step in cell division. *Molecular Microbiology, 59*(3), 989-999. doi:10.1111/j.1365-2958.2005.04987.x

Harris, L. G., Foster, S. J., & Richards, R. G. (2002). An introduction to *Staphylococcus aureus*, and techniques for identifying and quantifying *S. aureus* adhesins in relation to adhesion to biomaterials: review. *Eur Cell Mater, 4*, 39-60. doi:10.22203/ecm.v004a04

Helle, L., Kull, M., Mayer, S., Marincola, G., Zelder, M.-E., Goerke, C., . . . Bertram, R. (2011). Vectors for improved Tet repressor-dependent gradual gene induction or silencing in *Staphylococcus aureus*. *Microbiology, 157*(12), 3314-3323. doi:10.1099/mic.0.052548-0

Hesser, A. R., Matano, L. M., Vickery, C. R., Wood, B. M., Santiago, A. G., Morris, H. G., . . . Walker, S. (2020). The length of lipoteichoic acid polymers controls *Staphylococcus aureus* cell size and envelope integrity. *bioRxiv*, 2020.2003.2023.004671. doi:10.1101/2020.03.23.004671

Hilgarth, R. S., & Lanigan, T. M. (2020). Optimization of overlap extension PCR for efficient transgene construction. *MethodsX, 7*, 100759. doi:10.1016/j.mex.2019.12.001

Hiramatsu, K., Hanaki, H., Ino, T., Yabuta, K., Oguri, T., & Tenover, F. (1997). Methicillin-resistant *Staphylococcus aureus* clinical strain with reduced vancomycin susceptibility. *The Journal of antimicrobial chemotherapy, 40*(1), 135-136.

Hiramatsu, K., Ito, T., Tsubakishita, S., Sasaki, T., Takeuchi, F., Morimoto, Y., . . . Hishinuma, T. (2013). Genomic basis for methicillin resistance in *Staphylococcus aureus*. *Infection & chemotherapy, 45*(2), 117-136. doi:10.3947/ic.2013.45.2.117

Hollister, E. B., Brooks, J. P., & Gentry, T. J. (2015). Chapter 13 - Nucleic Acid-Based Methods of Analysis. In I. L. Pepper, C. P. Gerba, & T. J. Gentry (Eds.), *Environmental Microbiology (Third Edition)* (pp. 271-305). San Diego: Academic Press.

Horsburgh, M. J., Aish, J. L., White, I. J., Shaw, L., Lithgow, J. K., & Foster, S. J. (2002). sigmaB modulates virulence determinant expression and stress resistance: characterization of a functional *rsbU* strain derived from *Staphylococcus aureus* 8325-4. *Journal of bacteriology, 184*(19), 5457-5467. doi:10.1128/jb.184.19.5457-5467.2002

Horvath, P., & Barrangou, R. (2010). CRISPR/Cas, the Immune System of Bacteria and Archaea. *Science, 327*(5962), 167-170. doi:10.1126/science.1179555

Haag, A. F., & Bagnoli, F. (2017). The Role of Two-Component Signal Transduction Systems in *Staphylococcus aureus* Virulence Regulation. In F. Bagnoli, R. Rappuoli, & G. Grandi (Eds.), *Staphylococcus aureus: Microbiology, Pathology, Immunology, Therapy and Prophylaxis* (pp. 145-198). Cham: Springer International Publishing.

Jenkins, A., Diep, B. A., Mai, T. T., Vo, N. H., Warrener, P., Suzich, J., . . . Sellman, B. R. (2015). Differential Expression and Roles of *Staphylococcus aureus* Virulence Determinants during Colonization and Disease. *mBio, 6*(1), e02272-02214. doi:10.1128/mBio.02272-14

Jun, S., & Mulder, B. (2006). Entropy-driven spatial organization of highly confined polymers: Lessons for the bacterial chromosome. *Proceedings of the National Academy of Sciences, 103*(33), 12388-12393. doi:10.1073/pnas.0605305103

Jun, S., & Wright, A. (2010). Entropy as the driver of chromosome segregation. *Nature reviews. Microbiology, 8*(8), 600-607. doi:10.1038/nrmicro2391

Kajimura, J., Fujiwara, T., Yamada, S., Suzawa, Y., Nishida, T., Oyamada, Y., . . . Sugai, M. (2005). Identification and molecular characterization of an N-acetylmuramyl-l-alanine amidase Sle1 involved in cell separation of *Staphylococcus aureus*. *Molecular Microbiology, 58*(4), 1087-1101. doi:10.1111/j.1365-2958.2005.04881.x

Kapuscinski, J. (1995). DAPI: a DNA-Specific Fluorescent Probe. *Biotechnic & Histochemistry, 70*(5), 220-233. doi:10.3109/10520299509108199

Kho, K., & Meredith, T. C. (2018). Salt-Induced Stress Stimulates a Lipoteichoic Acid-Specific Three-Component Glycosylation System in *Staphylococcus aureus*. *Journal of bacteriology, 200*(12), e00017-00018. doi:10.1128/jb.00017-18

Kim, S. J., Singh, M., Preobrazhenskaya, M., & Schaefer, J. (2013). *Staphylococcus aureus* peptidoglycan stem packing by rotational-echo double resonance NMR spectroscopy. *Biochemistry, 52*(21), 3651-3659. doi:10.1021/bi4005039

Klein, E., Smith, D. L., & Laxminarayan, R. (2007). Hospitalizations and Deaths Caused by Methicillin-Resistant *Staphylococcus aureus*, United States, 1999–2005. *Emerging infectious diseases, 13*(12), 1840-1846. doi:10.3201/eid1312.070629

Kuru, E., Tekkam, S., Hall, E., Brun, Y. V., & Van Nieuwenhze, M. S. (2015). Synthesis of fluorescent D-amino acids and their use for probing peptidoglycan synthesis and bacterial growth *in situ*. *Nature protocols, 10*(1), 33-52. doi:10.1038/nprot.2014.197

Lee, P. Y., Costumbrado, J., Hsu, C.-Y., & Kim, Y. H. (2012). Agarose Gel Electrophoresis for the Separation of DNA Fragments. *JoVE*(62), e3923. doi:doi:10.3791/3923

Lesk, A. M. (2016). Chapter 9 - Proteomics and systems biology. In *Introduction to Protein Science - Architecture, Function, and Genomics (Third Edition)* (pp. 387-437). New York: Oxford University Press.

Liew, A. T. F., Theis, T., Jensen, S. O., Garcia-Lara, J., Foster, S. J., Firth, N., . . . Harry, E. J. (2011). A simple plasmid-based system that allows rapid generation of tightly controlled gene expression in *Staphylococcus aureus*. *Microbiology, 157*(3), 666-676. doi:10.1099/mic.0.045146-0

Linacero, R., Rueda, J., & Vázquez, A. M. (1998). Quantification of DNA. In A. Karp, P. G. Isaac, & D. S. Ingram (Eds.), *Molecular Tools for Screening Biodiversity: Plants and Animals* (pp. 18-21). Dordrecht: Springer Netherlands.

Liu , G. Y., Essex , A., Buchanan , J. T., Datta , V., Hoffman , H. M., Bastian , J. F., . . . Nizet , V. (2005). *Staphylococcus aureus* golden pigment impairs neutrophil killing and promotes virulence through its antioxidant activity. *Journal of Experimental Medicine, 202*(2), 209-215. doi:10.1084/jem.20050846

Liu, I., Liu, M., & Shergill, K. (2006). The effect of spheroplast formation on the transformation efficiency in *Escherichia coli* DH5α. *Journal of Experimental Microbiology and Immunology, 9*, 81-85.

Lory, S. (2014). The Family *Staphylococcaceae*. In E. Rosenberg, E. F. DeLong, S. Lory, E. Stackebrandt, & F. Thompson (Eds.), *The Prokaryotes: Firmicutes and Tenericutes* (pp. 363-366). Berlin, Heidelberg: Springer Berlin Heidelberg.

Lovering, A. L., Safadi, S. S., & Strynadka, N. C. J. (2012). Structural Perspective of Peptidoglycan Biosynthesis and Assembly. *Annual Review of Biochemistry, 81*(1), 451-478. doi:10.1146/annurev-biochem-061809-112742

Lowy, F. D. (1998). *Staphylococcus aureus* Infections. *New England Journal of Medicine, 339*(8), 520-532. doi:10.1056/nejm199808203390806

Lowy, F. D. (2003). Antimicrobial resistance: the example of *Staphylococcus aureus*. *The Journal of clinical investigation, 111*(9), 1265-1273. doi:10.1172/JCI18535

Mahmood, T., & Yang, P.-C. (2012). Western blot: technique, theory, and trouble shooting. *North American journal of medical sciences, 4*(9), 429-434. doi:10.4103/1947-2714.100998

Mardis, E. R. (2017). DNA sequencing technologies: 2006–2016. *Nature protocols, 12*(2), 213-218. doi:10.1038/nprot.2016.182

Matias, V. R., & Beveridge, T. J. (2007). Cryo-electron microscopy of cell division in *Staphylococcus aureus* reveals a mid-zone between nascent cross walls. *Mol Microbiol, 64*(1), 195-206. doi:10.1111/j.1365-2958.2007.05634.x

McCarthy, A. J., & Lindsay, J. A. (2010). Genetic variation in *Staphylococcus aureus* surface and immune evasion genes is lineage associated: implications for vaccine design and host-pathogen interactions. *BMC Microbiology, 10*(1), 173. doi:10.1186/1471-2180-10-173

Młynarczyk, A., Młynarczyk, G., & Jeljaszewicz, J. (1998). The Genome of *Staphylococcus aureus*: A Review. *Zentralblatt für Bakteriologie, 287*(4), 277-314. doi:10.1016/S0934-8840(98)80165-5

Monk, I. R., Tree, J. J., Howden, B. P., Stinear, T. P., & Foster, T. J. (2015). Complete Bypass of Restriction Systems for Major *Staphylococcus aureus* Lineages. *mBio, 6*(3), e00308-00315. doi:10.1128/mBio.00308-15

Monteiro, J. M., Pereira, A. R., Reichmann, N. T., Saraiva, B. M., Fernandes, P. B., Veiga, H., . . . Pinho, M. G. (2018). Peptidoglycan synthesis drives an FtsZ-treadmilling-independent step of cytokinesis. *Nature, 554*(7693), 528-532. doi:10.1038/nature25506

Morris, A., Kellner, J. D., & Low, D. E. (1998). The superbugs: evolution, dissemination and fitness. *Current Opinion in Microbiology, 1*(5), 524-529. doi:10.1016/S1369-5274(98)80084-2

Myrbråten, I. S., Wiull, K., Salehian, Z., Håvarstein, L. S., Straume, D., Mathiesen, G., & Kjos, M. (2019). CRISPR Interference for Rapid Knockdown of Essential Cell Cycle Genes in *Lactobacillus plantarum*. *mSphere, 4*(2), e00007-00019. doi:10.1128/mSphere.00007-19

Nelson, D. L., & Cox, M. M. (2017a). Chapter 3 - Amino Acids, Peptides and Proteins. In *Lehninger Principles of Biochemistry (Seventh edition)* (pp. 75-155). New York: Macmillan Higher Education.

Nelson, D. L., & Cox, M. M. (2017b). Chapter 8 - Nucleotides and Nucleic Acids. In *Lehninger Principles of Biochemistry (Seventh edition)* (pp. 279-317). New York: Macmillan Higher Education.

New England Biolabs. (2021). PCR Protocol for Phusion® High-Fidelity DNA Polymerase (M0530). Retrieved from https://www.neb.com/protocols/0001/01/01/pcr-protocol-m0530

Nishibori, A., Kusaka, J., Hara, H., Umeda, M., & Matsumoto, K. (2005). Phosphatidylethanolamine Domains and Localization of Phospholipid Synthases in *Bacillus subtilis* Membranes. *Journal of bacteriology, 187*(6), 2163-2174. doi:10.1128/jb.187.6.2163-2174.2005

Novick, R. (1967). Properties of a cryptic high-frequency transducing phage in *Staphylococcus aureus*. *Virology, 33*(1), 155-166. doi:10.1016/0042-6822(67)90105-5

Novick, R. P. (2003). Autoinduction and signal transduction in the regulation of staphylococcal virulence. *Molecular Microbiology, 48*(6), 1429-1449. doi:10.1046/j.1365-2958.2003.03526.x

Ogston, A. (1882). Micrococcus Poisoning. *Journal of anatomy and physiology, 16*(4), 526-567. Retrieved from https://pubmed.ncbi.nlm.nih.gov/17231444

Ogston, A. (1984). "On Abscesses". *Reviews of Infectious Diseases, 6*(1), 122-128. doi:10.1093/clinids/6.1.122

Oku, Y., Kurokawa, K., Matsuo, M., Yamada, S., Lee, B.-L., & Sekimizu, K. (2009). Pleiotropic Roles of Polyglycerolphosphate Synthase of Lipoteichoic Acid in Growth

of *Staphylococcus aureus* Cells. *Journal of bacteriology, 191*(1), 141-151. doi:10.1128/jb.01221-08

Olsen, J. E., Christensen, H., & Aarestrup, F. M. (2006). Diversity and evolution of *blaZ* from *Staphylococcus aureus* and coagulase-negative staphylococci. *Journal of Antimicrobial Chemotherapy, 57*(3), 450-460. doi:10.1093/jac/dki492

Otten, C., Brilli, M., Vollmer, W., Viollier, P. H., & Salje, J. (2018). Peptidoglycan in obligate intracellular bacteria. *Molecular Microbiology, 107*(2), 142-163. doi:10.1111/mmi.13880

Otto, M. (2014). *Staphylococcus aureus* toxins. *Current Opinion in Microbiology, 17*, 32-37. doi:10.1016/j.mib.2013.11.004

Painter, K. L., Krishna, A., Wigneshweraraj, S., & Edwards, A. M. (2014). What role does the quorum-sensing accessory gene regulator system play during *Staphylococcus aureus* bacteremia? *Trends in Microbiology, 22*(12), 676-685. doi:10.1016/j.tim.2014.09.002

Pasquina, L., Santa Maria, J. P., Jr., McKay Wood, B., Moussa, S. H., Matano, L. M., Santiago, M., . . . Walker, S. (2016). A synthetic lethal approach for compound and target identification in *Staphylococcus aureus*. *Nature chemical biology, 12*(1), 40-45. doi:10.1038/nchembio.1967

Pasquina, L. W., Santa Maria, J. P., & Walker, S. (2013). Teichoic acid biosynthesis as an antibiotic target. *Current Opinion in Microbiology, 16*(5), 531-537. doi:10.1016/j.mib.2013.06.014

Pichoff, S., & Lutkenhaus, J. (2005). Tethering the Z ring to the membrane through a conserved membrane targeting sequence in FtsA. *Molecular Microbiology, 55*(6), 1722-1734. doi:10.1111/j.1365-2958.2005.04522.x

Pinho, M. G., & Errington, J. (2003). Dispersed mode of *Staphylococcus aureus* cell wall synthesis in the absence of the division machinery. *Molecular Microbiology, 50*(3), 871-881. doi:10.1046/j.1365-2958.2003.03719.x

Pinho, M. G., Kjos, M., & Veening, J.-W. (2013). How to get (a)round: mechanisms controlling growth and division of coccoid bacteria. *Nature Reviews Microbiology, 11*(9), 601-614. doi:10.1038/nrmicro3088

Qi, Lei S., Larson, Matthew H., Gilbert, Luke A., Doudna, Jennifer A., Weissman, Jonathan S., Arkin, Adam P., & Lim, Wendell A. (2013). Repurposing CRISPR as an RNA-Guided Platform for Sequence-Specific Control of Gene Expression. *Cell, 152*(5), 1173-1183. doi:10.1016/j.cell.2013.02.022

Reed, P., Veiga, H., Jorge, A. M., Terrak, M., & Pinho, M. G. (2011). Monofunctional Transglycosylases Are Not Essential for *Staphylococcus aureus* Cell Wall Synthesis. *Journal of bacteriology, 193*(10), 2549-2556. doi:10.1128/jb.01474-10

Reichmann, N. T., & Gründling, A. (2011). Location, synthesis and function of glycolipids and polyglycerolphosphate lipoteichoic acid in Gram-positive bacteria of the phylum *Firmicutes*. *FEMS Microbiology Letters, 319*(2), 97-105. doi:10.1111/j.1574-6968.2011.02260.x

Reichmann, N. T., Piçarra Cassona, C., Monteiro, J. M., Bottomley, A. L., Corrigan, R. M., Foster, S. J., . . . Gründling, A. (2014). Differential localization of LTA synthesis proteins and their interaction with the cell division machinery in *Staphylococcus aureus*. *Molecular Microbiology, 92*(2), 273-286. doi:10.1111/mmi.12551

Reichmann, N. T., Tavares, A. C., Saraiva, B. M., Jousselin, A., Reed, P., Pereira, A. R., . . . Pinho, M. G. (2019). SEDS–bPBP pairs direct lateral and septal peptidoglycan synthesis in *Staphylococcus aureus*. *Nature Microbiology, 4*(8), 1368-1377. doi:10.1038/s41564-019-0437-2

Rismondo, J., Gillis, A., & Gründling, A. (2021). Modifications of cell wall polymers in Gram-positive bacteria by multi-component transmembrane glycosylation systems. *Current Opinion in Microbiology, 60*, 24-33. doi:10.1016/j.mib.2021.01.007

Roane, T. M., & Pepper, I. L. (2015). Chapter 9 - Microscopic Techniques. In I. L. Pepper, C. P. Gerba, & T. J. Gentry (Eds.), *Environmental Microbiology (Third Edition)* (pp. 177-193). San Diego: Academic Press.

Rosenbach, A. J. F. (1884). *Mikro-organismen bei den Wund-infections-krankheiten des Menschen*: JF Bergmann.

Saiki, R., Scharf, S., Faloona, F., Mullis, K., Horn, G., Erlich, H., & Arnheim, N. (1985). Enzymatic amplification of beta-globin genomic sequences and restriction site analysis for diagnosis of sickle cell anemia. *Science, 230*(4732), 1350-1354. doi:10.1126/science.2999980

Saleski, T. E., Chung, M. T., Carruthers, D. N., Khasbaatar, A., Kurabayashi, K., & Lin, X. N. (2021). Optimized gene expression from bacterial chromosome by high-throughput integration and screening. *Science Advances, 7*(7), eabe1767. doi:10.1126/sciadv.abe1767

Saraiva, B. M., Sorg, M., Pereira, A. R., Ferreira, M. J., Caulat, L. C., Reichmann, N. T., & Pinho, M. G. (2020). Reassessment of the distinctive geometry of *Staphylococcus aureus* cell division. *Nature communications, 11*(1), 4097. doi:10.1038/s41467-020-17940-9

Sass, P., & Brötz-Oesterhelt, H. (2013). Bacterial cell division as a target for new antibiotics. *Current Opinion in Microbiology, 16*(5), 522-530. doi:10.1016/j.mib.2013.07.006

Sauvage, E., Kerff, F., Terrak, M., Ayala, J. A., & Charlier, P. (2008). The penicillin-binding proteins: structure and role in peptidoglycan biosynthesis. *FEMS Microbiology Reviews, 32*(2), 234-258. doi:10.1111/j.1574-6976.2008.00105.x

Scheffers, D.-J., de Wit, J. G., den Blaauwen, T., & Driessen, A. J. (2002). GTP hydrolysis of cell division protein FtsZ: evidence that the active site is formed by the association of monomers. *Biochemistry, 41*(2), 521-529. doi:10.1021/bi011370i

Schito, G. C. (2006). The importance of the development of antibiotic resistance in *Staphylococcus aureus*. *Clinical Microbiology and Infection, 12*(s1), 3-8. doi:10.1111/j.1469-0691.2006.01343.x

Sewell, E. W. C., & Brown, E. D. (2014). Taking aim at wall teichoic acid synthesis: new biology and new leads for antibiotics. *The Journal of Antibiotics, 67*(1), 43-51. doi:10.1038/ja.2013.100

Sharif, S., Singh, M., Kim, S. J., & Schaefer, J. (2009). *Staphylococcus aureus* peptidoglycan tertiary structure from carbon-13 spin diffusion. *Journal of the American Chemical Society, 131*(20), 7023-7030. doi:10.1021/ja808971c

Shendure, J., & Ji, H. (2008). Next-generation DNA sequencing. *Nature Biotechnology, 26*(10), 1135-1145. doi:10.1038/nbt1486

Sieradzki, K., & Tomasz, A. (2003). Alterations of Cell Wall Structure and Metabolism Accompany Reduced Susceptibility to Vancomycin in an Isogenic Series of Clinical Isolates of *Staphylococcus aureus*. *Journal of bacteriology, 185*(24), 7103-7110. doi:10.1128/jb.185.24.7103-7110.2003

Silhavy, T. J., Kahne, D., & Walker, S. (2010). The bacterial cell envelope. *Cold Spring Harbor perspectives in biology, 2*(5), a000414. doi:10.1101/cshperspect.a000414

Skinner, D., & Keefer, C. S. (1941). Significance of bacteremia caused by *Staphylococcus aureus*: A study of one hundred and twenty-two cases and a review of the literature concerned with experimental infection in animals. *Archives of Internal Medicine, 68*(5), 851-875. doi:10.1001/archinte.1941.00200110003001

Stamsås, G. A., Myrbråten, I. S., Straume, D., Salehian, Z., Veening, J.-W., Håvarstein, L. S., & Kjos, M. (2018). CozEa and CozEb play overlapping and essential roles in controlling cell division in *Staphylococcus aureus*. *Molecular Microbiology, 109*(5), 615-632. doi:10.1111/mmi.13999

Stamsås, G. A., Restelli, M., Ducret, A., Freton, C., Garcia, P. S., Håvarstein, L. S., . . . Kjos, M. (2020). A CozE Homolog Contributes to Cell Size Homeostasis of *Streptococcus pneumoniae*. *mBio, 11*(5), e02461-02420. doi:10.1128/mBio.02461-20

Stapleton, M. R., Horsburgh, M. J., Hayhurst, E. J., Wright, L., Jonsson, I.-M., Tarkowski, A., . . . Foster, S. J. (2007). Characterization of IsaA and SceD, Two Putative Lytic Transglycosylases of *Staphylococcus aureus*. *Journal of bacteriology, 189*(20), 7316-7325. doi:10.1128/jb.00734-07

Steele, V. R., Bottomley, A. L., Garcia-Lara, J., Kasturiarachchi, J., & Foster, S. J. (2011). Multiple essential roles for EzrA in cell division of *Staphylococcus aureus*. *Molecular Microbiology, 80*(2), 542-555. doi:10.1111/j.1365-2958.2011.07591.x

Stevenson, K., McVey, A. F., Clark, I. B. N., Swain, P. S., & Pilizota, T. (2016). General calibration of microbial growth in microplate readers. *Scientific Reports, 6*(1), 38828. doi:10.1038/srep38828

Stryjewski, M. E., & Corey, G. R. (2014). Methicillin-Resistant *Staphylococcus aureus*: An Evolving Pathogen. *Clinical Infectious Diseases, 58*(suppl_1), S10-S19. doi:10.1093/cid/cit613

Swoboda, J. G., Campbell, J., Meredith, T. C., & Walker, S. (2010). Wall Teichoic Acid Function, Biosynthesis, and Inhibition. *ChemBioChem, 11*(1), 35-45. doi:10.1002/cbic.200900557

Taguchi, A., Welsh, M. A., Marmont, L. S., Lee, W., Sjodt, M., Kruse, A. C., . . . Walker, S. (2019). FtsW is a peptidoglycan polymerase that is functional only in complex with its cognate penicillin-binding protein. *Nature Microbiology, 4*(4), 587-594. doi:10.1038/s41564-018-0345-x

Tong, S. Y. C., Davis, J. S., Eichenberger, E., Holland, T. L., & Fowler, V. G., Jr. (2015). *Staphylococcus aureus infections*: epidemiology, pathophysiology, clinical manifestations, and management. *Clinical Microbiology Reviews, 28*(3), 603-661. doi:10.1128/CMR.00134-14

Typas, A., Banzhaf, M., Gross, C. A., & Vollmer, W. (2012). From the regulation of peptidoglycan synthesis to bacterial growth and morphology. *Nature Reviews Microbiology, 10*(2), 123-136. doi:10.1038/nrmicro2677

van Belkum, A., Melles, D. C., Nouwen, J., van Leeuwen, W. B., van Wamel, W., Vos, M. C., . . . Verbrugh, H. A. (2009). Co-evolutionary aspects of human colonisation and infection by *Staphylococcus aureus*. *Infection, Genetics and Evolution, 9*(1), 32-47. doi:10.1016/j.meegid.2008.09.012

Veiga, H., Jorge, A. M., & Pinho, M. G. (2011). Absence of nucleoid occlusion effector Noc impairs formation of orthogonal FtsZ rings during *Staphylococcus aureus* cell division. *Molecular Microbiology, 80*(5), 1366-1380. doi:10.1111/j.1365-2958.2011.07651.x

Vollmer, W., Blanot, D., & De Pedro, M. A. (2008). Peptidoglycan structure and architecture. *FEMS Microbiology Reviews, 32*(2), 149-167. doi:10.1111/j.1574-6976.2007.00094.x

Vollmer, W., & Seligman, S. J. (2010). Architecture of peptidoglycan: more data and more models. *Trends in Microbiology, 18*(2), 59-66. doi:10.1016/j.tim.2009.12.004

VWR. (2013). VWR Taq DNA Polymerase Master Mix. Retrieved from https://no.vwr.com/assetsvc/asset/no_NO/id/12367456/contents

Walter, A., Unsleber, S., Rismondo, J., Jorge, A. M., Peschel, A., Gründling, A., & Mayer, C. (2020). Phosphoglycerol-type wall and lipoteichoic acids are enantiomeric polymers

differentiated by the stereospecific glycerophosphodiesterase GlpQ. *Journal of Biological Chemistry, 295*(12), 4024-4034. doi:10.1074/jbc.RA120.012566

Wang, B., & Muir, Tom W. (2016). Regulation of Virulence in *Staphylococcus aureus*: Molecular Mechanisms and Remaining Puzzles. *Cell Chemical Biology, 23*(2), 214-224. doi:10.1016/j.chembiol.2016.01.004

Wang, J. D., & Levin, P. A. (2009). Metabolism, cell growth and the bacterial cell cycle. *Nature Reviews Microbiology, 7*(11), 822-827. doi:10.1038/nrmicro2202

Watson, J. D., Baker, T. A., Bell, S. P., Gann, A., Levine, M., & Losick, R. (2013). Chapter 7 - Techniques of Molecular Biology. In *Molecular Biology of the Gene (Seventh Edition)* (pp. 147-191). United States of America: Pearson Education.

Weart, R. B., Lee, A. H., Chien, A.-C., Haeusser, D. P., Hill, N. S., & Levin, P. A. (2007). A Metabolic Sensor Governing Cell Size in Bacteria. *Cell, 130*(2), 335-347. doi:10.1016/j.cell.2007.05.043

Wheeler, R., Turner, R. D., Bailey, R. G., Salamaga, B., Mesnage, S., Mohamad, S. A. S., . . . Foster, S. J. (2015). Bacterial Cell Enlargement Requires Control of Cell Wall Stiffness Mediated by Peptidoglycan Hydrolases. *mBio, 6*(4), e00660-00615. doi:10.1128/mBio.00660-15

Willey, J. M., Sherwood, L., & Woolverton, C. J. (2017a). Chapter 2 - Microscopy. In *Prescott's microbiology (Tenth Edition)* (pp. 22-41). New York: McGraw-Hill Education.

Willey, J. M., Sherwood, L., & Woolverton, C. J. (2017b). Chapter 3 - Bacterial Cell Structure. In *Prescott's microbiology (Tenth Edition)* (pp. 42-79). New York: McGraw-Hill Education.

Willey, J. M., Sherwood, L., & Woolverton, C. J. (2017c). Chapter 7 - Microbal Growth In *Prescott's microbiology (Tenth Edition)* (pp. 132-171). New York: McGraw-Hill Education.

Willey, J. M., Sherwood, L., & Woolverton, C. J. (2017d). Chapter 17 - Recombinant DNA Technology. In *Prescott's microbiology (Tenth Edition)* (pp. 400-418). New York: McGraw-Hill Education.

Willey, J. M., Sherwood, L., & Woolverton, C. J. (2017e). Chapter 18 - Microbal Genomics. In *Prescott's microbiology (Tenth Edition)* (pp. 419-442). New York: McGraw-Hill Education.

Williams, R. E. (1963). Healthy carriage of *Staphylococcus aureus*: its prevalence and importance. *Bacteriological reviews, 27*(1), 56-71. Retrieved from https://pubmed.ncbi.nlm.nih.gov/14000926

Wyke, A. W., Ward, J. B., Hayes, M. V., & Curtis, N. A. C. (1981). A Role in vivo for Penicillin-Binding Protein-4 of *Staphylococcus aureus*. *European Journal of Biochemistry, 119*(2), 389-393. doi:10.1111/j.1432-1033.1981.tb05620.x

Xia, G., Kohler, T., & Peschel, A. (2010). The wall teichoic acid and lipoteichoic acid polymers of *Staphylococcus aureus*. *International Journal of Medical Microbiology, 300*(2), 148-154. doi:10.1016/j.ijmm.2009.10.001

Yu, H.-W., Halonen, M. J., & Pepper, I. L. (2015). Chapter 12 - Immunological Methods. In I. L. Pepper, C. P. Gerba, & T. J. Gentry (Eds.), *Environmental Microbiology (Third Edition)* (pp. 245-269). San Diego: Academic Press.

Yu, W., Herbert, S., Graumann, P. L., & Götz, F. (2010). Contribution of SMC (Structural Maintenance of Chromosomes) and SpoIIIE to Chromosome Segregation in Staphylococci. *Journal of bacteriology, 192*(15), 4067-4073. doi:10.1128/jb.00010-10

Zarghampoor, F., Behzad-Behbahani, A., Azarpira, N., Khatami, S. R., Fanian, M., Hossein Aghdaie, M., & Rafiei Dehbidi, G. (2020). A Single Tube Overlap Extension PCR Method for Splicing of Multiple DNA Fragments. *Avicenna journal of medical*

biotechnology, 12(1), 37-43. Retrieved from https://pubmed.ncbi.nlm.nih.gov/32153737

Zerbib, D. (2017). Chapter 25 - Bacterial Cell Envelopes: Composition, Architecture, and Origin. In D. Miklavčič (Ed.), *Handbook of Electroporation* (pp. 417-436). Cham: Springer International Publishing.

Zhang, B., Liu, X., Lambert, E., Mas, G., Hiller, S., Veening, J.-W., & Perez, C. (2020). Structure of a proton-dependent lipid transporter involved in lipoteichoic acids biosynthesis. *Nature Structural & Molecular Biology, 27*(6), 561-569. doi:10.1038/s41594-020-0425-5

Zhao, C., Shu, X., & Sun, B. (2017). Construction of a Gene Knockdown System Based on Catalytically Inactive ("Dead") Cas9 (dCas9) in *Staphylococcus aureus*. *Applied and environmental microbiology, 83*(12), e00291-00217. doi:10.1128/AEM.00291-17

Zhou, X., Halladin, D. K., Rojas, E. R., Koslover, E. F., Lee, T. K., Huang, K. C., & Theriot, J. A. (2015). Mechanical crack propagation drives millisecond daughter cell separation in *Staphylococcus aureus*. *Science, 348*(6234), 574-578. doi:10.1126/science.aaa1511

Appendix

A1 Table of the mutant strains used in this work.

Table A1.1 Mutants used in this work.

Strain name	Genotype and characteristics	Reference
S. aureus NCTC8325-4		
MDB1	NCTC8325-4	Laboratory stock
MDB2	NCTC8325-4 Δ*cozEa*, spc^r	Laboratory stock
MDB3	NCTC8325-4 Δ*cozEb*, spc^r	Laboratory stock
MH225	MDB1 carrying pLOW-dCas9_extra_*lacO*, ery^r	Laboratory stock
MH223	MDB2 carrying pLOW-dCas9_extra_*lacO*, ery^r	Laboratory stock
MH224	MDB3 carrying pLOW-dCas9_extra_*lacO*, ery^r	Laboratory stock
MDB11	MH223 carrying pCG248-sgRNA(*cozEb*), ery^r, cam^r	This work
MDB12	MH224 carrying pCG248-sgRNA(*cozEa*), ery^r, cam^r	This work
MDB13	MH225 carrying pCG248-sgRNA(*cozEa*+*cozEb*), ery^r, cam^r	This work
MDB14	MH225 carrying pCG248-sgRNA(*cozEa*), ery^r, cam^r	This work
MDB15	MH225 carrying pCG248-sgRNA(*cozEb*), ery^r, cam^r	This work
MM75	MH225 carrying pVL2336-sgRNA(*luc*), ery^r, cam^r	Laboratory stock
MK1582	MDB1, but with *gfp* fused to the 3' end of *cozEa*, spc^r	Laboratory stock
MK1584	MDB1, but with *gfp* fused to the 3' end of *cozEb*, spc^r	Laboratory stock
MDB25	MH223 carrying pCG248-sgRNA(*cozEb*+*ugtP*-*ltaA*), ery^r, cam^r	This work
MDB26	MH223 carrying pCG248-sgRNA(*cozEb*+*ltaS*), ery^r, cam^r	This work
MDB27	MH223 carrying pCG248-sgRNA(*cozEb*+*dltA*), ery^r, cam^r	This work
MDB28	MH223 carrying pVL2336-sgRNA(*ugtP*-*ltaA*), ery^r, cam^r	This work
MDB29	MH223 carrying pVL2336-sgRNA(*ltaS*), ery^r, cam^r	This work
MDB30	MH223 carrying pVL2336-sgRNA(*dltA*), ery^r, cam^r	This work
MDB31	MH223 carrying pCG248-sgRNA(luc), ery^r, cam^r	This work
MDB35	MH225 carrying pVL2336-sgRNA(*ugtP*-*ltaA*), ery^r, cam^r	This work
MDB36	MH224 carrying pVL2336-sgRNA(*ugtP*-*ltaA*), ery^r, cam^r	This work
MDB58	MDB3 carrying pRAB11-*cozEa*, cam^r	This work
MDB62	MDB3 carrying pRAB11-*cozEb*, cam^r	Laboratory stock
MDB63	MDB3 carrying pRAB11-*lacA*, cam^r	Laboratory stock
MDB64	MDB1 carrying pLOW- *gfp_ugtP*, ery^r	This work
MDB65	MDB2 carrying pLOW- *gfp_ugtP*, ery^r	This work
MDB66	MDB3 carrying pLOW- *gfp_ugtP*, ery^r	This work
MDB77	MDB1, but with *gfp* fused to the 5' end of *ugtP*, spc^r	This work
MDB78	MDB77 carrying pLOW-dCas9_extra_*lacO*, ery^r	This work
MDB79	MDB78 carrying pCG248-sgRNA(*cozEa*+*cozEb*), ery^r, cam^r	This work

S. aureus NCTC8325		
MDB68	NCTC8325	Laboratory stock
MDB69	NCTC8325 Δ*ltaA*, spc^r	Laboratory stock
MDB70	MDB68 carrying pLOW-dCas9_extra_*lacO*, ery^r	This work
MDB71	MDB69 carrying pLOW-dCas9_extra_*lacO*, ery^r	This work
MDB75	MDB70 carrying pCG248-sgRNA(*cozEa*+*cozEb*), ery^r, cam^r	This work
MDB76	MDB71 carrying pCG248-sgRNA(*cozEa*+*cozEb*), ery^r, cam^r	This work
MDB80	NCTC8325 Δ*ugtP*, spc^r	This work
MDB81	MDB80 carrying pLOW-dCas9_extra_*lacO*, ery^r	This work
MDB82	MDB81 carrying pCG248-sgRNA(*cozEa*), ery^r, cam^r	This work
MDB83	MDB81 carrying pCG248-sgRNA(*cozEb*), ery^r, cam^r	This work
MDB84	MDB81 carrying pCG248-sgRNA(*cozEa*+*cozEb*), ery^r, cam^r	This work
S. aureus JE2		
MDB9	JE2	Laboratory stock
MDB10	JE2 Δ*cozEb*, ery^r	Laboratory stock
MDB16	MDB9 carrying pLOW-dCas9_aad9, spc^r	This work
MDB17	MDB16 carrying pCG248-sgRNA(*cozEa*), spc^r, cam^r	This work
MDB18	MDB16 carrying pCG248-sgRNA(*cozEb*), spc^r, cam^r	This work
MDB19	MDB16 carrying pCG248-sgRNA(*cozEa*+*cozEb*), spc^r, cam^r	This work
MDB20	MDB10 carrying pLOW-dCas9_aad9, spc^r	This work
MDB21	MDB20 carrying pCG248-sgRNA(*cozEa*+*cozEb*), spc^r, cam^r	This work
MDB37	JE2	Laboratory stock
MDB38	JE2 Δ*cozEa*, ery^r	Laboratory stock
MDB39	JE2 Δ*ugtP*, ery^r	Laboratory stock
MDB40	JE2 Δ*ltaA*, ery^r	Laboratory stock
MDB41	MDB39 carrying pLOW-dCas9_aad9, spc^r	This work
MDB42	MDB40 carrying pLOW-dCas9_aad9, spc^r	This work
MDB44	MDB16 carrying pCG248-sgRNA(luc), spc^r, cam^r	This work
MDB45	MDB41 carrying pCG248-sgRNA(*cozEa*+*cozEb*), spc^r, cam^r	This work
MDB46	MDB42 carrying pCG248-sgRNA(*cozEa*+*cozEb*), spc^r, cam^r	This work
MDB47	MDB41 carrying pCG248-sgRNA(*luc*), spc^r, cam^r	This work
MDB48	MDB42 carrying pCG248-sgRNA(*luc*), spc^r, cam^r	This work
MDB54	MDB41 carrying pCG248-sgRNA(*cozEa*), spc^r, cam^r	This work
MDB55	MDB41 carrying pCG248-sgRNA(*cozEb*), spc^r, cam^r	This work
MDB56	MDB42 carrying pCG248-sgRNA(*cozEa*), spc^r, cam^r	This work
MDB57	MDB42 carrying pCG248-sgRNA(*cozEb*), spc^r, cam^r	This work
MDB59	MDB10 carrying pRAB11-*cozEa*, cam^r	This work
MDB60	MDB10 carrying pRAB11-*cozEb*, cam^r	This work
MDB61	MDB10 carrying pRAB11-*lacA*, cam^r	This work

S. aureus COL		
MDB32	COL	Laboratory stock
MDB34	COL Δ*cozEb*, spc^r	Laboratory stock
E. coli IM08B		
MDB4	IM08B carrying pCG248-sgRNA(*cozEa*), amp^r	Laboratory stock
MDB5	IM08B carrying pCG248-sgRNA(*cozEb*), amp^r	Laboratory stock
MDB52	IM08B carrying pCG248-sgRNA(*cozEa*+*cozEb*), amp^r	Laboratory stock
MDB7	IM08B carrying pLOW-dCas9_extra_*lacO*, amp^r	Laboratory stock
IM225	IM08B carrying pLOW-dCas9_aad9, amp^r	Laboratory stock
MDB22	IM08B carrying pCG248-sgRNA(*cozEb*+*ugtP*-*ltaA*), amp^r	This work
MDB23	IM08B carrying pCG248-sgRNA(*cozEb*+*ltaS*), amp^r	This work
MDB24	IM08B carrying pCG248-sgRNA(*cozEb*+*dltA*), amp^r	This work
MK1794	IM08B carrying pVL2336-sgRNA(*ugtP*-*ltaA*), amp^r	Laboratory stock
MK1793	IM08B carrying pVL2336-sgRNA(*ltaS*), amp^r	Laboratory stock
MH274	IM08B carrying pVL2336-sgRNA(*dltA*), amp^r	Laboratory stock
IM210	IM08B carrying pCG248-sgRNA(*luc*), amp^r	Laboratory stock
MDB43	IM08B carrying pLOW-m(sf)*gfp*-SA1477, amp^r	Laboratory stock
MDB49	IM08B carrying pRAB11-*cozEa*, amp^r	Laboratory stock
MDB50	IM08B carrying pRAB11-*cozEb*, amp^r	Laboratory stock
MDB51	IM08B carrying pRAB11-*lacA*, amp^r	Laboratory stock
MDB53	IM08B carrying pLOW-*gfp_ugtP*, amp^r	This work
MK1008	IM08B carrying pMAD-I-SceI, amp^r	Laboratory stock
MK1544	IM08B carrying pMAD-ori_*parS*, amp^r	Laboratory stock
MDB72	IM08B carrying pMAD-Δ*ugtP*::*spc*, amp^r	This work
MDB73	IM08B carrying pMAD-*gfp_ugtP*::*spc*, amp^r	This work
E. coli DH5α		
MK1029	DH5α carrying pCN55, amp^r	Laboratory stock

a. spc^r = spectinomycin resistant, ery^r = erythromycin resistant, cam^r = chloramphenicol resistant, and amp^r = ampicillin resistant.

A2 Table of the primers used in this work.

Table A2.1 Primers used in this work.

Primer name	Sequence 5'-3'	Description	Reference
Primers to check for the presence of *cozEa*			
IM17	ATCGGTACCCAATAAAACTAGGAGGA AATTTAAATGTTAAACAAGGTTTGGTT CC	*cozEa* F w/ KpnI RS	Ine Myrbråten
IM18	GATGAATTCTTAGTCCTTAACATTACTG TTTG	*cozEa* R w/ EcoRI RS	Ine Myrbråten
Primers to check for the deletion of *cozEa*			
MK188	ATTGGGCCCACCTAGGATC	F upstream of *cozEa* deletion	Dr. Morten Kjos
MK187	CAAACATTTATCGTTGTAATACGT	R downstream of *cozEa* deletion	Dr. Morten Kjos
Primers to check for the presence of *cozEb*			
GS653	GATCGGATCCCAATGAAAATGAAAAG AATATAAGAAAG	*cozEb* F w/BamHI RS	Dr. Gro Stamsås
GS654	GATCGAATCCTTTATTCAACTATTTTAT TACTTTCTTTA	*cozEb* R	Dr. Gro Stamsås
Primers to check for the deletion of *cozEb*			
MK188	ATTGGGCCCACCTAGGATC	F upstream of *cozEb* deletion	Dr. Morten Kjos
MK195	GCGTCAACAATTACACCACAG	R downstream of *cozEb* deletion	Dr. Morten Kjos
Primers to check for the presence of ltaA			
MDB10	ACGTGGATCCGAAAGGTTCCTTTATAT GCAAG	*ltaA* F w/ BamHI RS	This work
MDB11	ACGTGAATTCCGTTTTAACCTTACTTAG CTTTT	*ltaA* R w/ EcoRI RS	This work
Primers to check for the presence of pCG248 plasmids			
MK26	GGATAACCGTATTACCGCCT	pCG248 F	Dr. Morten Kjos
MK25	AAATCTCGAAAATAATAGAGGGA	pCG248 R	Dr. Morten Kjos
Primers to check for the presence of pRAB11 plasmids			
MK23	GGATCCCCTCGAGTTCATG	pRAB11 F	Dr. Morten Kjos
MK24	GGGATGTGCTGCAAGGCGA	pRAB11 R	Dr. Morten Kjos
Primers to check for the presence of pMAD plasmids			
IM156	AATCTAGCTAATGTTACGTTACA	pMAD F	Ine Myrbråten
MK177	GATGCCGCCGGAAGCGAG	pMAD R	Dr. Morten Kjos
Primers for construction of pLOW-*gfp_ugtP*			
MDB9	ACGTGGATCCGTTACTCAAAATAAAAA GATATTGA	*ugtP* F w/ BamHI RS	This work
MDB2	ACGTGAATTCATGATTAGCGTAATTAT TTAACG	*ugtP* R w/ EcoRI RS	This work
Primers for construction of pMAD-*gfp_uptP*::*spc*			
MDB3	ACCTGAATTCGGTATCGCTAGCGATGG CT	ori_up F w/ EcoRI RS	This work
MDB4	TCGAACCCCGATGTTGTCG	ori_up R	This work

MDB5	CGACAACATCGGGGTTCGACAATATGTTTATTATACACGT	P_{ugtP} F overlapping ori_up	This work
MDB6	GTGAACAGCTCTTCTCCTTTTGACATTAATAGCCACCCTCCGTTAG	P_{ugtP} R overlapping *gfp*	This work
MK48	ATGTCAAAAGGAGAAGAGCTGTTCAC	*gfp* F	Dr. Morten Kjos
MDB7	GATCCTAGGTGGGCCCAATTTATTTAACGAAGAATCTTGCATATAAAG	*ugtP* R overlapping *spc*	This work
MK188	ATTGGGCCCACCTAGGATC	*spc* F	Dr. Morten Kjos
MDB8	AGGTGTCGACATTGGTGGTATCGCTGTTGC	Ori_down R w/ SalI RS	This work
Primers for construction of pMAD-Δ*ugtP*::*spc*			
MK501	CAACGCCTCGCAGTCGTCC	*ugtP*_up F	This work
MK502	TTTCCGTTAATCAAATTGCTCATTAATAGCCACCCTCCGTTAG	*ugtP*_up R overlapping *spc*	This work
MK503	ATGAGCAATTTGATTAACGGAAA	*spc* F	This work
MK504	CTAATTGAGAGAAGTTTCTATAG	*spc* R	This work
MK505	CTATAGAAACTTCTCTCAATTAGAAAATTAAGTATGCTACACAGAC	*ugtP*_down F overlapping *spc*	This work
MK506	ACGTGGATCCGATAGCTAAAGCGATAATCCAC	ugtP_down R w/ BamHI RS	This work

a. F = forward primer, R = reverse primer, and RE = restriction site.
b. The restriction sites are underlined.

A3 Table of the chemicals used in this work.

Table A3.1 Chemicals used in this work.

Chemical	Formula	Product number	Supplier
4–20% Mini-PROTEAN® TGX™ Precast Protein Gels	-	4561094	Bio-Rad Laboratories
4′,6-diamidino-2-phenylindole (DAPI)	$C_{16}H_{17}Cl_2N_5$	D1306	Invitrogen
5-Bromo-4-chloro-3-indolyl-β-D-galactopyranoside (X-gal)	$C_{14}H_{15}BrClNO_6$	B4252	Sigma-Aldrich
7-hydroxycoumarincarbonylamino-D-alanine (HADA)	$C_{13}H_{13}ClN_2O_6$	HY-131045	MedChemExpress
Acetic acid	CH_3CO_2H	1.00063	Merck
Acrylamide 4x (40%), 37.5:1	C_3H_5NO	BIAC41	Saveen Werner
Agar powder	$(C_{12}H_{18}O_9)_n$	20767	VWR International
Ammonium persulfate (APS)	$(NH_4)_2S_2O_8$	A3678	Sigma-Aldrich
Bacto™ Tryptic Soy Broth (TSB)	-	211825	Becton, Dickinson and Company
BODIPY FL vancomycin (VanFL)	$C_{80}H_{88}BF_2Cl_2N_{11}O_{25}$	V34850	Invitrogen
Bis-acrylamide	$(H_2C{=}CHCONH)_2CH_2$	146072	Sigma-Aldrich
Brain Heart Infusion (BHI) Broth	-	CM1135	OXOID
Bromophenol blue	$C_{19}H_9Br_4O_5S$	B5525	Sigma-Aldrich
Calcium chloride dihydrate	$CaCl_2 \cdot 2H_2O$	1.02382	Merck
Certified molecular biology agarose	-	1613100	Bio-Rad Laboratories
D-(+)-Glucose anhydrous	$C_6H_{12}O_6$	101176K	VWR International
Disodium hydrogen phosphate	Na_2HPO_4	1.06586	Merck
Disodium hydrogen phosphate dihydrate	$Na_2HPO_4 \cdot 2H_2O$	1.06580	Merck
Dithiothreitol (DTT)	$HSCH_2CH(OH)CH(OH)CH_2SH$	D0632	Sigma-Aldrich
Ethanol (96%)	C_2H_5OH	20824	VWR International
Ethylenediaminetetraacetic acid (EDTA)	$C_{10}H_{14}N_2Na_2O_8 \cdot 2H_2O$	20296.360	VWR International
Glass beads, acid-washed ≤ 106 µm	-	G4649	Sigma-Aldrich
Glutaraldehyde solution (Grade I, 25% in H_2O)	$OHC(CH_2)_3CHO$	G5882	Sigma-Aldrich
Glycerol solution (86-89%)	$HOCH_2CH(OH)CH_2OH \cdot aq$	49781	Sigma-Aldrich
Glycine	$NH_2CH_2CO_2H$	A13816	Alfa Aesar
Isopropanol prima (99.9%)	$CH_3CHOHCH_3$	600079	Arcus
Magnesium chloride hexahydrate	$MgCl_2 \cdot 6H_2O$	M2393	Sigma-Aldrich
Methanol (≥ 99.9%)	CH_3OH	1.06009	Merck Millipore

Mueller Hinton (MH) Broth	-	CM0405	OXOID
N,N-dimethylformamide (DMF)	$HCON(CH_3)_2$	227056	Sigma-Aldrich
Paraformaldehyde	$(CH_2O)_n$	8.18715	Sigma-Aldrich
Pellet Paint® Co-Precipitant	-	69049	EMD Biosciences
Potassium chloride	KCl	1.04936	Merck
Potassium dihydrogen phosphate	KH_2PO_4	1.04873	Merck
Skim milk powder	-	1.15363	Merck Millipore
Sodium acetate	$H_3CCOONa$	27650.292	VWR International
Sodium cacodylate trihydrate	$(CH_3)_2AsO_2Na \cdot 3H_2O$	C0250	Sigma-Aldrich
Sodium chloride	NaCl	27810	VWR International
Sodium dodecyl sulfate (SDS)	$CH_3(CH_2)_{11}OSO_3Na$	05030	Fluka
Sodium hydroxide	NaOH	1.06498	Merck
Sucrose	$C_{12}H_{22}O_{11}$	84100	Sigma-Aldrich
N,N,N′,N′-Tetramethylethylenediamine (TEMED)	$(CH_3)_2NCH_2CH_2N(CH_3)_2$	T9281	Sigma-Aldrich
Trizma® base	$NH_2C(CH_2OH)_3$	T1503	Sigma-Aldrich
Tryptone	-	LP0042	OXOID
Tween-20	-	1706531	Bio-Rad Laboratories
UltraPure™ Agarose	-	15510-027	Invitrogen
Yeast extract	-	LP0021	OXOID
peqGREEN	-	PEQL37-501	Saveen Werner

A4 Single *cozEb* deletion in the *S. aureus* COL strain does not affect growth.

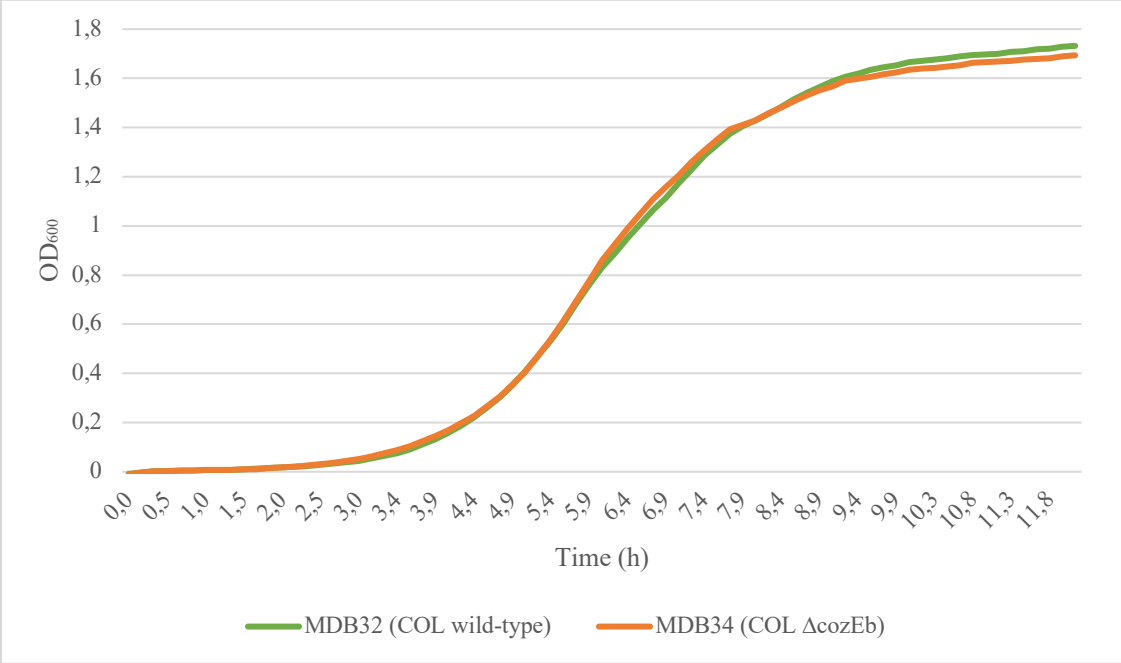

Figure A4.1 Growth curves for the COL wild-type strain (MDB32) and the COL Δ*cozEb* mutant strain (MDB34).

A5 No growth reduction is observed upon single knockdown of *cozEa* or *cozEb* in the Δ*ugtP* or Δ*ltaA* background (JE2 and NCTC8325).

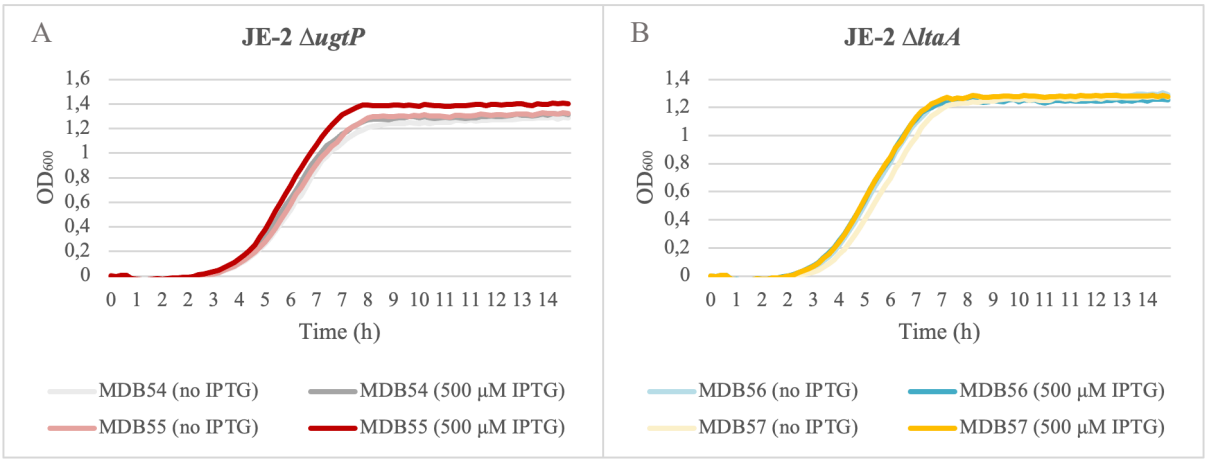

Figure A5.1 Growth of the JE2 Δ*ugtP* and Δ*ltaA* cells with single *cozE* knockdown.
A. Growth curves for the JE2 Δ*ugtP* strains targeting *cozEa* (MDB54) and *cozEb* (MDB55), with and without IPTG induction.
B. Growth curves for the JE2 Δ*ltaA* strains targeting *cozEa* (MDB56) and *cozEb* (MDB57), with and without IPTG induction.

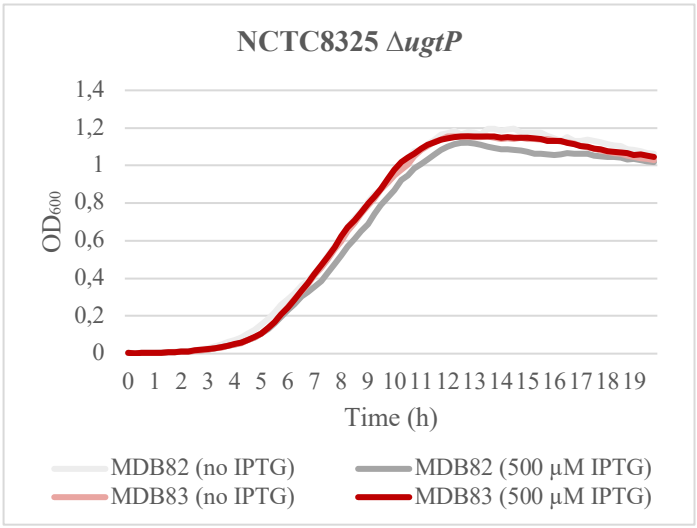

Figure A5.2 Growth of the NCTC8325 Δ*ugtP* cells with single *cozE* knockdown. Represented by the growth curves for the JE2 Δ*ugtP* strains targeting *cozEa* (MDB82) and *cozEb* (MDB83), with and without IPTG induction.

Norges miljø- og biovitenskapelige universitet
Noregs miljø- og biovitskapelege universitet
Norwegian University of Life Sciences

Postboks 5003
NO-1432 Ås
Norway